METHODOLOGY OF CITRIC ACID BASED FUNCTIONAL

BIOMATERIAL DEVELOPMENT

AND APPLICATION

by

YI ZHANG

Presented to the Faculty of the Graduate School of

The University of Texas at Arlington in Partial Fulfillment

of the Requirements

for the Degree of

DOCTOR OF PHILOSOPHY

THE UNIVERSITY OF TEXAS AT ARLINGTON

August 2012

ACKNOWLEDGEMENTS

It is my pleasure to acknowledge the professors, colleagues, family and friends who have made this work possible. I would like to gratefully and sincerely thank Dr. Jian Yang for his guidance, contributions, patience, and most importantly, his friendship to make my Ph. D. experience productive, stimulating, and rewarding. I will always remember "Chem-is-try", and everything you have done for me. For this dissertation, I would also like to thank my committee members: Yuanbao Hong, Xiankai Sun, Kytai Nguyen, and Liping Tang for their time, interest, and helpful comments. Special Thanks to Dr. Tang and Dr. Nguyen for all their help throughout my Ph. D. study, from comprehensive test to diagnostic test, and final defense. Without your helps, my work will always be missing the most important puzzle. Also, I need to thank the faculty of the Bioengineering Department, thank you for your open doors and minds, and all the great opportunities you offered me.

The members of the Yang research group have contributed immensely to my personal and academic life at the University of Texas at Arlington. This group has always been the source of inspiration, productivity, friendship, and fun time. I am especially grateful for the help provided by Dr. Richard Tran who have been kept our lab well organized all the time. I would also like to thank Dipendra Gyawali, Dr. Zhiwei Xie, and Dr. Jinshan Guo for their advice on my research work. Without those helps, I would not be where I am today.

I would also like to take this time to thank my family who were paramount in shaping my character and integrity. I owe the deepest gratitude to my parents, Libao and Qingwu, and my grandparents, Youqing and Juanru, who have always supported my decisions with no doubt. Although you were never able to offer me advice on my study and research, you never stop giving me love, support, and care. I would not have been able to pursue my dreams without the sacrifices you made from the day I came to this world. You were and would always be standing

iii

behind me, no matter what happened. I am at a loss for words adequate to the expression of my grateful feeling. Finally, I will always be indebted to my friends, Hongjun, Diana, KoKo, Haidong, and Yiwei, for your encouragement, support, and faith in me, that gave me the strength to make all of this work possible.

July 17, 2012

ABSTRACT

METHODOLOGY OF CITRIC ACID BASED FUNCTIONAL

BIOMATERIAL DEVELOPMENT

AND APPLICATION

Yi Zhang, Ph.D.

The University of Texas at Arlington, 2012

Supervising Professor: Jian Yang

Biomaterials play critical roles in modern strategies of biomedical applications, such as tissue engineering, and theranostic therapy. Attempts to design ideal biomaterials for each specific application have led to an enormous increase in the number of polymeric biomaterials. Different biomedical applications require specific functionality of biomaterials. Unfortunately, the limited versatility of currently available biodegradable polymers fails to meet the wide range of requirement for biomedical applications. Therefore, a methodology of functional biomaterials development would be beneficial to the biomaterial field.

It has been proved that citric acid can be utilized as a key element in the development of novel biodegradable polymers. This work presents the methodology of three citric acid based functional biomaterials design and application to meet the multifaceted needs of tissue engineering and theranostic therapy. Firstly, urethane doped biodegradable polyester with dual crosslinking mechanism is developed as scaffold materials to fulfill the wide range of mechanical properties of soft tissue engineering. We hypothesize that doping of urethane bond can greatly increase the mechanical strength and elasticity, and dual crosslinking mechanism

confers parameters to manipulate mechanical properties over a wide range. Secondly, novel family of biodegradable photoluminescent polymers (BPLPs) is developed meet the increasing needs of marriage between biodegradable polymers and bioimaging. We hypothesize that the intrinsic strong fluorescence of BPLPs can be exploited as theranostic probes, and provide possibility of real-time monitoring for implants. Lastly, BPLPs are doped with urethane bond (UBPLPs) to achieve an ultra strong elastomer with strong fluorescence. We hypothesize that the greatly increased mechanical strength makes UBPLPs suitable for engineering cardiovascular tissue. It also can improve the stability of nanoparticles for theranostic application. To test these hypotheses, we first developed the methodology of all three functional biodegradable polymers. The synthesis, characterization, fabrication, and application of those polymers were discussed. The relationship between materials chemistry and phenomenon were devoted to the understanding of basic biomaterials science.

The results presented in this work show that all three functional polymers succeed to fulfill the requirements of specific biomedical applications. The designing strategies can serve as a guide for developing of new citric acid based biodegradable polymers. These enabling new biodegradable polymers are able to address many of the existing challenges in tissue engineering, and theranostic applications.

TABLE OF CONTENTS

LIST OF ILLUSTRATIONS

xiii

LIST OF TABLES

CHAPTER 1

INTRODUCTION

1.1 Importance of Biodegradable Polymers

The development of novel biomaterials offers unique opportunities to tackle unmet clinical problems. Biomaterials are critical components to all medical devices, most of which require biodegradable materials, such as tissue engineering scaffolds, drug delivery vehicles, and bioimaging probes. Biodegradable polymers shoulder missions such as defining three-dimensional structure for neo-tissue formation, regulating cell differentiation and phenotype, facilitating targeted delivery and localized release of therapeutic agents, and visualizing diseased or abnormal tissue for diagnosis. Once those missions are completed, materials will degrade and be absorbed/cleared by body, thus leaving no foreign materials. Successes of biodegradable polymers have been previously demonstrated by tremendous number of studies on tissue engineering, drug delivery, and bioimaging. Large selection of biodegradable polymers provides desired mechanical properties, degradation rates, and functional groups for modification. Therefore, by careful choosing and design, biodegradable polymers with desired physical and chemical properties can be created for various biomedical applications.

1.2 Functional Biodegradable Polymers

As many biomedical applications require special properties, such as ultra-strong but elastic mechanical property, dual crosslinking (tunable mechanical property) mechanism, and fluorescence. For tissue engineering scaffold, a mismatch in mechanical compliance between the materials and host tissue interface causes scar tissue formation, improper tissue in growth, and much worse, failure of the implant. With the half century of development, only poly (L-lactide) (PLA), poly (glycolide) (PGA), and their copolymers (PLGA) have been approved by U. S. Food and Drug Administration (FDA) for medical device [1]. Although they are successfully

1

used to engineer hard tissues, their stiff nature compromises their success in soft tissue engineering [2]. Therefore, many efforts have been made to develop biodegradable polymers with wide range of mechanical properties. Soft tissue engineering with its complicated architecture and unique mechanical properties, presents an enormous challenge to tissue engineering [3, 4]. Choosing a biodegradable polymer with desired mechanical property is not enough to address the challenge. In order to replicate the complicate architecture of native tissue, such as heart valve and blood vessel, porous scaffolds are usually fabricated. Thus, there is a tremendous loss of mechanical property upon fabrication. Therefore, the chosen material should have ultra-strong but soft mechanical property cover this loss.

Recently, fluorescent labeling and imaging have fueled the significant growth of life science and medical research due to the increasing demands on analyzing biomolecules, tracking biological process, and visualizing diseases and therapeutic efficacy [5]. For tissue engineering, fluorescence incorporated scaffold can help to understand some fundamental elements of tissue engineering, such as predicting *in vivo* degradation [6]. It also provides the real-time monitoring of neo-tissue formation/infiltration. For drug delivery, it has been well established that polymeric drug delivery systems can enhance efficacy and safety for cancer therapy by transporting chemotherapy agents directly to targeted tissue [7]. Fluorescence enabled drug delivery vehicle can function as a theranostic probe which intertwines delivering therapeutic agents and diagnosis.

1.3 Functional Biomaterials Design and Requirements

In review of the recent literature, many important design criteria must be met when creating the functional materials for the intended biomedical application. The following sections will discuss the design criteria and concerns that should be taken into consideration when creating a functional biodegradable polymer.

2

1.3.1 Incorporation of Functionality

Due to the specific restrictions and requirements, many biomedical applications need functional biomaterials to fulfill the task. For example, ultra-strong and elastic polymer may be required for cardiovascular tissue engineering [8, 9]. Water solubility and *in situ* crosslinkability are required for injectable hydrogel. Fluorescence is needed for real-time monitoring of the implants. Two methods of incorporating functionality into biodegradable polymers are using monomers with functional groups to initial synthesis and creating functionality after synthesis. Due to the controllable manner of polymerization process, such as polycondensation and polyaddition reactions, monomers with functional groups can be easily incorporated. For example, vinyl containing monomers, such as maleic acid and poly (ethylene glycol) diacrylate (PEGDA), can be involved to synthesize free radical crosslinkable polymers [10]. Fluorescent labels, such as organic small molecule and inorganic quantum dots, can be conjugated to enable fluorescence [11]. On the other hand, creating functionality after synthesis is based on formation of new chemical bond or structure. For example, urethane bond can be formed by reaction between hydroxyl and isocyanate groups, which can dramatically increase mechanical property [12]. The presence of urethane bond can also bring the physical crosslinking point that offers elasticity.

1.3.2 Biocompatibility

Biocompatibility is a term used to describe the ability of a material to perform with an appropriate host response in a specific application. It is always the first concern to evaluate biocompatibility of materials for biomedical applications. Biocompatibility will be influenced by many effects, such as hydrophilicity, pH, and additives. Although there are many standards to characterize biocompatibility, comparison with FDA approved ones in the same category is able to provide strong evidence [13]. For biodegradable polymers, PLA, PGA, and their copolymer PLGA have been approved by FDA for biomedical applications [14, 15]. Thus, those materials can be set as standard for all biodegradable polymers [16]. Having one more concern than non-

3

degradable materials, biocompatibility of degradation products is also critical to biodegradable polymers. For most biodegradable polymers, such as polyesters, polyurethane, and polyamide, hydrolysis is the main process of biodegradation. Therefore, products of accelerated hydrolysis in strong base solution need to be evaluated.

1.3.3 Mechanical Property

To evaluated a polymer for tissue engineering scaffold, mechanical strength is critical character. Generally, stress-strain curve obtained from mechanical test is used to define many important parameters. However, various kinds of mechanical tests are addressed for different applications. Compression test is usually performed to test the toughness of engineered scaffolds or tissues, such as bone tissue engineering. The toughness can be determined by compressive strength-strain curve. Tensile test is used to evaluate polymers for engineering elastic tissues, such as blood vessel, heart valve, and tendon. Tensile strength, elongation at break, and Young's modulus can be determined. Except for usual tensile test, some tissues require specific mechanical test for materials. For example, for vascular tissue engineering, burst pressure and suture retention strength are both critical. Burst pressure determines the suitability for vascular implants, and suture retention strength represents the suitability for surgical handling. Engineered heart valve is subjected to accelerated wear test to evaluate the endurance of the implant.

1.3.4 Degradation

For biodegradable polymers, degradation can be concluded into two types, hydrolysis and enzymatic degradation [17]. Although *in vivo* degradation is more complicate than *in vitro*, degradation rate after implantation is usually predicted by *in vitro* study. In previous work, *in vitro* degradation in PBS or enzymatic solution was carried out to evaluate the property of the polymers [18].

Several factors can influence degradation rate, such as hydrophilicity and hydrolytic resistance. Hydrophilicity influences rate of water uptake, which is considered to be the first step

4
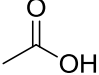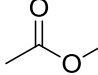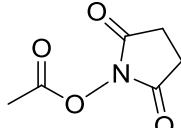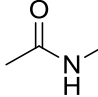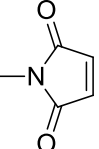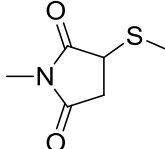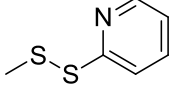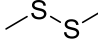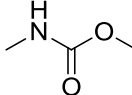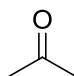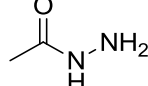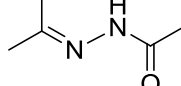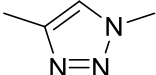
of polymer degradation. It is determined by chemical structure of polymers. More hydrophilic groups, such as hydroxyl and carboxyl groups, lead to high hydrophilicity. Normally, a more hydrophilic polymer will have higher degradation rate. Moreover, water uptake rate will also be raised by lower glass transition temperature (Tg). Hydrolytic resistance is determined by chemical bonds that consist of polymer backbone or network. For example, urethane bond is more resistant to hydrolysis than ester bond. Thus, polyurethane normally has lower degradation rate than polyester.

1.3.5 Functional Groups for Conjugation

For many biomedical applications, free chemical group for conjugation of biofunctional moieties are critical. Various conjugation strategies have been developed covering all the functional groups that exist in conjugating moieties and biodegradable polymers. The most commonly used conjugation chemistry is listed in table 1.1. Carboxyl group is present in many biodegradable polymers, most of which are synthesized via ring-opening polymerization, such as PGA, Poly (α-malic acid), and their copolymers. Carboxyl group can be easily activated by carbodiimide for condensation. N,N'-dicyclohexylcarbodiimide (DCC) is suitable for water insoluble condition, while 1-ethyl-3-(3-dimethylaminopropyl) carbodiimide (EDC) is for aqueous environment. Although carbodiimide is able to conjugated both carboxyl and amino group, N-Hydroxysuccinimide ester (NHS-ester) is more specific to amidation. Thiol group has its specialty in quantum dot chemistry, and is present in many proteins, and peptides. Meanwhile, thiolation for different molecule has been well established in organic chemistry. Polymers with maleimide and pyridyidisulfide can be conjugated with thiolated molecules. Hydroxyl groups can also be found in many organic compounds. Except for carbodiimide chemistry, hydroxyl group can react with isocyanate group to form urethane bond in an active –H free environment. In addition, hydroxyl group can also be oxidized into aldehyde group by some mild oxidant, such as sodium periodate. Then aldehyde groups can be conjugated with hydrazide group. Recently, click chemistry has been extensively studied, due to the easy introduction of azides and alkynes

[19]. Reaction can be conducted in a wide range of solvents (including water). Although the use of Cooper-based catalyst has been a concern for biomedical application, catalyst free click chemistry has been well established recently [20].

Table 1.1 Commonly used conjugation chemistry in biomedical application

Conjugating site	Conjugated Group	Chemistry	Final bond
—COOH	—OH	Carbodiimide (EDC, DDC)	ester
—NH₂	NHS structure	NHS ester	amide
—SH	maleimide structure	Maleimide	thioether
	pyridyldisulfide structure	Pyridyldisulfide	disulfide
—OH	−N=C=O	Isocyanate	carbamate
ketone	hydrazide structure	Hydrazide	hydrazone
—C≡CH	—N₃	click chemistry	triazole

1.4 Biodegradable Polymers with Tunable Mechanical Property

1.4.1 Mechanical Requirements of Soft Tissue Engineering Scaffold

As tissue engineering scaffold, it was expected to shoulder at least one or more of following tasks, supporting and regulating cell growth and proliferation, defining space for neo-tissue formation, delivering and retaining cells and biochemical factors, and exerting mechanical stimuli to modify cell behavior and tissue regeneration [21]. Various scaffold fabrication techniques, such as salt leaching, thermal-induced phase separation (TIPS) [22], gas foaming

[23], and electrospinning, are exploited to offer different structure and morphology for intended tissue engineering. Biofunctional moieties, such as growth factors, differentiation inducers, and drugs, are incorporated to achieve biological functions. However, the mismatch in mechanical compliance between tissue engineering scaffold and host tissue remains the issue for scientists. Due to the varsity of soft tissues/organ in human body (Table 1.2), biodegradable polymers with wide range of mechanical properties need to be prepared. From Table 1.2, it is shown that human soft tissues and organs have a wide range of mechanical properties. Although many biodegradable polymers have been developed as scaffold materials for tissue engineering, there is no family of polymers that has tunable mechanical property in a wide range. It is urgent to develop a family of elastic materials to fulfill the mechanical requirement of soft tissue engineering.

Table 1.2 Mechanical properties of human soft tissues

Soft Tissue	Tensile Strength (MPa)	Young's Modulus (MPa)	Elongation (%)	Reference
Human Bladder	0.27±0.14	0.25±0.18	0.69±0.17	[24]
Smooth muscle relaxed	N/A	0.006	300	[25]
Smooth muscle contracted	N/A	0.01	300	[25]
Aortic valve leaflet (circumferential)	N/A	15±6	21±12	[26]
Ulnar cadaveric peripheral nerve	9.8 – 21.6	N/A	8 – 21	[27]
Medial cadaveric peripheral nerve	9.8 – 30.4	N/A	6 – 22	[27]
Cerebral artery	N/A	15.7	50	[28]
Cerebral vein	N/A	6.85	83	[28]
Achilles Tendon	79±22	819±208	8.8±1.9	[29]
Medial Collateral Ligament	84.4±22.2	1107.27±126.3	10.6±2.8	[30]

1.4.2 Existing Biodegradable Polymers for Soft Tissue Engineering

Due to the mechanical behavior, polymers can be divided into three categories, thermoset, thermoplastic, and elastomer. Biodegradable elastomers has been widely used as scaffold materials for soft tissue engineering due to that their soft and elastic behavior is similar

to soft tissue. They can sustain and recover from multiple deformations without causing irritation to the surrounding tissue in a mechanically demanding environment [31]. Different from traditional biodegradable polymers, every biodegradable elastomer need physical or/and chemical crosslinking to form three-dimension (3D) structure. Elastomers with only physical crosslinking exhibits thermoplastic behavior, so called thermoplastic elastomer. Physical crosslinking is formed by Van der Waals forces or hydrogen bonding, usually accompanied by the crystalline regions or the high glass transition temperature (Tg) regions as crosslinking points [32]. Elastomer with chemical crosslinking has thermoset behavior that expressing high elasticity. The chemically crosslinked 3D network significantly reduces the relaxation and creep of molecular chain, thus, maintaining the shape of final products.

1.4.2.1 Thermoplastic Biodegradable Elastomer

Segment polyurethane (SPU) is the most commonly used thermoplastic biodegradable elastomer [33, 34]. Due to the isocyanate chemistry, various diol can be exploited as precursor to synthesis SPU. Therefore, SPU family has a wide range of physical and chemical properties. With the hydrolyzable urethane bond, biodegradability was endowed to SPU with biodegradable or water-soluble precursors, such as PLA, poly caprolactone (PCL), poly (ethylene glycol) (PEG), and polyhydroxyalkanotes (PHAs) [32]. Those low-molecular weight polymers (with a molecular weight from 400 to 5000 g/mol) work as soft segments that have low Tg and high elasticity. Hard segments are formed by strong intermolecular bonding among urethane bonds. With different choice of diol and diisocyanate, 55 MPa of tensile strength and 1300% of elongation at break can be obtained (Table 1.3). SPU is extensively used to engineer ligament [35], meniscus [36], blood vessel [12], and heart valve [37].

Poly (ether ester) [38] and Poly (ester amide) [39] are two families of thermoplastic elastomers. Polyester acts as hard segment in the former and soft segment in the later. Both of them have many choices of soft and hard segments, thus, resulting in wide range of mechanical properties and tunable degradation rate. With PEG as soft segment and poly (butylenes

8

terephthalate) (PBT) as hard segment, tensile strength of obtained poly (ether ester) can be tuned from 8-23 MPa, and elongation from 500% to 1300% (Table 1.3).

Due to the wide accepted biocompatibility of PLA, many strategies of making thermoplastic elastomers based on PLA have been developed [40, 41]. Since lactic acid has a chiral nature, several distinct forms of PLA exist. Poly (D,L-Lactide) (PDLLA) is amorphous which can serve as soft segment, such as in SPU. PDLA and PLLA are semicrystalline which usually act as hard segment. Mechanical property of PLA based thermoplastic elastomers is listed in Table 1.3. As shown, elongation at break can be as high as 1800% of chain-extended PLA-PEO-PLA. Poly (1,3-trimethylene carbonate)-PLA diblock copolymer has a tunable tensile strength from 1 to 38 MPa (Table 1.3).

Table 1.3 Mechanical properties of thermoplastic bioelastomers

Thermoplastic bioelastomer	Tensile Strength (MPa)	Young's Modulus (MPa)	Elongation (%)	Reference
PCL Diol/ 1,4-butanediisocyanate	38–55	30.1–263.9	870–1200	[42]
PCL-PEO-PCL Diol/ 1,4-butanediisocyanate	8-20	4.6-75	325–560	[43]
PCLA Diol 1,6-hexanediisocyanate	19.8–38.5	10.6–29.5	526–1300	[44]
PCL PHC Diol 1,4-butanediisocyanate	14–34	8-24	660-875	[45]
PDMEA Diol 1,6-hexanediisocyanate	22.9	20.2	560	[46]

1.4.2.2 Thermoset Biodegradable Elastomer

Chemically crosslinked elastomer exhibits thermoset behavior. It can be further divided into two classes, thermal-cured and photo-cured. The general similarity of thermal-cured elastomer is having reacting groups as side chain along polymer backbone. Those side chains are normally hydroxyl and carboxyl groups that can be thermally cured to form ester bond. However, thermal-cure elastomer is not suitable for in-situ crosslinking and delivering cells and thermo-sensitive molecule. Photo-curable double bond is incorporated into biodegradable

polymers to enable photocrosslinkability. Mechanical property of thermoset biodegradable elastomers is listed in table 1.4 and 1.5.

There are two types of thermal-cured biodegradable elastomers. One is based on polyol and dicarboxylic acid, and the other one is based on diol and tricarboxylic acid. Polyol represents a set of alcohols that containing more than two hydroxyl groups. After polycondensation reaction with dicaboxylic acid, the extra hydroxyl groups along polymer chain can be thermal-cured to form a 3D network. The most popular elastomer of this type is poly (glycerol sebacate) (PGS). After the first report of PGS in the late 1990's [47], Wang and co-workers started to explore its use for biomedical application [31]. With a two-step synthesis, a linear PGS prepolymer was obtained in the first step, and the pendant free hydroxyl groups served as thermal-curable points in the second step. PGS is a soft (Young's modulus of 0.282 MPa) and elastic (elongation at break of 267%) (Table 1.4) material that has potential for engineering soft tissues such as arteries, veins, and nerves [9, 48, 49]. Except for glycerol, many other biocompatible polyols have been involved to form a family of poly (polyol sebacate) (PPS), such as poly (xylitol sebacate) (PXS), poly (sorbitol sebacate) (PSS), and poly (mannitol sebacate) (PMS). Compared with PGS, more hydroxyl groups resulted in stronger (tensile strength as high as 17.64 MPa) and stiffer (Young's Modulus as high as 378 MPa) (table 1.4). To adjust the mechanical property and degradation rate of PGS, sebacic acid has been partially replaced with lactic acid to form PGSL, and fully replaced with dodecanedioic acid to form PGD. However, the tensile strength and elasticity has not been significantly improved.

The other type of thermoset elastomer is based on polycondensation of diol and tricarboxylic acid. Citric acid is key monomers for this family of elastomers. Citric acid is a nontoxic, FDA approved, inexpensive, and robust multifunctional monomer. It is a ubiquitous metabolite in citric acid circle. The valuable side carboxylic and hydroxyl groups can be thermal-cured to form degradable ester-crosslinked 3D network. Citric acid based elastomers have succeeded in small diameter vascular graft, bone tissue engineering, nerve tissue engineering,

and biodegradable photoluminescent polymers. First citric acid based elastomer for biomedical application was reported in 2004 [50]. Yang and co-workers synthesized poly (diol citrates) (PDC) via a convenient and cost effective polycondensation reaction. It has a similar two-step polymerization as PGS. Different aliphatic diols ranging from 3 to 16 carbon chain lengths were involved in synthesis to obtain wide range of mechanical properties [51]. Controlling the post-polymerization (thermal-cure) temperature and time provide another manipulation on mechanical property. For poly (1,8-octanediol citrate) (POC), tensile strength of 6.7 MPa and elongation at break of 265% can be achieved (Table 1.4). Except for aliphatic diols, xylitol and PEG can also be involved in synthesis to obtain water soluble pre-polymers. The rationale behind this design was to create polymers with non-toxic FDA approved monomer (xylitol) or diols with outstanding biological properties (PEG). The hydrophilicity of those two diol will have great contribution on controlling degradation rate [32]. More interestingly, those thermal-curable water soluble polymers can also be conferred with photo-curability to achieve a dual-crosslinkable hydrogel, which will be discussed later this section.

Although there has been many ways to manipulate the mechanical properties, no significant improvement on the strength has been achieved. Those elastomers with relatively low tensile strength are not suitable for engineering strong soft tissues, such as blood vessel, heart valve, and ligament. There is also a significant loss in mechanical property on porous scaffold fabrication and in wet condition, which will worsen the mechanical mismatch between polymeric scaffold and native tissues. Recently, urethane-doped POC (CUPE) elastomers were prepared as stronger and more elastic (100% recovery after a stretch) degradable elastomers than PGS and POC for use in scaffold fabrication of dynamic tissues like blood vessels and ligaments [8]. The incorporation of urethane bond provided physical crosslinking point. Since diisocyanate consumes the pendant hydroxyl and carboxyl groups of citric acid, CUPE is still considered as thermoset biodegradable elastomer [52]. With different ratio between POC and diisocyanate, tensile strength of CUPE can be increased to 41.07 MPa, which is seven-fold as

high as POC (Table 1.4). The elongation at break of CUPE can also achieve as high as 291.26%. Although CUPE has a relatively long degradation time (16% mass loss within 60 d), thi rate can be significantly accelerated by partially replacing POC with Poly (ethylene glycol citrate) (PEC) [52]. After fabrication of biphasic tubular scaffold for vascular tissue engineering, a burst pressure of 2602.50 mmHg can be obtained, which meets the standard of saphenous veins [53]. Suture retention of 2.45 N is strong enough for surgical handling [54]. Those results indicate that incorporation of urethane bond into a citric acid based elastomer has great potential to offer strong and elastic materials for soft tissue engineering.

Table 1.4 Mechanical properties of thermo-cured bioelastomers

Thermo-cured bioelastomer	Tensile Strength (MPa)	Young's Modulus (MPa)	Elongation (%)	Reference
PGS	0.5	0.28	267	[9]
PPS	0.57-17.64	0.37-378	10.9-205.2	[55, 56]
PGSL	0.15	6.5-21	133	[57, 58]
PGD	0.46-7.2	1.08-136.55	123.2-225	[59]
POC	Up to 6.7±1.4	0.92-11.4	265±10	[50]
CUPE	15.62-33.35	2.53-29.82	252.37-291.26	[12]

Although thermal-cured elastomers showed promising results for soft tissue engineering, the heat dependence of the preparation and crosslinking restricts the abilities of the elastomers to provide localized delivery of thermo-sensitive drugs and proteins for site-specific action by in situ polymerization and crosslinking in or on a tissue, and makes it difficult to process the elastomers into complex 3D scaffolds with cell entrapment and bioactive molecules [60]. The photo-cured elastomers can overcome the shortcoming of thermal-cured ones. The photo-curability can be conferred to polymers by incorporating vinyl group containing monomers, such as acrylic units, maleic acid, and fumaric acid. The non-crosslinkable polycarbonate (PC) and poly (ε-caprolactone) (PCL) can be conferred with photo-curability by incorporating vinyl groups [61, 62]. The mechanical property of those elastomers is listed in Table 1.5. Tensile strength reaches 35 MPa, and elongation at break can be as high as 1500%.

Another unique family of photo-curable elastomers is developed based on PGS and POC. Those thermal-curable elastomers are conferred with photo-curability to enable dual-crosslinking mechanism. PGS was reacted with acryloyl chloride to obtain acrylated PGS (PGSA) [63]. For POC, citric acid was partially replaced with maleic acid/maleic anhydride to obtain double bonding containing (POMC) [64]. With controlled degree of vinylation, PGSA has a tensile strength between 0.05 - 0.5 MPa, and elongation at break between 42 - 189%. POMC has a tensile strength between 0.7 - 1.29 MPa, and elongation at break between 38 - 382% (Table 1.5). The dual-crosslinking mechanism not only provides more variables to manipulate mechanical property, but also improves the processability of those elastomers. However, both PGSA and POMC can only be dissolved in organic solvent. The harshness of solvent will limit their use for cell encapsulation and gene/protein delivery. Therefore, maleic acid has been incorporated into the synthesis of PEC to obtain a photo-curable elastomer (PPEGMC) [60]. PPEGMC has a tensile strength of 0.64 MPa, and elongation at break of 723% (Table 1.5). The mild crosslinking condition (redox initiator, 37°C) and short cure time (less than 5 min) make PPEGMC an injectable in situ crosslinkable hydrogel for cell delivery. Recent research showed that hydrogel mimics the nature of cardiovascular system in the early development [65]. PPEGMC showed promising potential for stem cell encapsulation addressing cardiovascular tissue engineering.

Table 1.5 Mechanical properties of photo-cured bioelastomers

Photo-cured bioelastomer	Tensile Strength (MPa)	Young's Modulus (MPa)	Elongation (%)	Reference
PGSA	0.05-0.5	0.05-1.38	42-189	[18]
POMC	0.7-1.29	0.07-1.06	38-382	[64]
PPEGMC	0.311-0.638	0.389-0.777	138-723	[60]
Photo-cured poly(trimethylene carbonate)	0.95-35	1.12-10.5	108-847	[66, 67]
Photo-cured PCL	2.0-9.2	0.6-100	90-1500	[68]

1.5 Biodegradable Fluorescent Materials

The marriage of biodegradable polymer and fluorescent imaging has resulted in an important area of polymeric biomaterials: biodegradable fluorescent polymers. Researchers have put significant efforts on developing versatile fluorescent biomaterials due to their promising in biological/biomedical labeling, tracking, monitoring, imaging, and diagnostic applications, especially in drug delivery, tissue engineering, and cancer imaging applications. Biodegradable fluorescent polymers can function not only as implant biomaterials but also as imaging probes. Currently, there are two major classes of biodegradable polymers used as fluorescent materials. The first class is the combination of non-fluorescent biodegradable polymers and fluorescent agents such as organic dyes and quantum dots (Qdots). Another class of polymers shows intrinsic photoluminescence as polymers by themselves carrying integral fluorescent chemical structures in or pendent to their polymer backbone, such as Green Fluorescent protein (GFP). In the present section, we will review the fluorescent biodegradable polymers with emphases on material fluorescence mechanism, design criteria for fluorescence, and their cutting-edge applications in biomedical engineering.

1.5.1 Design Criteria of Fluorescent Materials for Biomedical Application

To develop an ideal biodegradable fluorescent material for various bioimaging, the physiological, physicochemical, and photophysical properties should all be taken into consideration. For different bioimaging application, fluorophore should be chosen with careful consideration of its photophysical, physiological, and physicochemical property.

To better describe the photophysical property of a fluorescent material, there are several parameters to be understood. Firstly, excitation and emission, they determine the color of the fluorescence. As we discussed above, emission of quantum dots is size dependent, while the one of inorganic compounds can be manipulated by chemical modification [69-71]. Considering the biomedical application, penetration depth in the biological tissue is important, too. Light with the longer wavelength has longer penetration depth [71]. Brightness of

14

fluorescence is second consideration after fluorescence color. Precisely speaking, the brightness is determined by two parameters, extinction coefficient, and quantum yield. Extinction coefficient stands for how many photons a substance can absorb under a given wavelength, which is excitation wavelength. Quantum yield shows the efficiency of a substance emits light, specified at a given emission wavelength. In common word, it represents that how many protons can be emitted, when 100 of them are absorbed. In the comparison of the brightness of different fluorescent proteins, the product of molar extinction coefficient and quantum yield has been used [72]. Although each fluorophore has a fixed value of extinction coefficient and quantum yield at given wavelength, but those values can be varied under different circumstances, such as solvent, temperature, and pH. The endurance of fluorescent materials to photobleaching is also a very important optical property. It is determined by the time to bleach from an initial emission rate of 1,000 photons/s down to 500 photons/s [70, 72]. In most cases, it stands for the photostability. The optical properties of some typical fluorescent materials were listed in Table 1.6, 1.7 and Figure 1.1. Autofluorescence from the examined objective is another concern. For in vivo imaging application, biological tissue has strong light scattering and autofluorescence [73]. Plasma also has massive absorption at 400-670 nm (hemoglobin) [74]. Therefore, near infrared (NIR) fluorophore is usually preferred for tissue imaging to avoid an overlap with tissue-autofluorescence and light scattering/absorption.

Table 1.6 Optical properties of different fluorescent materials (for quantum yield and extinction coefficient, sample was tested using water as solvent, unless specified)

Category	Fluorescent Material	Emission (nm)	Quantum Yield	Extinction Coefficient ($M^{-1}cm^{-1}$)	$t_{1/2}$ for Bleach (s)
Quantum Dot	CdS	370-500	<0.60	100,000-950,000	
	CdSe	470-660	0.65-0.85	100,000-700,000	
	CdTe	520-750	0.30-0.75	130,000-600,000	
Organic Dye	FITC	541	0.97 (ethanol)	92,000 (ethanol)	
	Rhodamine B	610	0.49 (ethanol)	106,000 (ethanol)	
	Texas Red	615	0.93	140,000 (ethanol)	

Table 1.6 – *Continued*

			(ethanol)		
Fluorescent Protein	Cerulean	475	0.62	43,000	36
	T-Saphire	511	0.60	44,000	25
	mOrange	562	0.69	71,000	9.0
	mPlum	649	0.10	41,000	53
Biodegradable Photoluminescent Polymers (BPLP)	BPLP-Cys	437	0.62	133 (1,4-dioxane)	
	BPLP-Ser	441	0.32 (1,4-dioxane)	117 (1,4-dioxane)	
		535	0.12 (1,4-dioxane)	51 (1,4-dioxane)	
		540	0.02 (1,4-dioxane)	10 (1,4-dioxane)	

Table 1.7 Comparison of properties among fluorescent materials

Property	Organic Dye	Quantum Dot	Fluorescent Protein	BPLPs
Emission Range	All range from UV to IR	All range from UV to IR (size dependent)	440nm – 649nm	434nm – 725nm
Molar Extinction coefficient	2.5x104-2.5 x 105 M^{-1}cm^{-1}	105-106 M-1cm-1	103-1.5 x 105 M^{-1}cm^{-1} (per chain)	100 – 200 M^{-1}cm^{-1}
Quantum Yield	0.5-1.0 (visible), 0.05-0.25 (NIR)	0.1-0.8 (visible), 0.2-0.7 (NIR)	0.10-0.79	0.02-0.62
Size/Mw	Up to 0.5nm	6-60nm	~27kD	1000-1500 g/mol
Fluorescent lifetime	1-10ns	10-100ns	1-10ns	1-5ns
Solubility	Depending on the chemical structure	Depending on surface chemistry	Can be water-soluble via a series of site-directed mutations	Different solubility based on various monomers

Table 1.7 – *Continued*

Bioconjugation	Using conjugation chemistry based on functional group, usually multi-dyes on single biomlecule	Well-established protocol of ligand chemistry	Can be conjugated easily via conjugation chemistry, due to the ubiquitous presence of cysteine and lysine residues	Rich of –COOH, and –OH group, which can be used for bioconjugation
Processability	Small molecule, usually loaded with polymeric carrier	Normally used as fluorescent label	Working individually as biosensor, but not as any devices, like nanoparticles, scaffold	Used for scaffold, nanoparticle, and biosensor
Body clearance	Retention and clearance depending on dyes	<5.5nm, Rapid and efficient renal clearance; >15 nm, prevented renal excretion	Clearance from body via renal proximal tubules	Completely degradation into non-toxic monomers
Toxicity	Potential cellular toxicity due to the aromatic structure	Main issue for the use of QDots due to the heavy metal, and potential nanotoxicity	Generally nontoxic to cell, but still have issues due to the over-expression, and protein aggregation	Have the comparable toxicity with PLA
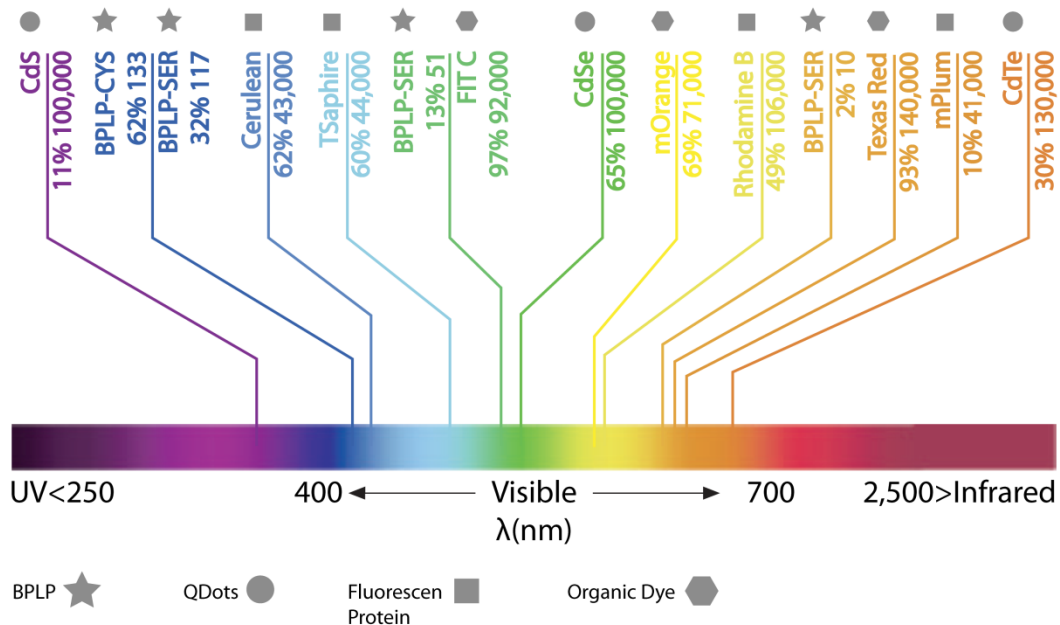
Figure 1.1 Extinction coefficient, optimal emission wavelength, and corresponding quantum yield of different fluorescent materials

From physiological point of view, biocompatibility of the fluorescent materials has the first priority. Generally, traditional fluorescent probes, including organic dyes, quantum dots, and GFPs, have different degrees of cytotoxicity [75-78]. Conjugation with or encapsulation in polymers are the most common and effective way to considerably reduce the cytotoxicity. It has been found that polymer coating can be effectively block the release of heavy metal ion from the core, which is considered as the main course of its alarming cytotoxicity [79]. Polymers can also provide potential for targeted delivery, and protection against physiological environment. The dosage of fluorophore can be considerably reduced, in other words, lowering cytotoxicity. Although there is no standard protocol to evaluate biocompatibility of custom-made fluorescent materials, comparison with FDA approved ones in the same category is able to provide strong evidence. For examples, biodegradable polymer should be compared with PLA, PGA, or PLGA.

Indocyanine green (ICG) can be a standard to all organic dyes. To our knowledge, there is no FDA approved quantum dot by now. However, the silicon based quantum dot, Cdot, has been recently approved by FDA for clinical trial [80]. Therefore, Cdot can be set as a control for all quantum dots. The body clearance should also be given great concern. Research has shown that a nanosphere with a dynamic diameter smaller than 5.5nm can be rapidly cleared by renal. However, like a double-edge sword, rapid body clearance greatly reduces the toxicity, but it also increases the needed dosage of fluorophore for a sustained window. Biodegradable polymer seems like a perfect solution. Increased size after conjugation or encapsulation with polymers helps to avoid renal clearance. Some surface modification, such as PEGylation, confer propensity to evade scavenging by the Reticuloendothelial system (RES) [81]. Thus, a prolonged window period can be obtained, while everything can be still renal clearable after the full degradation of polymers.

Meanwhile, the physicochemical property can also be improved by incorporation of biodegradable polymers. Due to the aromatic nature of organic dyes and hydrophobic surface of Qdots from synthesis, conjugation with water-soluble polymer or encapsulated with polymeric colloids will considerably increase their aqueous solubility. Aggregation stability of the fluorophore should also be concerned. For examples, Qdots with smaller size and damaged surface shield exhibits low stability against aggregation [79, 82] . Moreover, negative surface charge also causes unexpected ionic interactions with biological environment [79]. Sufficient free functional groups are also crucial, due to the need for further conjugation of multiple moieties, such as PEG, drug, and targeting moiety. Although numerous derivates of traditional organic dyes have been synthesized with functional groups present, the limit number of functional groups hinders multiple conjugations for various purposes such as targeting and longer circulation time. Incorporating fluorophore within biodegradable polymers with sufficient functional groups, such as PLGA, Poly (L-glutamic acid), and PCL has been a common solution for the above concern.

19

1.5.2 Organic Dyes Enabled Biodegradable Fluorescent Polymers

The first synthetic organic dye, Mauveine, was discovered by William Henry Perkin in 1856. It has been proved to be effective in dyeing silk and textile. Since its inception, thousands of organic dyes have been prepared for a wide range of applications. For bioimaging purposes, a large number of organic dyes have been developed to examine the fundamental processes at the organ, tissue, cellular, and molecular levels [83, 84]. Based on chemical structure, they can be divided into several classes, cyanine, porphyrin, squaraine, BODIPY, and xanthenes. All the commonly used dyes are derivates from these classes, such as indocyanine green from cyanine, fluorescein and rhodamineB from xanthenes. In order to meet the requirement for different biomedical applications, various chemical modifications have been made upon traditional dyes to tune emission wavelength, increase fluorescence intensity, and introduce functional groups. A series of commercial organic dyes have been developed, such as Cy® and Alex Flour® by Molecular Probes, and DyLight® by Thermo Fisher Scientific.

Of all the currently available organic dyes, only indocyanine green (ICG) have been approved by the FDA for clinical use as diagnostic agents. Bare organic dyes tend to be non-specific to target tissue, unstable, toxic, and rapidly cleared from the body. Major limitations of bare organic dyes include the potential carcinogenesis, which comes from aromatic structure, low threshold of photobleaching, and the lack of functional groups for further conjugation. Incorporation with biodegradable polymers shows great potential to solve these obstacles. In the present section, two approaches will be discussed thoroughly. One is single water-soluble macromolecule conjugation, and the other is encapsulation with polymeric colloids. Organic dye-conjugated polymeric scaffold will also be discussed.

1.5.2.1 Water-soluble Fluorescent Polymers

Tremendous efforts have been made to prepare polymer-dye conjugates. The conjugates have several advantages over the bare organic dyes: (1) since the major content of organic dyes is their aromatic structure, which is usually non-water soluble, conjugation with a

water soluble polymer can dramatically increase the hydrophilicity; (2) conjugation with a polymer can protect dyes from rapid metabolism and body clearance; (3) polymer provides additional functional groups for conjugation of targeting and therapeutic moieties. With the rapid growth of pharmaceutical and material science, various polymers have been considered for the formulation. To include above benefits in one formulation, the chosen polymer should meet several requirements: (1) biocompatible; (2) water solubility; (3) biodegradable for body clearance; and (4) having functional groups that can be reacted with organic dye and conjugation with other molecules, such as drugs and targeting moieties.

Among numerous water soluble polymers, poly (ethylene glycol) (PEG) is the most commonly studied polymer, and its prodrug formulation with anti-cancer drug have received regulatory approval in different countries [85]. The end-group chemistry of PEG has been intensively studied. PEG with different molecular weight, and with different end groups are commercially available, or can be synthesized with reported protocol. Multi-armed PEG provides the multiple conjugation sites for different functional molecules. Although PEG is not biodegradable, it can be served as a standard for PEG-based polymers and many other water soluble polymers. Meanwhile, many efforts have been put on the strategies to produce biodegradable derivatives of PEG. Zhao et al. [86] described the synthesis of a biodegradable multiarm PEGs, and it has entered clinical trials. Poly (L-glutamic acid) (PG) is a biodegradable polymer, and its breakdown product, L-(glutamic acid) can enter normal cellular metabolism. Every repeating unit has carboxyl groups, so PG has sufficient sites for conjugation. The prodrug of PG and Paclitaxel is now under phase III clinical development in US [87]. Melancon et al. [88] conjugated PG with a cyanine derivate, near infrared dyes (NIRF). After conjugation of NIRF, there are still numerous free carboxyl groups for conjugation of targeting moieties, and drug. Although this PG-NIRF was used to study *in vivo* degradation of PG based polymer-drug conjugates, it showed great potentials for whole body imaging or tumor imaging. A number of biodegradable N-(2-Hydroxypropyl)methacrylamide (HPMA) based copolymers (co-pHPMA)

21

caught many attentions over the last 30 years [89]. Co-pHPMA can be conjugated with different imaging moieties through copolymerization and chemical conjugation. Jensen et al. [90] conjugated co-pHPMA with fluorescein-cadaverine, and used it to study the intracellular metabolism of the copolymer. Dextran is another polymer that has been conjugated with organic dyes for imaging. Helmchen et al. [91] used dextran-FITC/Rhodamine conjugates for high resolution brain imaging. The vicinal diol structure could be oxidized by periodate and further conjugated with various functional molecules [92].

In addition to linear polymers, dendrimer is a class of branched macromolecules forming a star-like structure. The physiochemical properties can be easily tuned due to its step-wise fashion synthesis. Theoretically, a generation 5 (G5) dendrimers will have 128 free functional end-groups on surface. Thus, high density of functional groups on the outer layer of dendrimer confers sufficient sites for the conjugation of organic dyes, targeting moieties, and drugs. A major advantage of dendrimers over linear polymer is that hydrophobic molecules can be encapsulated in the cavity formed by adjacent branch [93]. Some dendrimers with positive surface charges, such as poly (ethyleneimine), have also been investigated as carries for negatively charged DNA [94]. Polyamidoamine (PAMAM) is the most commonly used dendrimer. Biodegradable PAMAM were prepared by many labs via different strategies, and have been used for drug delivery and gene therapy [95]. Majoros et al. [96] conjugated fluorescein isothiocyanate (FITC) onto PAMAM, and investigated it for both *in vivo* and *in vitro* imaging. Interestingly, some of PAMAM have been found to have fluorescent properties [97-99]. The fluorescent mechanism has been discussed above. This unique property makes PAMAM a dye-free imaging probe. Therefore, complexity of the design can be greatly reduced.

1.5.2.2 Dye Encapsulation

Biodegradable polymers can be fabricated into nanoparticles of different structures, such as nanocapsules, nanospheres, and micelles depending on physicochemical properties of polymers, and fabrication techniques. Nanocapsule is a core-shell structure with a polymer

membrane and cavity inside, which can be a reservoir for organic dyes. Whereas nanosphere is a polymeric matrix in which dye molecule can be evenly dispersed. Polymeric micelles can be self-assembled in aqueous solution by amphiphilic polymers. Diblock, triblock, and random copolymers of both hydrophobic and hydrophilic blocks can self-assemble into micelles. They have a generally small size (<100nm), depending on the critical micelle concentration (CMC), and a propensity to evade scavenging by the Reticuloendothelial system (RES). Those structures confer protection to organic dye, and considerably improve the stability. Targeted delivery can also be achieved by surface conjugation of targeting moieties. Organic dye encapsulated nanoparticles have been generally exploited for the study of pure imaging purpose, such as cellular uptake, intracellular fate, metabolism, and biodistribution [100-102].

1.5.2.3 Chemically Conjugation

Biodegradable polymeric colloids have been intensively investigated as delivery vehicle for drugs, gene, protein, and cells. To save more loading space for those components and avoid interference with aromatic fluorophore, organic dyes are chemically conjugated with polymeric colloids either during the synthesis of polymers or via surface conjugation of polymeric colloids. Poly (alkyl cyanoacrylate) (PACA) and its copolymers are a family of biodegradable polymers. Droumaguet et al. [103] synthesized PACA copolymers by three monomers, hexadecyl cyanoacetate, methoxypoly (ethylene glycol) cyanoacetate, and Rhodamine B conjugated cyanoacetate. The fluorescent intensity can be tuned by varying the feeding ratios of dye conjugated monomers. The resulted amiphiphilic polymers were self-assembling into nanoparticles. Those nanoparticles have been demonstrated suitable for *in vitro* imaging of human brain endothelial cells. Numerous of biodegradable polymeric colloids have functional groups on surface, such as colloids made from PLGA, Poly (L-glutamic acid), poly (ε-caprolactone) (PCL), and their amphiphilic copolymers with PEG as hydrophilic block, as well as nature polymers, such as chitosan, and gelatin. PLGA nanoparticles have been surface labeled with FITC, Cy®, Alex Fluor®, and Rhodamine for various imaging studies [104-106]. The label

23

of Near-Infrared cyanine dye (NIR-797) helped the real-time biodistribution study of PCL based micelles [107]. For natural polymer-based nanoparticles, Nam et al. [108] conjugated Cy5.5 was labeled on the surface of chitosan nanoparticles. This fluorescent nanoparticle has been successfully used for the study of nanoparticle biodistribution and tumor accumulation.

1.5.2.4 In Situ imaging of biodegradable fluorescent polymeric scaffold

With the rapid development of biodegradable polymers for in situ tissue engineering, non-invasively or minimal-invasively monitoring the behavior of polymeric implants becomes crucial. Although the properties of biodegradable polymers have been carefully evaluated *in vitro*, such as degradation speed and mechanical properties, understanding these material properties remains elusive as the physiological environment provides a more complicated degradation or erosion than *in vitro*. There is an urgent need to assess material properties in situ and in real time.

Recently, Edelman et al. [6] presented a decent study on tracking polymeric scaffold using fluorescence imaging. In this study, fluorescein was conjugated onto PEG, and then mixed with dextran to form fluorescent hydrolyzable hydrogel. Enzymatically degradable collagen labeled with Texas-red was also used to assess its enzymatic degradation. *In vitro* and *in vivo* degradation were both performed for comparison. It was found that the *in vivo* hydrolytical degradation rates of the PEG-based scaffolds could well correlate with the *in vitro* degradation of the samples, while the enzymatic degradation of collagen samples has more complicate behavior in different sites of body. This study represents an advance in tissue engineering where there has been a dearth of understanding on the scaffold degradation and tissue replacement in situ and in real time. Fluorescent scaffolds enable a real-time quantitative evaluation of the scaffold evolution over time via a fluorescence imaging method. This study also implies the added fluorescent properties can be beneficial in the design of next wave of tissue engineering scaffolds to function as both implants and imaging probes.

1.5.3 Inorganic Dyes Enabled Biodegradable Fluorescent Polymers

Generally, naked Qdots are not ready for bioimaging, due to the easy surface oxidation, insufficient functional groups, and most importantly the water-insolubility [79]. To address these problems, polymers have been introduced to make Qdots more suitable for bioimaging. Various polymers can be incorporated with Qdots focusing on the different facets of benefits, such as greatly increasing the stability and hydrophilicity of Qdots, lowering the toxicity, offering sufficient sites for further modification, and providing a reservoir for drug loading [109]. As illustrated in Figure 1.2A, polymer coating converts the hydrophobic surface of Qdots to hydrophilic. Figure 1.2B showed that the tunable fluorescence of Qdots has been investigated for multicolor fluorescence imaging of cancer cells under *in vivo* environment. Polymer layer also improves the colloidal stability, and lower the chance of aggregation [110]. In addition, simple polymer coating has proved to act as a significant barrier for heavy metal ion (Cd^{2+}) diffusion, which was considered as a major cause of toxicity of Qdots [79]. Polymers with various functional groups, such as amine, carboxyl group, and maleimide, can be exploited to further conjugate with antibodies, peptides, hydrophilic therapeutics, or aptamers. From therapeutic point of view, the polymer network provides sufficient room for hydrophobic drug, comparing to the solid semiconductor component of Qdots which is simply an imaging probe. A large pool of polymers have been studied to encapsulate or conjugate with Qdots via various techniques [111]. All those techniques can be classified into two ways, surface coating, and bulky embedding. There are also numberous studies on incorporating Qdots with inorganic substances, such as silica or titania, non-biodegradable polymers, such as Poly (maleic anhydride alt-1-tetradecene), and dendrimers, such as poly (amido amine) [112, 113]. However, we will only focus on the strategies of incorporating inorganic dyes with biodegradable polymers below.
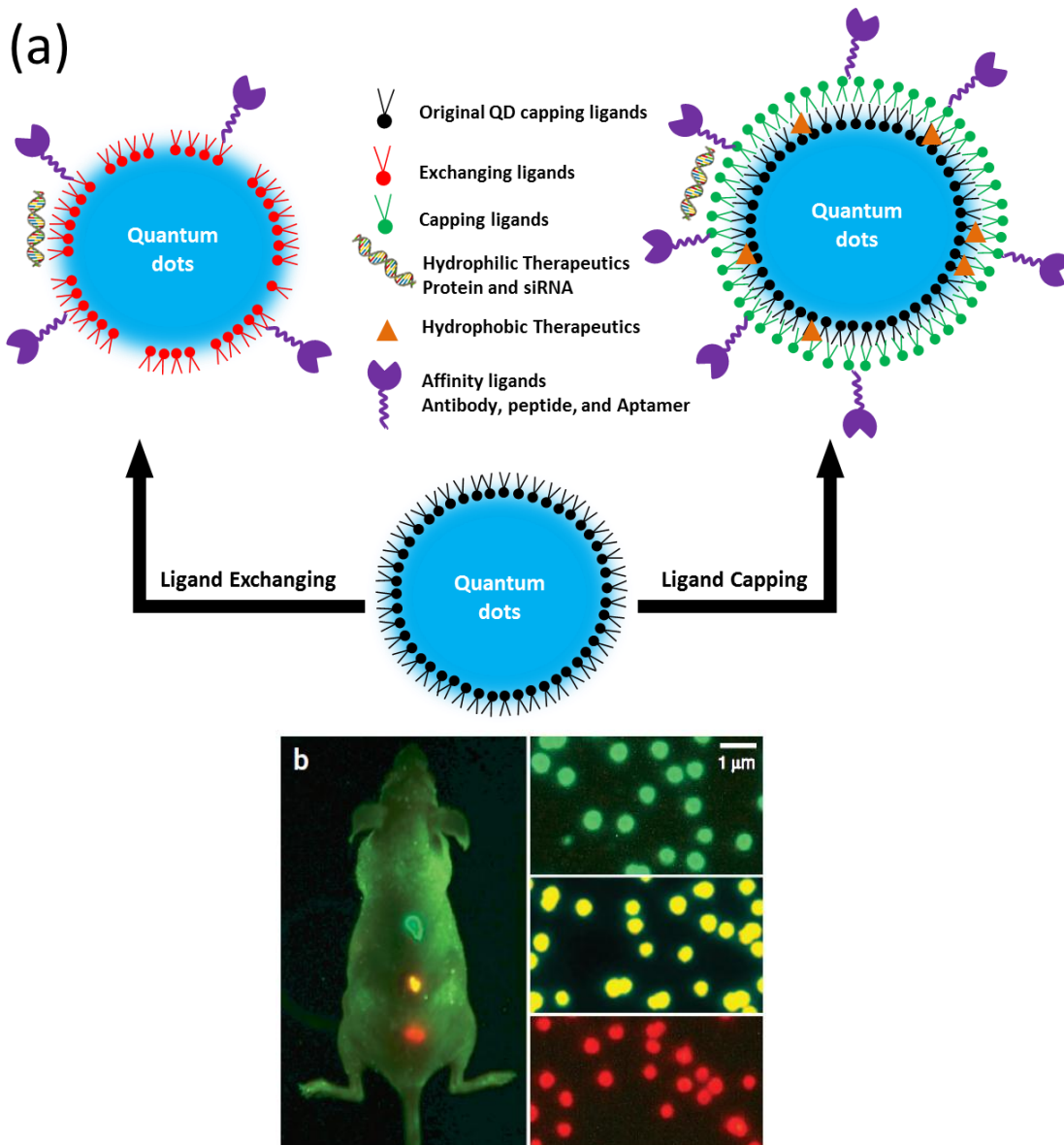
Figure 1.2 Quantum Dots for biomedical applications (a) Schematic illustration of a multifunctional Qdots coated with biodegradable polymers. (b) Cellular and animal imaging showing Qdots with different color under same light source.

1.5.3.1 Biodegradable Polymers Coating on Qdots

Qdots are usually characterized for their photophysical properties, such as emission wavelength, quantum yield, photostability, and physicochemical properties, such as size, surface charge, and aggregation stability. Both of them may change after surface coating with

biodegradable polymers [79]. There are two distinct strategies usually adopted for Qdot coating, ligand exchange, and ligand capping.

Ligand exchange strategy involves completely replacing the surface bound ligands remained during the decomposition of metal-organic or organometallic precursors at elevated temperatures [114]. Those ligands include trioctylphosphine oxide (TOPO) and lipophilic trioctylphosphine for most cases. Physicochemically, the advantage of ligand exchange is maintaining the small final diameter. Choi et al. [115] pointed out that Qdots with a hydrodynamic diameter smaller than 5.5 nm can be cleared rapidly from the body by renal filtration and urinary excretion. Therefore, keeping a small final diameter after surface coating can be beneficial in reducing toxicity. However, Qdots with small diameter after ligand exchange suffer from low stability against aggregation [79]. From photophysical point of view, replacing the original ligand of Qdots may result in several disadvantages. The exchange process raises the risk of surface damage of Qdots, leading to a decrease of quantum yield. It also increases the likelihood for surface oxidation, which will leads to a poor photostability, and blue shift of emission wavelength.

Since there is a specific interaction between thiol group and heavy metal, such as gold, silver, cadmium and so forth, thiolated polymers are the most common ligands involved in ligand exchange strategy [116]. Thiolated PEG has been extensively exploited, due to its easy synthesis, ease of handling, and versatile applications. Hou et al. [117] reported a disulfide bond-bearing and symmetric PLLA-SS-PLLA synthesized by ring-opening polymerization, and its reduced product PLLA-SH. The thiolated PLLA has been successfully coated onto CdSe with ligand exchange strategy. A quantum yield of 53% was reported by tuning the molecular weight of PLLA-SH, and the feeding ratios between ligand and Qdots. The hydroxyl groups on the other end of PLLA-SH also provide sites for further conjugation. The synthesis of thiolated PLLA sets as a protocol for thiolation of various biodegradable polymers that can be synthesized through ring-opening polymerization, such as family of cyclic lactone, and morpholine-2,5-dione

27

[118]. Except for thiol group, amine bond and phosphine bond have also been exploited for ligand exchange [79]. However, rarely any biodegradable polymer has been reported involving the latter two chemical groups.

Different from ligand exchange, ligand capping only caps the original ligands on Qdots with suitable amphiphilic polymers. Without damaging the protecting ligands of Qdots, the photophysical property will be better retained. The thicker layer of coating provides not only a better protection against surface oxidation, but also a good chemical stability and a reliable protection against aggregation. Typically, the coating will also increase the particle size by as much as 5-10 nm [119]. This number depends on the molecular weight of both hydrophilic and hydrophobic blocks. Larger size of Qdots after ligand capping may have a low renal clearance. However, the bare Qdots still can undergo renal clearable after polymer coating is fully degraded. On the other hand, longer circulation time can extend the targeting and potential drug delivery window once injected in the blood circulation.

The surfaces of naked Qdots are occupied by hydrophobic ligands from theorganometallic compounds during the syntheses of Qdots, such as the stabilizing ligand, trioctylphosphine oxide (TOPO), or hexadecylamine [120]. Ligand capping strategy exploits the physical interaction between hydrophobic ligand from Qdots and hydrophobic part of an amphiphilic polymer. After the first successful case of coating amphiphilic polymers on Qdots by Dubertret et al [121], many others have explored this approach to coat Qdots with small organic molecule and non-degradable polymers. Although there have been extensive researches on biodegradable amphiphilic block copolymers [122], however, very few studies have reported coating Qdots with these polymers via physical interactions due to their weak binding. Stabilization of the coating layer has been proved by crosslinking the coating polymers. Various crosslinking methods have been introduced to stabilize the polymer layer, such as lysine or diamine for polymers with abundant carboxylic group, and free radical crosslinking for polymers with abundant double bond [79].

Currently, most studies have focused on non-degradable amphiphilic polymers. Nevertheless, those work provided general protocols for coating biodegradable polymers on Qdots via ligand capping. Pellegrino et al. [123] have reported a general route to coat various Qdots with poly (maleic anhydride alt-1-tetradecene) via ligand capping, and further crosslinked the layer with bis (6-aminohexyl) amine. Gao et al. [69] reported that CdSe/ZnS was coated with triblock copolymer consisting of polybutylacrylate segment, polyethylacrylate segment, and polymethacrylic acid segment. Polymer layer was further crosslinked by peptide. This polymer coated Qdots showed great potential in cancer imaging. These reports can serve as standard approaches for any –COOH containing biodegradable amphiphilic polymers, such as PEG/PLGA, and PEG/Poly (aspartic acid).

1.5.3.2 Qdots-embedded Biodegradable Polymers

A number of studies have attempted to embed Qdots into polymers such as polymeric nano/microparticles, micelles. Similar to organic dye incorporation, techniques of incorporating Qdots in polymers can be divided into two methods: chemical bonding, and physical encapsulation.

To chemically bond Qdots with biodegradable polymers, functional groups should be introduced on Qdots first, which can be achieved with either ligand exchange or ligand capping strategies. Different from organic dyes, Qdots can be chemically bonded into polymer colloids during the polymerization. Various polymers can be synthesized and form particles via emulsion and dispersion polymerization. Many studies successfully demonstrated the incorporation Qdots into polymer colloids [124]. During the process, Qdots are required to be dissolved in oil droplets. In other word, there is no need for surface modification of Qdots to make them hydrophilic. However, polymers that are applicable for emulsion polymerization are normally non-degradable. Interestingly, a biodegradable polyurethane nanoparticle was fabricated via miniemulsion techniques by Cramail et al [125]. Although no further research has been

conducted on these polyurethane nanoparticles, it represents a new way of synthesizing biodegradable polymer colloids in the presence of Qdots.

Although conjugating Qdots onto the surface of polymer spheres has been rarely reported, Yeh et al. [126] reported a Qdots conjugated PLGA nanoparticles as a potential candidate for gene delivery. By conjugating nuclear localization signal (NLS) on the surface of nanoparticles, HeLa cells exhibit fluorescence at the nuclei region after incubating with the NLS-nanoparticles. However, Qdots are normally encapsulated inside the polymer sphere due to their relatively poor stability and potential cellular toxicity. Like organic dyes, Qdots can be encapsulated into biodegradable polymeric colloids via different fabrication techniques. Desai et al. [127] encapsulated CdSe/Zns into PLGA nanoparticles via nanoprecipitation. Kim et al. [128] encapsulated CdTe/CdSe into PLGA nanoparticles via a double emulsion technique. The Qdots loaded nanoparticles have a similar value of quantum yields to the bare Qdots (52%), and the emission wavelength remained the same (760nm). Another group also reported the encapsulation of protein-conjugated Qdots into PLGA via double emulsion technique [129]. The carboxylic groups on the polymers were conjugated with Herceptin, a monoclonal antibody that targets ErbB2 cell membrane receptors. Specific targeting to ErbB2-positive SKBR3 breast tumor cells and intracellular controlled release of quantum dots was achieved. As we discussed above, amphiphilic copolymers have been intensively studied for the surface modification of Qdots. Due to the ability to self-assemble into micelles, those copolymers have been used for encapsulation of Qdots. Due to the hydrophobic core/hydrophilic shell structure of micelles, Qdots can be distributed within the hydrophobic core. Cao et al. [130] reported a PbS loaded N-succinyl-N'-octyl chitosan micelles for targeted imaging of liver cancer. The emission wavelength of PbS loaded micelles presents a red shift (800nm to 870nm) due to the stabilization and energy transfer of Qdots. The unnoticeable toxicity both *in vitro* and *in vivo* implied that low leakage of QDs from the micelle. However, the long term toxicity of the micelle need to be further studied. After 12h of intravenously injection, micelle has been found to

accumulate at tumor site via enhanced permeability and retention (EPR) effect. The strong fluorescence can be observed up to 96h. Liu et al. loaded hydrophilic CdSe/ZnS into PLA-b-poly (2-metharcyloyloxyethylphosphorylcholine) (PLA-b-PMPC). TEM imaging indicated that most of the Qdots were located in the core of nanoparticles.

Stimulus-responsive polymers have also been used to load Qdos. The external stimulus can trigger the conformation change of those polymers. Most notable stimulus-responsive polymers are pH or temperature sensitive ones. The mechanism of loading Qdots in such polymers is an expansion-uptake/shrink-entrap process. Xu et al. [131] reported a pH-sensitive copolymer of N-isopropylacrylamide and 4-vinylpyridine (PNIPVP), and the loading of CdTe into the PNIPVP nanoparticles. Qdots were loaded during expansion of PNIPVP nanoparticle under pH 3, and entrapped within the particles at pH 3-10. Eventually, the Qdots can be released when pH>11. Poly (N-isopropylacrylamide) (PNIPAM) also proved to be thermo-sensitive. When the temperature is below lower critical solution temperature (LCST), PNIPAM microparticles expand. Therefore, they are able to entrap Qdots, when temperature is higher than LCST. However, the release of Qdots remains a problem when the temperature is lowered below LCST. Gong et al. [132] loaded CdTe into PNIPAM microparticles, and exploited the hydrogen bonding between surface ligands from CdTe and amide groups from PNIPAM to stabilize the loaded Qdots. Although PNIPAM and its copolymers are not biodegradable, these studies serve as good references for Qdots embedding in various biodegradable pH or thermo-sensitive polymers. A number of polypeptides with pendant ionizable groups present pH-sensitive property, such as poly (aspartic acid), poly (glutamic acid), poly arginine, poly histidine, poly lysine, and their copolymers [118]. Meanwhile, many PNIPAM based polymers have been proved to be biodegradable. Biodegradable PNIPAM-b-PLA has been synthesized by ring-opening polymerization of lactide initiated by PNIPAM-OH [133]. Similar approach has been used to prepare PNIPAM-b-poly (glutamic acid), and PNIPAM-b-Poly (L-lysine) [118]. Radical polymerization techniques, including Reversible Addition-Fragmentation chain Transfer

(RAFT), and Atom transfer radical polymerization (ATRP), have been used to prepare PNIPAM-based copolymers, such as PNIPAM-poly (3-hydroxybutyrate)-PNIPAM triblock copolymer [118]. All these polymers could potentially be used for Qdots embedding.

1.5.4 Green Fluorescent Proteins

In 1956, Shimomura et al discovered green fluorescence from Aequorea jellyfish as a companion protein to aequorin. Since then, this green fluorescent protein (GFP) has become one of the most useful biological tool in the past decade [134, 135]. The primary structure of Aequorea GFP was deduced from the cDNA sequence. Aequorea GFP is a protein of 238 amino acids with a molecular weight of 27 or 30 kDa. The chromophore of GFP is formed from the primary amino acid sequence, residues 65-67, which are Ser-Tyr-Gly (Figure 1.3a). After conformational folding and a series of reactions, including cyclization, dehydration, and oxidation, the chromophore, (*p*-hydroxybenzylidene)-5-imidazolinone is formed. This structure has later been confirmed by two-dimensional NMR and the cDNA sequence [134]. To fulfill the requirements for various applications, tremendous effort have been placed on preparing yellow and red fluorescent proteins. The GFP variants can be classified by different emission colors, from cyan (475nm) up to far-red (649nm) [72]. Shaner et al. [70, 72] have made significant contributions to the family of GFP, such as the only bright and photostable far-red FP, mPlum, superior photostable red FP, mCherry, brightest orange FP, mOrange, yellow FP, mCitrine, brightest cyan FP, Cerulean, and the UV-excitable GFP, T-Sapphire (Figure 1.3b).
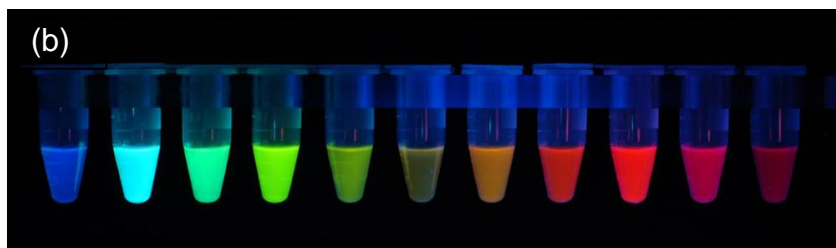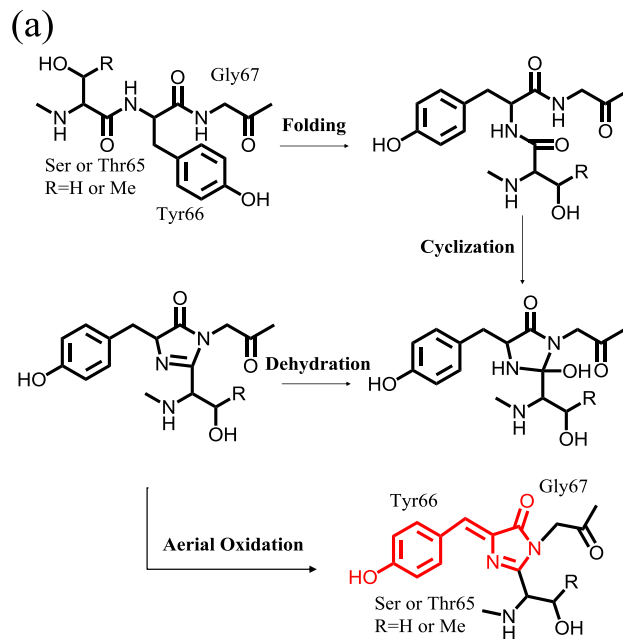
Figure 1.3 Green Fluorescent Proteins for biomedical applications (a) The formation and final chemical structure of the fluorophore of GFP. (b) Different color from various fluorescent proteins

The most important advantage of GFP is that it can be genetically encoded into protein and expressed in living cells and organisms [136]. Due to this distinct benefit, GFP has been extensively used as an intrinsic intracellular indicator of a specific protein, other than an imaging probe for many drug/gene delivery systems. There are rarely any reports on combining GFP with biodegradable polymers. The criteria on how to choose a fluorescent protein and specific application of GFP has been summarized elsewhere [70]. GFP has been exploited as pH sensitive and redox sensitive indicator for dynamic intracellular activity. Based on the variety of fluorescent protein, there are many chances of crosstalk in excitation and emission channels

from two fluorescent proteins, which confers great opportunity for fluorescence resonance energy transfer (FRET) on pair of fluorescent proteins [137]. The FRET effect of fluorescent proteins has been exploited for studying protease action and Ca^{2+} sensitivity [138].

1.6 Specific Aims

In the present work, we aim to address the aforementioned challenges by developing citric acid based functional biomaterials. The governing hypotheses are: 1) Citric acid can be used as a versatile multifunctional monomer to produce biodegradable polymers with low cytotoxicity, good processability. 2) Introduction of maleic acid and urethane doping into polymers confer multiple ways to manipulate the mechanical property to cover a wide range. 3) Incorporation of amino acid brings inherent fluorescent property to BPLP, therefore reducing the need of complex conjugation or encapsulation with other fluorescent materials. 4) The abundance of functional group for modification and the excellent processability of BPLPs make them appealing for various applications. 5) BPLP with urethane doping can achieve strong and elastic fluorescent materials.

The Impacts of this work lie in that: 1) Developing a family of biodegradable polymers with tunable mechanical properties may address the issue of scaffold/tissue mechanical mismatch in soft tissue engineering; 2) unveiling the intriguing fluorescence mechanism and the design strategies for the syntheses of biodegradable photoluminescent polymers will significantly advance fluorescent biomaterials science; and 3) the development of BPLPs and Urethane doped BPLPs can potentially bring a paradigm shift in the use of biodegradable implant biomaterials in a broad range of biological and biomedical fields including biosensing, cellular imaging, drug delivery, tissue engineering, and theranostic nanomedicine.

To achieve these goals, we propose the following specific aims:

1) Syntheses and characterization of crosslinked urethane doped poly poly (octamethylene maleate citrate) (CUPOMC) with enhanced processability and tunablemechanical properties for soft tissue engineering.

2) Syntheses and characterization a family of biodegradable photoluminescent polymers (BPLPs) and their applications for tissue engineering, drug delivery, and bioimaging.

3) Development of BPLPs under controlled syntheses and unveiling the intriguing fluorescence mechanism of BPLPs.

4) Development of super strong and elastomeric urethane doped BPLPs (UBPLPs) and their application for blood vessel tissue engineering.

.

CHAPTER 2

DUAL-CROSSLINKABLE URETHANE DOPED POLYESTER

2.1 Introduction

Finding an ideal biomaterial is one of the major goals in the field of tissue engineering. Many of the native tissues in the human body have elastomeric properties. Thus, the biomaterials selected to repair these tissues should have similar elastic properties in order to sustain and recover from multiple deformations without causing irritation to the surrounding tissues [9]. It has been proven that mechanical stimuli can enhance cellular growth, alignment, and extracellular matrix production. Previous research has also shown that the appropriate mechanical constraints can help yield both fibril alignment and the geometry of a native heart valve [139, 140]. Moreover, the addition of mechanical stimuli has also been shown to have an influence on the stem cell differentiation [141, 142]. Mechanical mismatch between host blood vessels and vascular grafts may contribute to the development of myointimal hyperplasia, a major reason for graft failure [143]. Therefore, a suitable biomaterial for soft tissue engineering should have the appropriate mechanical properties similar to the target tissue, and be capable of transmitting mechanical stimulus to the seeded cells.

Recently, many researchers have focused their work on the development of biodegradable polyester and polyurethane elastomers for soft tissue engineering. Biodegradable polyurethanes (BPUs) are a family of elastomers, which have been used in a wide variety of biomedical applications due to their good mechanical properties (up to 29 MPa tensile strength) and elasticity (up to 895% elongation) [34, 144-147]. However, due to their aliphatic nature BPUs are susceptible to permanent creep under cyclic mechanical loading. Therefore, the potential long-term success of polyurethanes as scaffold materials for dynamic tissues like blood vessels and ligament is still questionable [12].

36

Elastomeric polyesters are another family of polymers that have attracted interest due to the appropriate biodegradability, biocompatibility, and elasticity for various biomedical applications [8, 52]. Thereof, crosslinked polyester elastomers have attracted much attention recently due to their excellent elasticity without permanent deformation under cyclic deformation such as poly (glycerol sebacate) (PGS) and poly(octamethylene citrate) (POC) [9, 50, 51, 148]. PGS and POC have shown excellent biocompatibility in vitro and in vivo. The crosslinking nature of PGS and POC also confer excellent elasticity to these polymers. However, the mechanical strength of PGS and POC are still relatively weak which range from 0.5±0.2 MPa to 2.9±0.1 MPa, especially when they are made into porous scaffolds. The reported tensile mechanical strength of POC porous scaffolds are only 0.3±0.1 MPa [143]. The processability of PGS and POC is also limited with only a salt-leaching method reported for this type of polymer. A commonly used thermally induced phase separation (TIPS) or freeze-drying method for scaffold fabrication cannot be applied to these polymers due to the sticky nature of their low molecular weight pre-polymers, which are the only processable forms for these polymers.

To improve the mechanical properties of POC but retain the excellent elasticity, we have recently reported a crosslinked urethane-doped polyester (CUPE) elastomer. 1,6-hexamethylene diisocyanate (HDI) is used to extend the POC pre-polymer chains to obtain a pre-CUPE polymer. Pre-CUPE can be further thermally crosslinked into a urethane-doped polyesters (CUPE) elastomeric network. The tensile strength of CUPE was as high as 41.07±6.85 MPa with corresponding elongation at break of 222.66±27.84% [12].

Given that there has been great interest in using photopolymerization techniques for various biomedical applications such as 3-dimensional (3-D) tissue construction and cell entrapment [149-151], an in situ crosslinkable biodegradable polyester network which was referred to as poly(octamethylene maleate citrate) (POMC) has been recently synthesized based on POC. Unsaturated maleic acid is reacted with citric acid and 1,8-octanediol to form a photocrosslinkable POMC pre-polymer (pre-POMC). However, similar to POC in addition to the

37

photocrosslinkability, POMC is still relatively weak and the processability of pre-POMC is still limited due to its low molecular weight.

Aiming at synthesizing a biodegradable elastomer with photocrosslinkability and excellent processability, we have synthesized and characterized a new family of polymers, crosslinked urethane-doped poly (octamethylene maleate citrate) (CUPOMC), in the present study. The rationale behind this polymer is: (1) the major chemical structure of CUPOMC is composed of urethane and ester bonds that have been used in many biodegradable polymer designs [8, 34]. (2) The presence of vinyl groups makes it possible for free radical polymerization such as photocrosslinking. (3) The unused pendant functional groups (-COOH and –OH) after free radical polymerization can be used for post polymerization through polycondensation or for bioconjugation [50]. (4) The urethane-doped structure should result in a material with strong mechanical properties similar to CUPE [12]. In addition, controlling the feeding ratio of the different monomers should create a material with tunable the mechanical properties and degradation rates. In this work, we describe the synthesis, characterization and cytocompatibility of the CUPOMCs. Porous scaffolds are also fabricated using a thermally induced phase separation (TIPS) method to demonstrate the processability and potential of CUPOMC in soft tissue engineering applications.

2.2 Experimental

2.2.1 Polymer Synthesis

The synthesis of the CUPOMCs was carried out in following steps. The synthesis schematic is shown in Figure 2.1. Briefly, 0.11 mole of 1,8-octanediol, 0.8 mole of maleic acid, and 0.2 mole of citric acid were melted in a round bottom reaction flask under 160°C. Once all the monomers had been melted, the temperature was reduced to 140°C, and the mixture was bulk polymerized through polycondensation for 4h to obtain the POMC prepolymer. The prepolymer was purified by drop wise precipitation in deionized water. After purification, the prepolymer was then lyophilized. The molecular weight of the POMC prepolymer was

characterized by Matrix assisted laser desorption/ionization mass spectroscopy (MALDI-MS) as 680 Da. 0.02 mole of POMC prepolymer was dissolved in 1,4-dioxane to obtain a 3% W/V solution. Next, 0.02 mole of 1,6-hexamethylene diisocyanate (HDI) was added into reaction system to synthesize pre-CUPOMC. The reaction was carried out under constant stirring with stannous octoate as a catalyst (0.1% wt). The reaction temperature was maintained at 55°C. A small amount of reaction solution was taken out and checked by Fourier transform infrared (FT-IR) after 48h. The reaction was terminated when the isocyanate peak at 2267cm-1 disappeared.
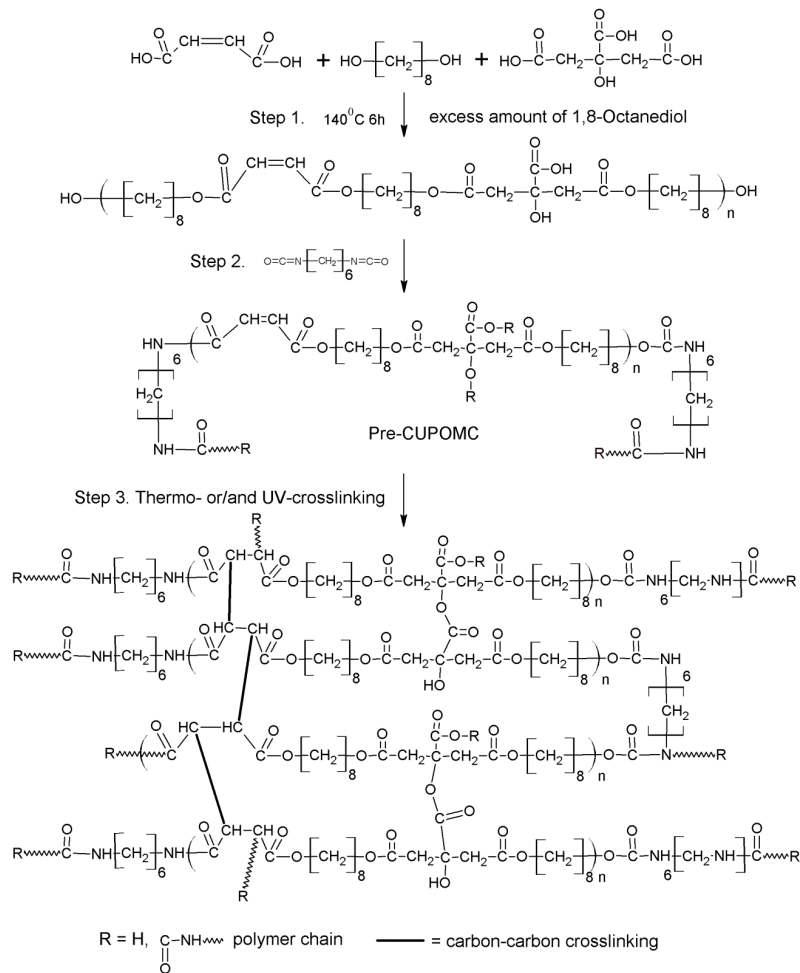
Figure 2.1 Synthesis schematic of CUPOMC polymers

To obtain a thermo-crosslinked polymer, the pre-CUPOMC polymer solution was cast into a Teflon mold and dried in a chemical hood equipped with laminar airflow to evaporate all

39

the solvent. The resulting thermo-CUPOMC film was placed into an oven under 80°C for predetermined time periods.

The free radical reaction was carried out by UV-crosslinking. Briefly, the pre-CUPOMC solution was mixed with 0.3% w/v Irgacure 784, which was used as the photoinitiator. Then the polymer solution was casted into a Teflon mold and placed under UV light for predetermined time period to synthesize photo-CUPOMC.

Polymers with different feeding ratios of 1,8-octanediol, citric acid, and HDI were synthesized using the same steps. Different CUPOMCs were abbreviated as follows: CUPOMC-ratio of citric acid-maleic acid-1,8-octanediol-HDI (ex. CUPOMC-0.2-0.8-1.1-1.0). The prepolymer of CUPOMCs was abbreviated as Pre-CUPOMC. In our following study, CUPOMC represents thermo-CUPOMC unless otherwise specified.

2.2.2 Mechanical Test

The mechanical tests of different Pre-CUPOMC and CUPOMC films were conducted on an MTS Insight 2 machine equipped with a 500N load cell. The testing samples were cut into a dog bone shape samples, as per ASTM D412a (25 x 6 x 0.5 mm, length x width x thickness). The testing sample was pulled at a rate of 500 mm/min and elongated to failure. The initial modulus was calculated from the initial slope. 8-10 samples were measured and averaged.

2.2.3 In Vitro Degradation Study

For the in vitro degradation study, the polymer films were cut into disk-shaped specimens 7mm in diameter and 0.5mm in thickness. The degradation studies were conducted in both phosphate buffer saline (PBS, pH 7.4) and 0.05M NaOH solutions. To rapidly obtain relative degradation rates, each specimen was placed in a clean glass tube containing 10ml NaOH solution, and then incubated under 37°C for predetermined time points. At each time point, the samples were washed three times with deionized water and lyophilized. The mass loss was calculated by comparing the initial mass (W_0) with the mass measured after lyophilized (M_t), as shown in equation:

$$Mass\ loss\ (\%) = \frac{W0 - Wt}{W0} \times 100$$

The final result was obtained from the average value of six individual samples.

2.2.4 Toxicity Test of Degradation Products

NIH 3T3 fibroblasts (3T3) were cultured in a 50 mL culture flask with Dulbecco's modified eagle's medium (DMEM) supplemented with 5% fetal bovine serum. Cell culture was maintained in a water-jacket incubator equilibrated with 5% CO_2 and 95% humidity at 37 °C. After confluence of cell proliferation, the cells were trypsinized, centrifuged, and suspended in culture media before seeding. According a method described previously [152], the cytotoxicity of the CUPOMC degradation products was carried out by completely degrading the materials and exposing the degraded product solution to the cultured cells. Polymers were hydrolytically degraded in accelerated conditions. The difference between CUPOMC and CUPE with 2 d oven crosslinking was compared. Poly (D,L-lactide-co-glycolide) (PLGA 75/25) was used as control. All polymers were placed in 50ml 1N NaOH solution and incubated under 37 °C. The polymers took 24 h to be completely degraded. The solution was then filtered through a cellulose acetate membrane filter (0.2 μm pore diameter). The pH was adjusted to 7.4 with 1N HCl. The solution was filtered again for sterilization and then diluted by 2, 10, 50 and 100 times with culture media. Then the solutions with culture media were added to the cultured cells in 96 well plates (100 μl/well) and incubated at 37 °C and 5% CO2 for 24h. After incubation, cell viability was testified using methylthiazole tetrazolium (MTT) assay. Six samples were tested for each polymer.

2.2.5 In Vitro Cell Proliferation

Both CUPOMC and CUPE films were oven-crosslinked for 2 d and cut into discs with a diameter of 6 mm. PLGA films were selected as a control. All the samples were sterilized by incubation in 70% v/v ethanol for 15 min followed by UV light exposure for 1 h. 3T3's were seeded on the films at a density of $2.0\text{x}10^5$ cells/ml in a 96-well plate. After 1 h pre-incubation, 200 μL of culture media was added into each well. After incubation for predetermined time

points, the cell viability on each sample was testified using MTT assay. The result was obtained from average value of six samples. The morphology of 3T3 on the CUPOMC films was observed directly under microscopy.

2.2.6 Scaffold Fabrication

The CUPOMCs were fabricated into porous scaffolds by a thermally induced phase separation (TIPS) method as described previously [153]. Briefly, a 3% w/v pre-CUPOMC solution in 1,4-dioxane was frozen under -80°C for 2h and then freeze-dried to obtain a porous scaffold. The morphology of the TIPS scaffold was observed by scanning electron microscope (SEM).

2.2.7 Statistical Method

Data were expressed as the mean ± standard deviation. The statistical significance between two sets of data was calculated using a One-way ANOVA. Data were considered to have significant difference, when a p-value of 0.05 or less was obtained.

<u>2.3 Results and Discussion</u>

The FT-IR spectra of pre-CUPOMC-0.8-1.1-1.0, pre-POMC, and pre-CUPE were compared in Figure 2.2. All the three polymers had a sharp peak at $1730cm^{-1}$, which was assigned to the carbonyl group (C=O). Amide I at $1670cm^{-1}$ and amide II at $1560cm^{-1}$ vibrations were found on the spectra of pre-CUPOMC and pre-CUPE, which indicates the successful doping of urethane [12]. The characteristic peak of the double bond at $1647cm^{-1}$ was overlapped by the amide I peak. However, the peak of trans-double bond at $980cm^{-1}$ could be observed from the spectra of the pre-POMC and pre-CUPOMC. These results indicated that the double bond was maintained after the chain extension reaction. It also demonstrated that during the synthesis of pre-POMC, the cis- structure of double bond from maleic acid had turned into trans- structure.
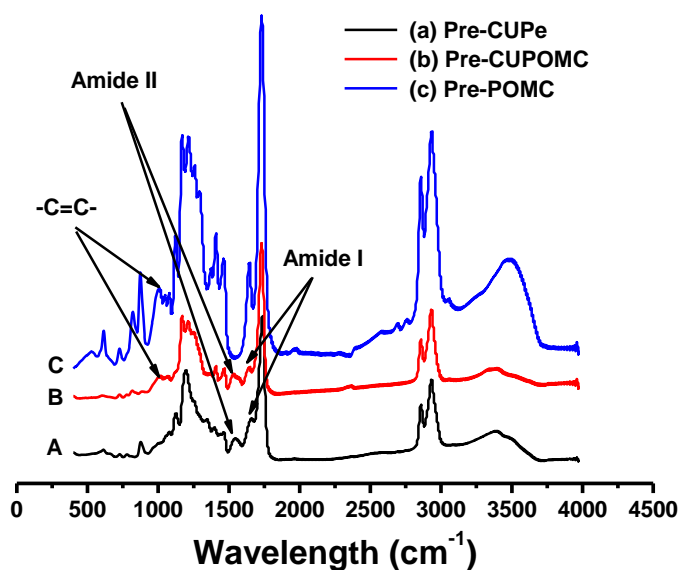
Figure 2.2 FT-IR spectra of representative prepolymers.
(a) Pre-CUPe; (b) Pre-CUPOMC; (c) Pre-POMC.

The mechanical properties of different polymers were compared through tensile tests. To evaluate the impact of the HDI ratio, mechanical tests were performed on prepolymers of CUPOMC-0.2-0.8-1.1-0.5, CUPOMC-0.2-0.8-1.1-1.0 and CUPOMC-0.2-0.8-1.1-1.5. The results are shown in Figure 2.3A and B. With the increase of the HDI, the tensile strength and initial modulus ranged from 0.94±0.08 and 5.60±0.48 respectively. Compared with POMC, the tensile strength of which is lower than 1MPa [154], the presence of the urethane bond dramatically increased the tensile strength of the materials. The materials' elongation ranged from 181.92±10.64% and 295.85±30.06, which covers the elongation of native arteries and veins (~260%).

CUPOMC-0.2-0.8-1.1-1.5 was selected to analyze the impact of different thermo-crosslinking times on the material mechanical properties. From Figure 2.3C, it showed an increasing trend with the increasing thermo-crosslinking times from 0 day to two days. Since

there was only 0.2 molar ratio of citric acid in the polymer, there was no significant difference for the tensile strength and initial modulus after two-day thermo-crosslinking suggesting the crosslinking reactions were completed within two days. The elongation of the polymers remained similar after one-day crosslinking (Figure 2.3D).

CUPOMC-0.2-0.8-1.1-0.5 was UV-crosslinked with Irgacure 784 for 20 and 30min. As shown in Figure 2.3E and F, the polymer crosslinked for 20 min under UV irradiation was almost three times as strong as the original pre-polymer. However, the additional UV-crosslinking times seemed to not change the mechanical properties significantly. Since UV-crosslinking only consumed vinyl groups from the polymer chain, the functional groups on the pendent chain can be saved for thermo-polymerization or further chemical modification. The UV-crosslinking is a much milder polymer processing method than the thermo-crosslinking providing advantages when thermo-sensitive biomolecules have to be incorporated or conjugated to the polymers.
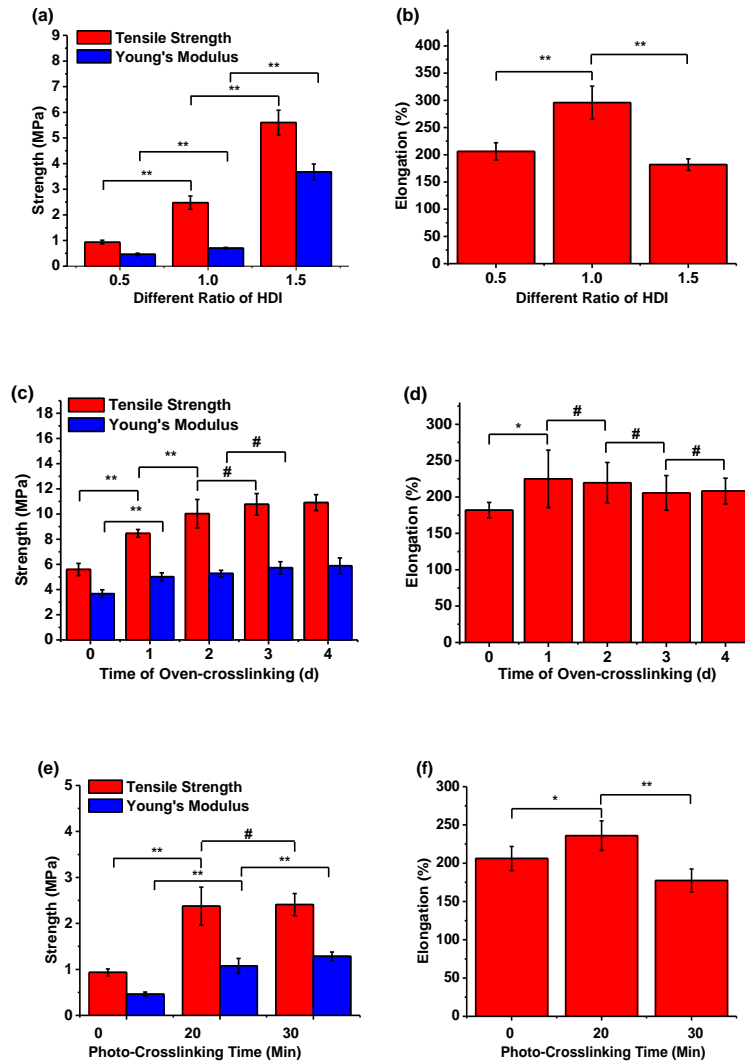
Fig. 2.3 Different impacts influencing the mechanical property of CUPOMCs. (a) Tensile strength and Young's Modulus, and (b) Elongation of Pre-CUPOMC-0.2-0.8-1.1 synthesized with various molar ratio of HDI, 0.5, 1.0, and 1.5. (c) Tensile strength and Young's Modulus, and (d) Elongation of CUPOMC-0.2-0.8-1.1-1.5 with different thermo-crosslinking time, from 1d to 4d, and its prepolymer. (e) Tensile strength and Young's Modulus, and (f) Elongation of CUPOMC-0.2-0.8-1.1-0.5 with different UV-crosslinking time and its prepolymer. **$p<0.01$, *$p<0.05$, #$p>0.05$; N=8.

The mechanical properties of the selected biodegradable elastomers and soft tissues were listed in Table 2.1. The tensile strength of pre-CUPOMC and CUPOMCs under the known synthesis conditions ranged from 0.73±0.12 and 10.91±0.63MPa (Figure 2.3A and C), which

45

are similar to POC and much stronger than PGS and POMC. Importantly, the elongation range of pre-CUPOMC and CUPOMCs covered all the selected polymers and the soft tissues in Table 2.1. These results indicated that doping urethane bonds in POMCs created strong CUPOMCs without losing the elasticity. It should be noted that even the tensile strength of pre-CUPOMCs synthesized under the known conditions ranged from 0.73 ± 0.12 and 5.60 ± 0.48. This is very different from the other published pre-POC, pre-PGS and pre-POMC polymers which could not even be tested for their tensile mechanical properties due to their sticky nature. In other words, pre-CUPOMCs can be used as implant materials for various applications without even a further post-polymerization (thermo- or photo-). The tunable mechanical properties of CUPOMCs suggested that CUPOMCs may be viable candidate materials for soft tissue engineering applications.

Table 2.1 Mechanical properties of selected biodegradable elastomers and soft tissues

Tissue/Polymer	Tensile Strength (MPa)	Young's Modulus (MPa)	Elongation (%)	Reference
Human Bladder	0.27±0.14	0.25±0.18	0.69±0.17	[24]
Smooth muscle relaxed	N/A	0.006	300	[25]
Smooth muscle contracted	N/A	0.01	300	[25]
Aortic valve leaflet (circumferential)	N/A	15±6	21±12	[26]
Ulnar cadaveric peripheral nerve	9.8 – 21.6	N/A	8 – 21	[27]
Medial cadaveric peripheral nerve	9.8 – 30.4	N/A	6 – 22	[27]
Cerebral artery	N/A	15.7	50	[28]
Cerebral vein	N/A	6.85	83	[28]
Poly (octanediol-citrate)	~ 5.80±0.76	6.44±0.28	367±15	[51]
Poly (glycerol sebacate)	>0.5	0.282±0.025	>267	[9]
PLGA	41.4 – 55.2	1.4 – 2.8	3 - 10	[155]
Caprolactone soft segment polyurethane	1.5	3.7	60	[156]

The degradation rates of pre-CUPOMCs could be varied by changing the feeding ratio of monomers. As shown in Figure 2.4A, pre-CUPOMC-0.2-0.8-1.1-1.0 polymers were fully degraded after 14 weeks of incubation in PBS. Increasing the HDI ratio and decreasing the diol

ratio resulted in slower degradation rates (Figure 2.4B and C). This was explained that increasing the HDI ratio and decreasing the diol ratio could both increase more hydrolysis-resistant urethane and amides bonds than ester bonds, which were in agreement with previous findings on POC and CUPE [12, 50, 51]. Compared to the long degradation times for some polyesters (18-60 months for PLLA and 24 months for PCL), the 14-week in vitro degradation time period for pre-CUPOMC can potentially be more suitable for tissue engineering. Normally, polyurethanes undergo even longer degradation times [17]. The degradation study in base solution also provided strong evidence that the degradation rate of CUPOMCs could be controllable in vivo.
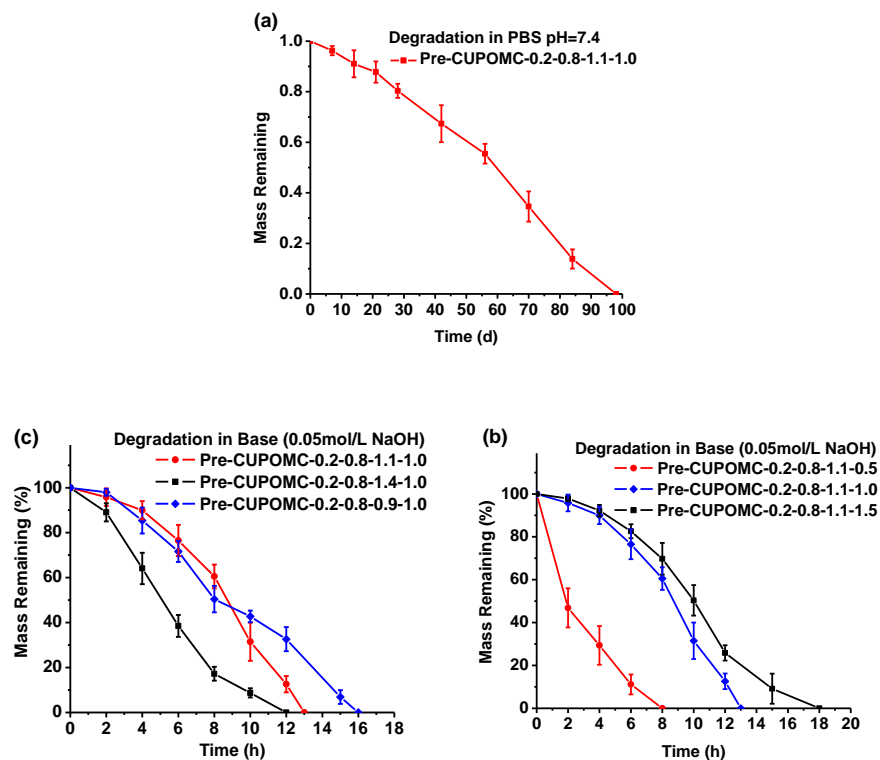
Fig. 2.4 (a) In vitro degradation of Pre-CUPOMC-0.2-0.8-1.1-1.0 in PBS (b) In vitro degradation of Pre-CUPOMC with different ratio of HDI in NaOH (c) In vitro degradation of Pre-CUPOMC with different ratio of 1,8-Octanediol in NaOH

The cell morphology of 3T3s on pre-CUPOMC-0.2-0.8-1.1-1.0 films are shown in Figure 2.5A and B with different magnifications. It was observed that 3T3 fibroblasts had a stretched morphology on Pre-CUPOMC-0.2-0.8-1.1-1.0 films, which indicates that this polymer supported 3T3 fibroblast adhesion.
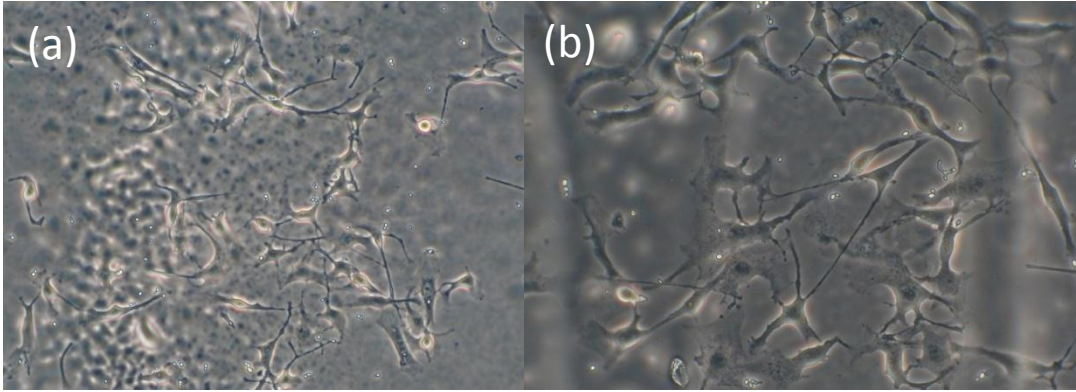
Fig. 2.5 Images of fibroblast on the Pre-CUPOMC-0.2-0.8-1.1-1.0 film under microscopy with 20X (a) and 32X (b) magnification.

To study the cytotoxicity of the CUPOMC degradation products, the maximum release of degradation products was achieved by an accelerated degradation in strong base solution [152]. The degradation solution of the polymers was then incubated with 3T3 fibroblasts. All the values of absorbance were normalized to the PLGA at 100x dilution. The results are shown in Figure 2.6A. The viability of 3T3s cultured in the presence of the CUPOMC degradation products was 1.80±0.07%, 5.66±0.66%, 40.53±4.63%, and 81.96±11.23% for 2×, 10×, 50×, and 100× dilutions, respectively. The results indicated that CUPOMC had a dose-dependent cytotoxic effect. CUPOMC degradation products produced similar or slightly higher cytotoxicity compared to the PLGA degradation products at 100× dilution.

The cytocompatibility of CUPOMC was evaluated by cell adhesion and proliferation on CUPOMC-0.2-0.8-1.1-1.0 films. From the MTT assay results (Figure 2.6B), PLGA had a higher cell adhesion than both CUPe and CUPOMC during the initial phase of cell adhesion and proliferation. After 3 days cell culture, there was no significant difference in the cell number

between CUPOMC and PLGA. CUPOMC displayed higher cell viability than PLGA after 5 and 7 days cell culture, but CUPe was even higher. It was demonstrated that although the presence of double bond from maleic acid slightly affects the biocompatibility of the resulting polymer, CUPOMC still supported higher cell proliferation rates than PLGA. The cytotoxicity studies demonstrated that CUPOMCs have the potential to be used as cell delivery carrier such as in tissue engineering applications.
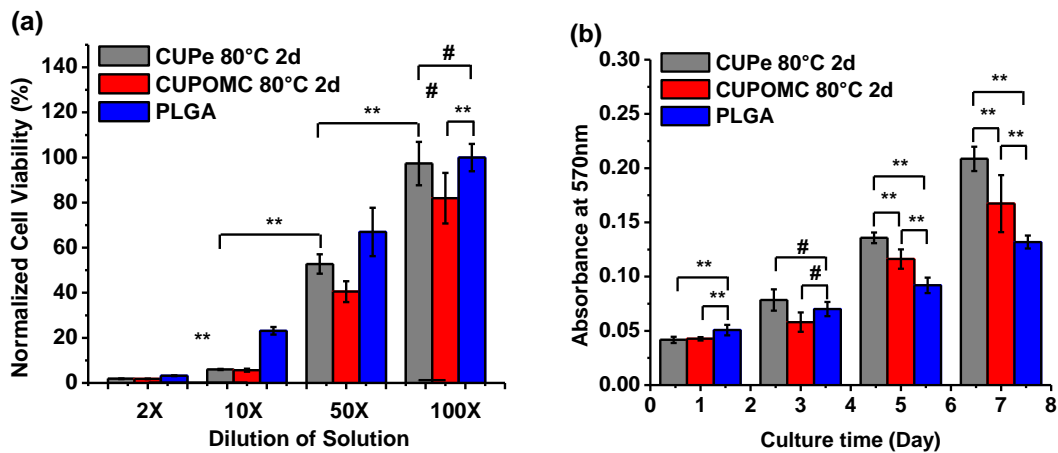
Fig. 2.6 In vitro cell proliferation evaluation (a) Cytotoxicity evaluation of degradation products of CUPOMC-0.2-0.8-1.1-1.0 with 2d thermo-crosslinking under 80°C at 2×, 10×, 50×, and 100× dilutions. (b) Cell viability and proliferation assay (MTT assay) for 3T3 fibroblasts cultured on CUPOMC-0.2-0.8-1.1-1.0 film with 2d thermo-crosslinking under 80°C. **$p < 0.01$, *$p < 0.05$, #$p > 0.05$; N=8.

As we have studied, pre-CUPOMC possessed excellent mechanical properties even without further crosslinking. We have also studied the processability of pre-CUPOMC by scaffold fabrication. The morphology of the TIPS scaffold fabricated from pre-CUPOMC-0.2-0.8-1.1-1.0 was observed on a Hitachi 3000 SEM. CUPOMC-0.2-0.8-1.1-1.0 TIPS scaffolds are shown in Figure 2.7. Pictures of both the surface and cross section were taken. Figure 2.7A and B shows that the TIPS fabrication technique could form a scaffold with a highly interconnected porous structure. The morphology of the scaffold was also observed after 1d thermo-

crosslinking. The porous structure was maintained in both the surface and cross section of the scaffold as shown in Figure 2.7C and D.
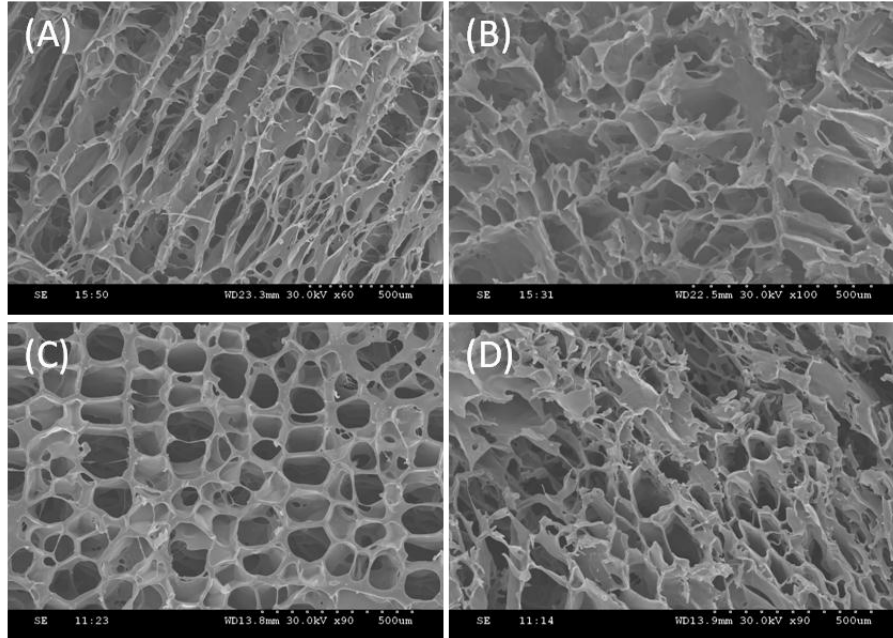
Figure 2.7 SEM images of the TIPS scaffold. Surface area (a) and cross section (b) for Pre-CUPOMC-0.2-0.8-1.1-1.0 prepolymer. Surface area (c) and cross section (d) for 80 °C1d CUPOMC-0.2 -0.8-1.1-1.0

2.4 Conclusion

We have developed a new family of polyester elastomers, poly (1,8- octamethylene maleate citrate) urethane (CUPOMCs). CUPOMCs possess tunable mechanical properties and degradation rate. CUPOMCs could be either thermo-crosslinkable and/or UV-crosslinkable providing flexibility to use these polymers in various applications. CUPOMC prepolymers exhibited excellent processability offering advantages over the previous developed biodegradable elastomers. Preliminary biocompatibility evaluation in vitro supported that CUPOMCs may be good candidate materials for cell delivery carriers. The development of CUPOMCs should expand the choices of available biodegradable elastomers for broad biomedical applications such as soft tissue engineering.

CHAPTER 3

BIODEGRADABLE PHOTOLUMINESCENT POLYMERS

3.1 Introduction

Biodegradable polymers have been central in biomaterial science for a wide variety of biomedical applications such as drug delivery, tissue engineering, and medical devices [8, 14, 157]. Owing to their chemical stability, sufficient functional groups, and fully body clearance, they have succeeded as a vehicle for therapeutic or diagnostic molecules [157, 158]. Fluorescent diagnostic dyes, such as quantum dots and small organic dyes, have been incorporated into biodegradable polymers, and utilized as biological imaging probes [159, 160]. These dyes require protection from *in vivo* circumstances due to their unstable physical or chemical properties. Biodegradable polymers are perfect candidates to protect the aforementioned fluorescent dyes in that they can provide not only increased biocompatibility and stability, but also sufficient functional groups for further modification. Unfortunately, the intrinsic toxicity from the heavy metal and aromatic structure still remains an issue, which substantially hinders the clinical use in patients. In addition, in many instances the polymer layer coating can also be a barrier blocking the fluorescence. In the search for a less toxic fluorescent material, green fluorescent protein has attracted increased interest due to its high fluorescence and alleviated toxicity [70, 161]. Green fluorescent proteins bring a beam of dawn light on the field, and have succeeded as many cell-biology tools. However, research has shown that these proteins are hard to manipulate, suffer from photobleaching, and are toxic at cell level [70, 78]. Recently, great effort has been made to create new fluorescent materials that are highly fluorescent, biocompatible, easy to process, and most importantly, fully biodegradable. However, the conventional fluorescent mechanism of many organic compounds is a conjugation system [84], which is normally based on an aromatic structure. By obeying the conventional rule

51

of a conjugation system [162], fluorescence seems to be an irreconcilable conflict with biodegradability as water and fire. Clearly, to achieve both fluorescence and biodegradability, simultaneously, remains the bottleneck in the development of the next generation of fluorescent materials.

In this section, we introduce a new philosophy of polymer design to solve the puzzle. A methodology of inherently fluorescent polymer design based on ester and amide bonds, both of which are biodegradable, is introduced with exciting results prompting the need for further understanding and application. Biodegradable photoluminescent polymers (BPLPs) are synthesized from three monomers, 1,8-octanediol, citric acid, and α-amino acids [52]. BPLP has shown complete degradation, and high fluorescence, which can be tuned by choice of amino acids, monomer feeding ratio, and even excitation. These unique properties make BPLP the first biodegradable polymer with inherent fluorescence circumventing the need for toxic dyes. The rationale behind the fluorescent polymer design are: 1) polymers with inherent fluorescence circumvent the use of toxic dyes, and are implantable with no need of modification; 2) using polycondensation reaction to form polymers with hydrolyzable bonds (ester and amide bond), which confers the fully biodegradability of the polymer; 3) Citric acid and essential amino acids are involved in many human metabolism and 1,8-octanediol has been used many other biomaterials. Those monomers promise the biocompatibility of polymer; 4) to increase the manufacturing potential, we chose to use inexpensive monomers and a cost-effective synthesis procedure performed under mild heating without the use of any catalysts; 5) functional monomers, such as PEG and Maleic acid, can fully or partially involved in synthesize to create water-soluble and photocrosslinkable fluorescent polymers.

The following sections will discuss the development of new family of biodegradable photoluminescent polymers (BPLPs), including water-soluble BPLP (wsBPLP), and photocrosslinkable BPLP (pcBPLP). The synthesis and characterization of all polymers will be discussed. The results show that BPLPs are a family of biodegradable and implantable

52

biomaterials with tunable fluorescence and low cytotoxicity. It has great potential for various applications from drug delivery to tissue engineering.

3.2 Experimental

3.2.1 Synthesis of BPLP pre-polymers

All chemicals were purchased from Sigma-aldrich (St. Louis, MO) and used as received, unless stated otherwise. All amino acids are L isomer unless stated otherwise. All BPLPs are named with the abbreviation of the amino acid. Polymer synthesis and characterization were conducted for BPLP-Cys as a representative BPLP, except where otherwise specified. BPLP-Cys pre-polymers were first synthesized by carrying out a controlled condensation reaction as described in Figure 3.1. Briefly, citric acid (CA), 1,8-octanediol (OD), and cysteine were added to a 250 mL three-necked round bottom flask fitted with an inlet and outlet adapter. Next, a flow of nitrogen gas was introduced into the flask, and the contents were melted at 160 °C while stirring at 360 rpm. The temperature of the system was subsequently lowered to 140 °C and allowed to react for 2 h to form the unpurified pre-polymer. Next, the pre-polymer was dissolved in 1,4-dioxane and purified by drop wise precipitation in deionized water to remove any of the unreacted monomers. The undissolved pre-polymer was collected and lyophilized in a Freezone 6 Freeze Dryer (Labconco, Kansas City, MO) to obtain the purified BPLP-Cys. The ratio of CA to OD was kept as 1: 1.1. Various BPLP-Cys were synthesized at different molar ratios of cys/CA 0.05, 0.2, 0.4, 0.6, and 0.8 to yield BPLP-Cys 0.05, BPLP-Cys 0.2, BPLP-Cys 0.4, BPLP-Cys 0.6, and BPLP-Cys 0.8. Each of the 20 essential amino acids was used to synthesize a family of BPLP-amino acid polymers.
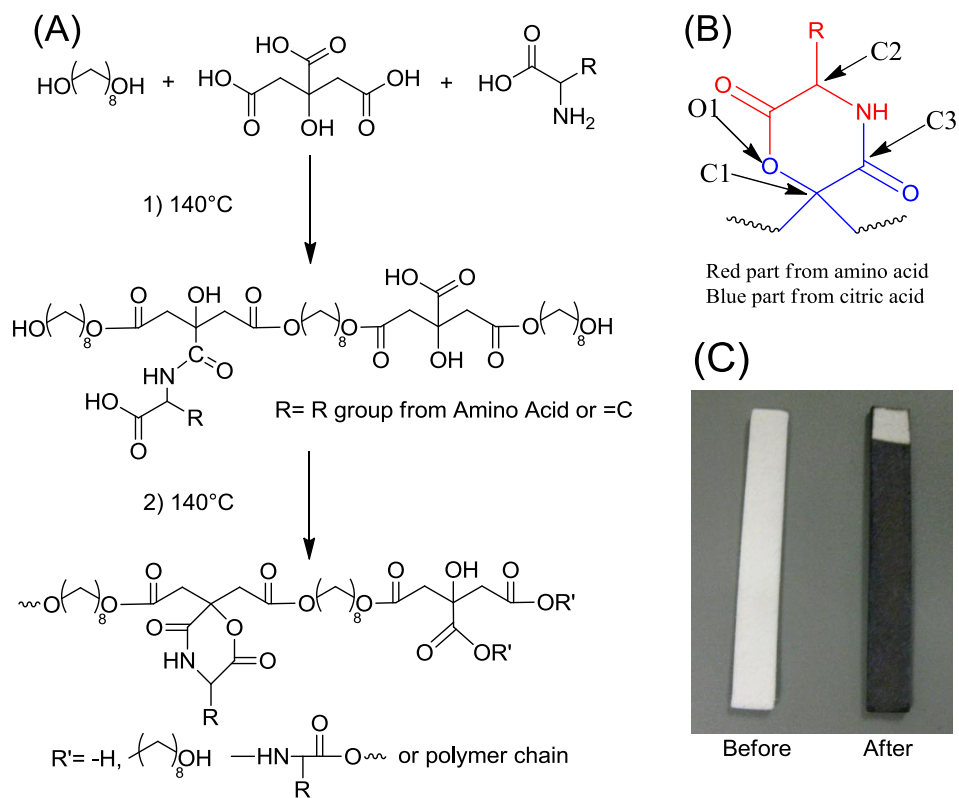
Figure 3.1 Synthesis of BPLPs (a) Synthesis schematic of BPLPs, (b) Chemical Structure of six-member ring, (c) Test stripe turning black shows the release of Hydrogen sulfide

Water soluble BPLP (wsBPLP) was synthesized by completely replacing OD with PEG (MW 200) (Figure 3.2A). Briefly, CA, PEG, and Cys were reacted together as previously described above. For purification, the prepared wsBPLP-Cys was dissolved in deionized water and dialyzed with a 500 Da molecular weight cutoff membrane for 2 days followed by lyophilization to achieve a purified pre-polymer. To synthesize photocrosslinkable BPLP (pcBPLP), CA was partially replaced by maleic acid (MA). Two ratios of MA to CA were used for synthesis as 8/2 and 6/4. The synthesis (Figure 3.2B) and purification were as same as BPLP-Cys.

54
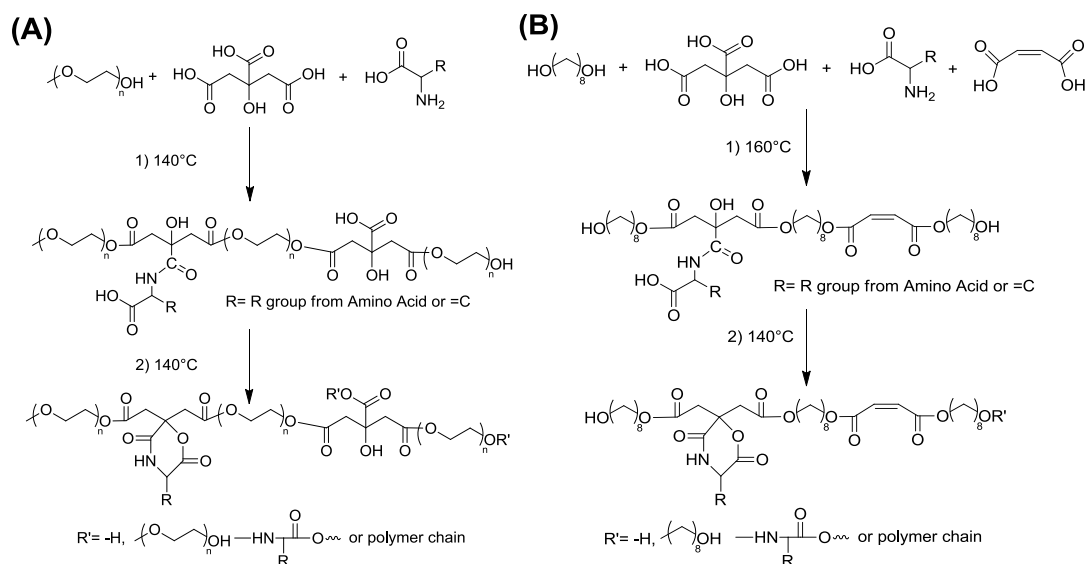
Figure 3.2 Synthesis schematic of (A) wsBPLPs and (B) pcBPLPs.

3.2.2 BPLP Fabrications

To evaluate the processability of BPLP and its potential for various biomedical applications, BPLP-Cys was fabricated into 2D dense film, 3D porous scaffold, and aqueous nanoparticle solution. To fabricate 2D dense films, purified BPLP-Cys was dissolved in 1,4-dioxane to obtain a 10% w/v solution. Next, solution was cast into a poly (tetrafluoroethylene) (PTFE) dish, and placed in chemical hood for 24 h to remove solvent. Polymers were cured in oven for desired time period to yield 2D dense films. To fabricate 3D porous scaffold, purified BPLP-Cys was dissolved in 1,4-dioxane to form a 30% w/v solution, followed by addition of sieved salt with desired size. The resulting slurry was cast into PTFE dish and placed in chemical hood for 24 h to evaporate solvent. The mixture was transferred into an 80 °C oven. The salt in the resulting composites was leached out by deionized water every 12 h for 96 h. The resulting porous sponge-like scaffold was lyophilized for 24 h and stored in desiccators. For nanoparticle preparation, 0.4 g of BPLP-Cys was dissolved in acetone (10 mL). The polymer solution was added dropwisely to deionized water (20 mL) under magnetic stirring (600 rpm).

55

The setup was left in chemical hood for 6 h in chemical hood to evaporate acetone. Desired concentration of nanoparticle solution can be achieved by evaporating water and dilution.

3.2.3 BPLPs Chemical Characterization

^{1}H NMR and ^{13}C NMR spectra for BPLP-Cys and BPLP-Ser were recorded on a JNM ECS 300 (JOEL, Tokyo, Japan) at 300 MHz. The pre-polymers were dissolved in dimethyl sulfoxide-d6 (DMSO-d6) (10 mg mL^{-1}). The chemical shifts in parts per million (ppm) were referenced relative to tetramethylsilane (TMS, 0.00 ppm) as the internal reference. The number average molecular weight (Mn) was determined by matrix assisted laser desorption/ionization mass spectroscopy (MALDI-MS) using an Autoflex MALDI Mass Spectrometer (Bruker Daltonics, Manning Park, MA). Fourier transform infrared (FT-IR) spectra were obtained using a Nicolet 6700 FT-IR spectrometer (Thermo Fisher Scientific, Waltham, MA) at room temperature. Pre-polymer samples were prepared by a solution casting technique. A dilute solution of the pre-polymer in anhydrous 1,4-dioxane (3% w/v) was smeared onto a potassium bromide (KBr) pellet and allowed to dry for 12 h in a vacuum hood before being tested.

3.2.4 Characterization of Crosslinked BPLPs

In this study, BPLPs prepolymers were thermo-crosslinked to yield an elastic polymer network. Briefly, BPLP-Cys pre-polymer was dissolved in 1,4-dioxane at 30% w/v. The solution was cast into a PTFE circular dish, and then placed in oven for thermo-crosslinking at 80 °C for 1, 2, 3, and 4 d. PcBPLP was photocrosslinked to form a gel. Briefly, pcBPLP was dissolved in dimethyl sulfoxide (DMSO) and mixed with photoinitiator (PI) 2-hydroxy-1-[4(hydroxyethoxy)phenyl]-2-methyl-1 propanone (Irgacure 2959) (1 wt. %). The solution was cast into a polypropylene microcentrifuge tubes, and exposed to a 365 nm long wave ultraviolet light (UVP, Upland, CA) at room temperature.

Tensile mechanical testing was conducted according to ASTM D412A on an MTS Insight 2 fitted with a 500 N load cell (MTS, Eden Prairie, MN). Briefly, the dog bone shaped samples were cut, and dimension (length, width, and thickness) was measured and noted.

Samples were loaded and pulled at a rate of 500 mm min^{-1}, and elongated to failure. Values were converted to stress-strain and initial modulus was calculated from the initial gradient of the curve (0 – 10% elongation). The results are presented as means ± standard deviation (n = 6).

The water uptake of crosslinked BPLP (cBPLP) was measured by the mass differential after the incubation in PBS (pH = 7.4). Briefly, cBPLP film with 1 d oven crosslinking was cut into discs (1 mm thick) using a cork borer. The discs were weighted and noted as initial mass (W_0), and placedin 10 mL PBS. Samples were removed from PBS at pre-determined time points and weighted for wet mass (Wx), until it reaches equilibrium. The water uptake percentage at each time point was calculated using the formular from equation (3.1):

Water Uptake (%) = $\frac{Wx - W0}{W0}$ x 100

The reported values are the means ± standard deviation (n = 6).

3.2.5 In Vitro Degradation

Degradation studies were performed in PBS (pH = 7.4) and NaOH solutions (0.05 M). NaOH degradation was used to screen the polymer degradation in a relatively short period of time. Briefly, 6 disc specimens (6 mm in diameter; 1 mm thick) were cut from films of cBPLP using a cork borer. The samples were weighted (W_0), placed in a tube containing 10 mL PBS or NaOH for up to 32 weeks or 24 h respectively, and incubated at 37 °C. After pre-determined time point, samples were taken out and thoroughly washed with deionized water for 3 times, lyophilized for 1 week. The weight of dry sample was measured (W_x). The remaining mass was calculated by comparing the initial mass (W_0) with the remaining mass (W_x), as shown in equation (3.2):

Remaining mass (%) = $\frac{Wx - W0}{W0}$ x 100

The reported values are the means ± standard deviation (n = 6).

3.2.6 Characterization of BPLPs fluorescent properties

All photoluminescence spectra were acquired on a Shimadzu RF-5301 PC fluorospectrophotometer. Both the excitation (exc) and the emission (emi) slit widths were set at

1.5 nm for all samples unless otherwise stated. BPLP solutions (2% w/v) in 1,4-dioxane were loaded in a quartz cuvette with a path length of 10 mm. The spectra of BPLP nanoparticle solution was evaluated in the same manner. To collect the excitation and emission spectra for scaffolds and films (size of ≈ 12 mm x 40 mm), samples were held diagonally in a quartz cuvette with a path length of 10 mm. The absorbance spectra were collected on Shimadzu 1501 ultraviolet-visible (UV-Vis) spectrophotometer. All tested solutions were loaded in a quartz cuvette with a path length of 10 mm, and same volume of pure solvent was place in same cuvette as control. The absorbance was scanned from 700 nm to 200 nm, with UV/Vis sources switching at 355 nm.

The extinction coefficient (ε) of each sample was measured by standard protocol [163]. Briefly, 5% BPLP solution was prepared. Extinction coefficient of all samples was measured in 1,4-dioxane unless noticed otherwise. The emission spectra of sample solution were obtained at various excitation wavelengths. Optimal excitation wavelength was determined as the one that generated the highest emission intensity. Next, absorbance spectrum was collected at a series of solution with gradient concentration, and the absorbance (within the range of 0.01–0.1 Abs units) at the optimal excitation wavelength was noted. Graphs of absorbance vs. concentration were plotted. The slope was determined as extinction coefficient. The quantum yields of the BPLP polymers were measured by the Williams' method [164]. Briefly, 5% BPLP solution was prepared. Quantum yield of all samples was measured in 1,4-dioxane unless noticed otherwise. The solution was scanned at various excitation wavelengths. Optimal excitation wavelength was determined as the one that generated the highest emission intensity. Then, UV-vis absorbance spectrum was collected with the same solution and the absorbance at the optimal excitation wavelength was noted. Next, a series of solution was prepared with gradient concentration, so that the absorbance of the each solution was within the range of 0.01–0.1 Abs units. The fluorescence spectrum was also collected for the same solution in the 10 mm fluorescence cuvette. The fluorescence intensity, which is the area of the fluorescence

spectrum, was calculated and noted. Five solutions with different concentrations were tested and the graphs of integrated fluorescence intensity vs. absorbance were plotted. The quantum yields of the BPLP polymers were calculated according to equation (3.3):

$$\Phi_x = \Phi_{ST} \left(\frac{Slope\ x}{Slope\ st}\right) \left(\frac{\eta x}{\eta st}\right)^2$$

where, Φ = quantum yield; Slope = gradient of the curve obtained from the plot of intensity versus absorbance; η = Refractive index of the solvent; x = subscript to denote the sample, and ST = subscript to denote the standard. Anthracene was a commercially available organic dye with a quantum yield of 0.27 in ethanol. It was used as a standard.

3.2.7 In Vitro Evaluation of cytotoxicity

Cell compatibility of cBPLP-Cys and cBPLP-Ser was evaluated *in vitro* using both qualitative and quantitative methods. cBPLP films with 2 d oven crosslinking were cut into discs (6 mm in diameter) and sterilized in 70% ethanol for 3 h. After incubation in ethanol, the samples were exposed to UV light for another 30 min and washed with sterilized PBS. NIH 3T3 fibroblasts were used as model cells for evaluation of cytotoxicity. The cells were cultured in Dulbecco's modified eagle's medium (DMEM), which had been supplemented with 10% fetal bovine serum (FBS) and 1% penicillin streptomycin. The T75 culture flasks were kept in an incubator maintained at 37 °C, 5% CO_2, and 95% relative humidity. The cells were allowed to grow to confluence at fourth passage, and washed with sterilized PBS twice before treatment of trypsin. Next, the cell suspension was centrifuged, and resuspended into complete culture media to obtain a seeding density of 1 x 10^5 cells mL^{-1} for seeding on samples.

For qualitative evaluation, cells were allowed to attach, grow, and proliferate on cBPLP films for 3 days, and 7 days. After incubation, the cells were fixed with the addition of a 2.5% w/v gluteraldehyde PBS solution. The films with fixed cells were then sequentially dehydrated by treatment with a graded series of ethanol, lyophilized, and sputter coated with silver. The samples were then observed under scanning electronic microscope (SEM) to view the cell morphology.

The quantitative assessment of the cell proliferation on cBPLP films was also performed using a methylthiazoletetrazolium (MTT) cell proliferation and viability assay kit. Disc shape samples were prepared and sterilized as mentioned above. PLLA films were used as a relative control. Fibroblasts were seeded on disc samples in the same manner as mentioned above using 96-well plate. MTT assay analysis was performed at 1, 3, and 7 days of culture as specified by the manufacturer's protocol. Briefly, at each time point, the old media were discarded, and each sample was washed with sterilized PBS twice to remove any dead or loosely attached cells. Next, incomplete media (100 µL) (free of FBS) was added to each well. A 3-(4,5-dimethylthiazol-2yl)-diphenyltetrazolium bromide solution (10 µL) was then added to the well, and allowed to incubate for 3 h. At the end of incubation period, DMSO (100 µL) was added to the media. Dissolution of the formazan crystals was facilitated by constant agitation of the well plate on an orbital shaker for 20 min. The absorbance was measured on an Infinite200 microplate reader (Teacan Group Ltd., Switzerland) at 570 nm.

The cytotoxicity of the cBPLP degradation products was also evaluated with MTT assay. cBPLP-Cys and cBPLP-Ser films with oven crosslinking for 4 days were incubated in 0.1 M NaOH for accelerated degradation. Following complete polymer degradation, the pH of the solution was adjusted to 7.4 with 0.1 M HCl. The degradation solutions were then diluted in complete media into various concentrations to create the cytotoxic media. All solutions were passed through a 0.22 µm syringe filter for sterilization. Next, approximately 10,000 3T3 mouse fibroblasts were seeded into each well of a 96-well plate and incubated for 24 h to reach a 60% confluence. After 1 day of culture, the normal media was replaced with 200 µL of cytotoxic media, and cells were allowed to incubate for an additional 4 h and 24 h. MTT assay was performed on each time point in the same way mention above. The degradation products of PLLA were used as a control. Viability of cells in the presence of degradation products was normalized to the viable cells cultured with complete media only.

3.2.8 In Vivo Imaging of Tumor Targeting

For nanoparticle bioimaging in vivo, BPLP-Ser 1.2 nanoparticles (2% wt in DI Water, 80 nm in diameter) were sterilized by filtering through a syringe filter (0.22 μm) and injected subcutaneously in Black mice (C57BL/6 J). 100 μL of nanoparticle solution was injected at each spot. The mice were then imaged using a Kodak Imaging System, as described previously immediately after the implantation. To evaluate the *in vivo* tumor targeting efficiency of BPLP nanoparticles via Enhanced Permeability and Retention (EPR) effect, B16F10 malenoma cells were implanted orthotopically on the back of Black mice. After the size of tumor reached 1 x 1 x 1 cm^3, 100 μL of BPLP-Ser nanoparticle solution was injected intravenously via tail. The accumulation of nanoparticles on tumor site was monitored at pre-determined time point. Animals were cared for in compliance with the regulations of the animal care and use committee of The University of Texas at Arlington.

3.2.9 Statistical Methods

Data ware expressed as means ± standard deviation. The statistical significance between two sets of data was performed using two-tail student's t-test or non-parametric one-way ANOVA tests. Data were considered to be significantly different, when $p < 0.05$ was obtained.

3.3 Results and Discussion

Although traditional fluorescent dyes, such as quantum dots and small organic dyes have been widely used in biomedical application, they have to be incorporated with other implantable materials to accomplish the task. There has been tremendous research on combination of biodegradable polymers and fluorescent dyes [79, 100, 158]. However, the incorporation of biodegradable polymers will have some negative effect on property of fluorescent dyes in both photophysical and physicochemical way [79]. Many efforts have been made to develop implantable and biodegradable polymers with inherent fluorescence. Unfortunately, there has not been any report of such material to our knowledge.
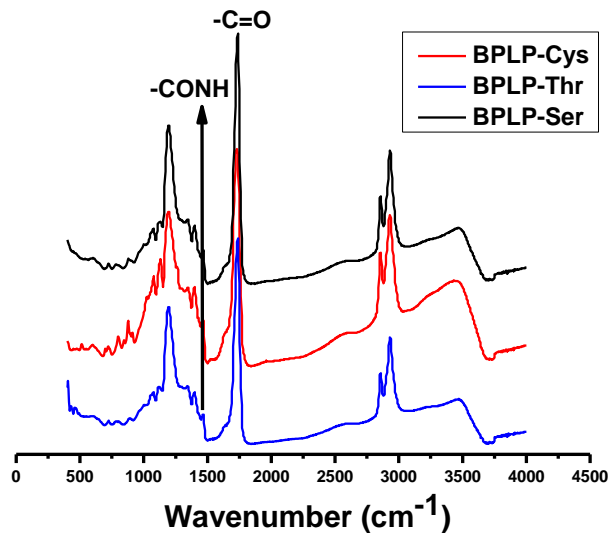
3.3.1 Characterization of Chemical Structure

Figure 3.3 FT-IR Spectra of BPLP-Cys, BPLP-Thr, and BPLP-Ser

FT-IR spectrum of BPLP-Cys, BPLP-Ser, and BPLP-Thr is depicted in Figure 3.3. It show the presence of -C(=O)NH- at 1,527 cm^{-1}, -C=O at 1,731 cm^{-1}, -CH$_2$- at 2,931 cm^{-1}, and –OH at 3,467 cm^{-1}. The formation of amide bond confirms the successful corporation of amino acids into the polymers. In the ^{1}H-NMR spectrum of BPLP-Cys (Figure 3.4), peaks at 1.23 ppm and 1.50 ppm represent -C$\underline{H}_2$- from 1,8-octanediol, and the multiple peaks at 2.75 ppm represent –C$\underline{H}_2$- from citric acid. Interestingly, release of hydrogen sulfide was detected by hydrogen sulfide test strip during the synthesis of BPLP-Cys (Figure 3.1C). Two small peaks at 5.85 and 6.57 ppm was assigned to –(C=C$\underline{H}_2$)- from cysteine [165]. In the ^{13}C-NMR spectrum of BPLP-Cys (Figure 3.5), the peaks ≈ 170 ppm were assigned to carbonyl (-$\underline{C}$=O) groups from citric acid and cysteine. The peaks ≈ 63.8 ppm and 28.5 ppm were assigned respectively to –O-$\underline{C}$H$_2$CH$_2$- and –O-CH$_2$$\underline{C}H_2$- from 1,8-octanediol. The –C(=O)-$\underline{C}$H$_2$- carbon from citric acid was assigned to the peak at 61.2 ppm. The –NH-$\underline{C}$H- carbon from cysteine was assigned to the peak at 54.5 ppm. There were 4 peaks assigned to the central carbon atom of citrate units in

62

various chemical environments (inset of Figure 3.5). Peaks at 72.9 and 73.4 ppm were assigned to central carbon when –COOH and –OH group on the central carbon was reacted with 1,8-octanediol and remained unreacted respectively. Those two peaks were also found on ^{13}C-NMR of pre-POC. Peaks at 72.1 and 72.4 ppm were assigned to the central carbon when it formed amide bond with cysteine only and a six-member ring structure respectively. The ^{13}C-NMR results suggests the presence of a 6-membered ring formed on BPLP-Cys as depicted in Figure 3.1B. This ring structure is proposed to be the fluorophore of BPLP, which will be discussed in next section. The number average molecular weight of BPLP-Cys measured by MALDI-MS was 1,334 Da.
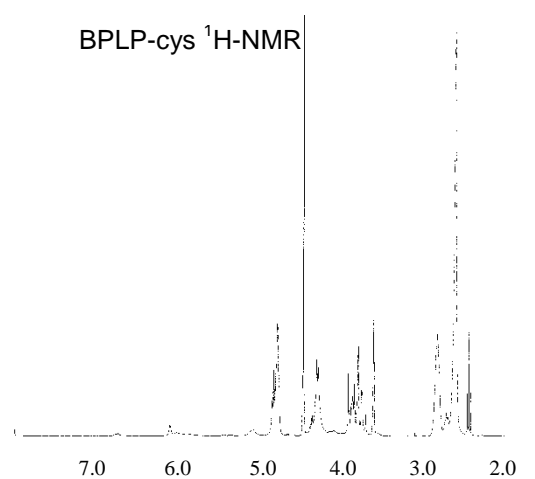
BPLP-cys ^{1}H-NMR

Figure 3.4 ^{1}H-NMR spectra of BPLP-Cys
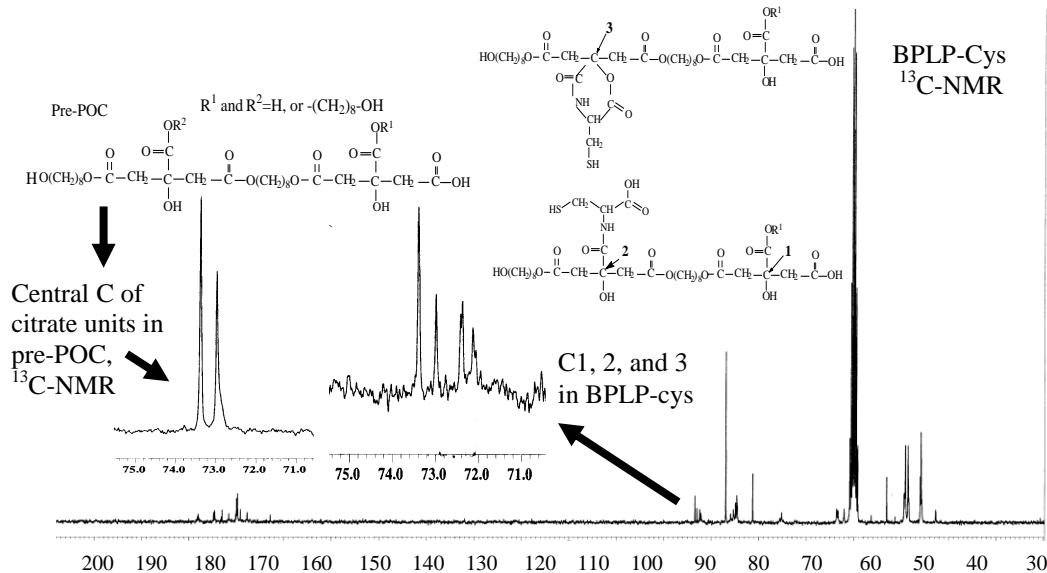
Figure 3.5 ^{13}C-NMR spectra of BPLP-Cys

3.3.2 Fluorescent Properties

Fluorescent properties of every synthesized BPLP were listed in Table 3.1. Polymers include BPLPs with 20 essential amino acids, wsBPLP-Cys, and pcBPLP-Cys. All 22 polymers have significant fluorescence. This indicates that fluorescence of BPLPs can be control by using different amino acids. It is not only restricted within 20 essential amino acids, but also includes large pool of unessential ones.

Table 3.1 Fluorescent properties of BPLPs

Name	Diol	Diacid	Amino Acid	Extinction Coefficient (M^{-1} cm^{-1})	Quantum Yield (%)
wsBPLP-Cys	PEG	Citric acid	L-Cysteine	67.3	32.3
pcBPLP-Cys	1,8-octanediol	Citric acid 0.2 + Maleic acid 0.8	L-Cysteine	90.2	11.1
BPLP-Ala	1,8-octanediol	Citric acid		6.2	5.3

64

Table 3.1 – *Continued*
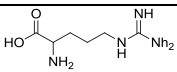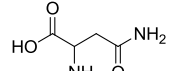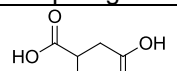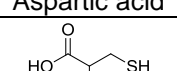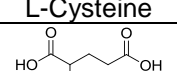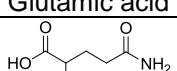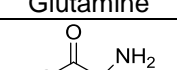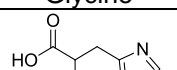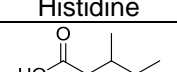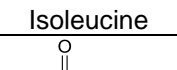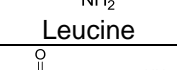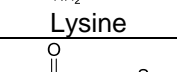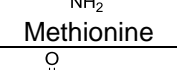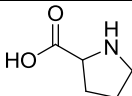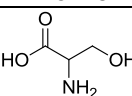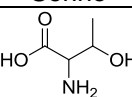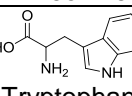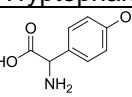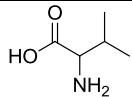
			Alanine		
BPLP-Arg	1,8-octanediol	Citric acid	Arginine	4.6	0.9
BPLP-Asn	1,8-octanediol	Citric acid	Asparagine	16.6	11.0
BPLP-Asp	1,8-octanediol	Citric acid	Aspartic acid	170.2	11.3
BPLP-Cys	1,8-octanediol	Citric acid	L-Cysteine	90.2	62.3
BPLP-Glu	1,8-octanediol	Citric acid	Glutamic acid	17.8	0.3
BPLP-Gln	1,8-octanediol	Citric acid	Glutamine	14.4	13.9
BPLP-Gly	1,8-octanediol	Citric acid	Glycine	679	10.9
BPLP-His	1,8-octanediol	Citric acid	Histidine	7.2	1.9
BPLP-Ile	1,8-octanediol	Citric acid	Isoleucine	9.2	1.2
BPLP-Leu	1,8-octanediol	Citric acid	Leucine	4.8	1.0
BPLP-Lys	1,8-octanediol	Citric acid	Lysine	3.2	9.4
BPLP-Met	1,8-octanediol	Citric acid	Methionine	8.4	0.5
BPLP-Phe	1,8-octanediol	Citric acid	Phenylalanine	4.6	0.8

Table 3.1 – *Continued*

BPLP-Pro	1,8-octanediol	Citric acid	Proline	10.6	0.4
BPLP-Ser	1,8-octanediol	Citric acid	Serine	97.8	26.0
BPLP-Thr	1,8-octanediol	Citric acid	Threonine	84.0	34.2
BPLP-Trp	1,8-octanediol	Citric acid	Tryptophan	93.8	12.1
BPLP-Tyr	1,8-octanediol	Citric acid	Tyrosine	2.4	3.1
BPLP-Val	1,8-octanediol	Citric acid	Valine	22.6	1.0

The successful fabrication of films, scaffolds, gel, and nanoparticles demonstrated the good processability of BPLPs. Strong fluorescence of BPLP was inherited to all forms of products. The exc and emi spectra were depicted in Figure 3.6, and final form of each product was put in inset. Compared with fluorescence of BPLP-Cys in solution, the optimal emission wavelength remains the same for all products. It demonstrated that fluorophore was preserved intact through fabrication procedure. Those results indicated that BPLP is an implantable and ready to use material with strong inherent fluorescence. However, there is significant lost in fluorescent intensity for all products compared to the solution. This is because of the self-quenching of fluorescence when fluorophore are getting too close to each other [166].
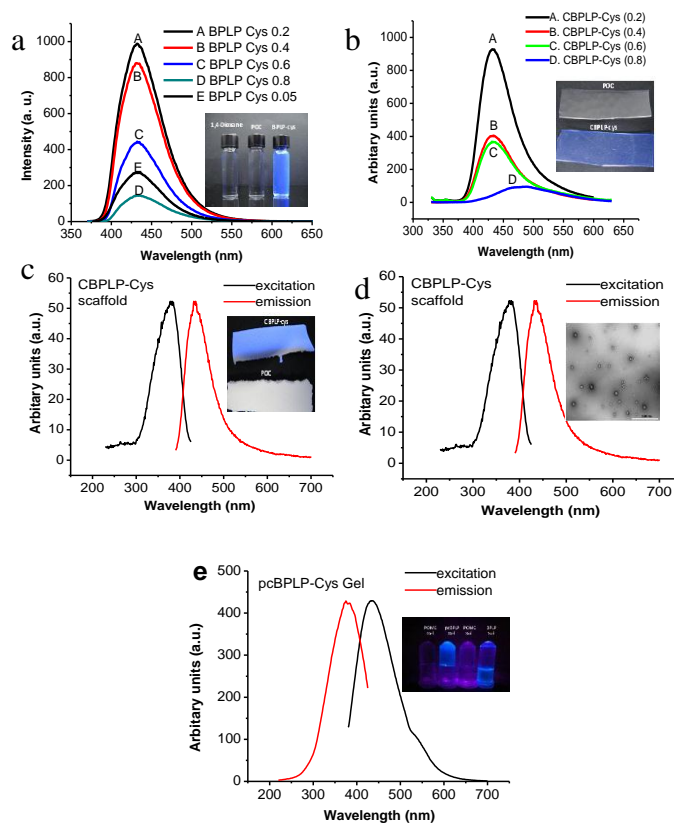
Figure 3.6 Emission Spectra of (a) BPLP-Cys Solution and (b) BPLP-Cys Film. Excitation and Emission Spectra of (d) BPLP-Cys Scaffold, (d) BPLP-Cys Nanoparticles, and (e) pcBPLP gel.

3.3.3 Mechanical Properties

Figure 3.7 shows the tensile strength and the Young's modulus of BPLP-Cys films with different postpolymerization time. The tensile strength ranged from 2.44±0.28 MPa to 4.54±0.59 MPa. Young's Modulus was in a range of 1.96±0.04 MPa to 5.88±0.35 MPa. It was found that the tensile strength and the modulus of BPLP-cys increased with an increased postpolymerization time. However, it caused a decrease of elongation from 137.61±13.27 to 82.02±13.63. Mechanical properties can also be controlled by feeding ratio of cysteine (Figure 3.8). With increased feeding ratio of cysteine, both strength and elasticity of BPLPs have significantly increased. After 2 d of postpolymerization, BPLP-Cys 0.8 has a tensile strength of 7.35±0.58, Young's modulus of 5.05±0.28, and elongation of 222.341±6.711%. Those results

indicated that the mechanical properties could be adjusted by varying ratios of monomers and by altering polymerization conditions. Increased amount of cysteine will result in more amide bonds, which will increase the mechanical property of polymer. Film of BPLP-Cys can be elongated up to 222%, which is comparable with reports of such values for arteries and veins [50]. Although pre-BPLPs have low molecular weight and sticky nature, postpolymerization improves the processability, and makes BPLP an implantable material.
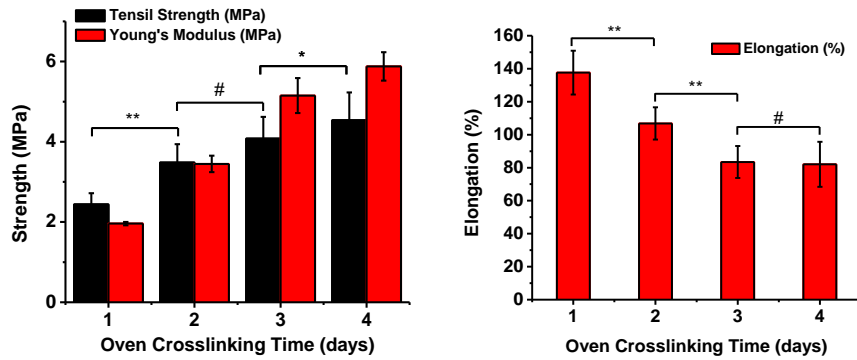
Figure 3.7 Mechanical Properties of BPLP-Cys 0.2 Films with Different Oven Crosslinking Time **$p<0.01$, *$p<0.05$, #$p>0.05$; N=8.
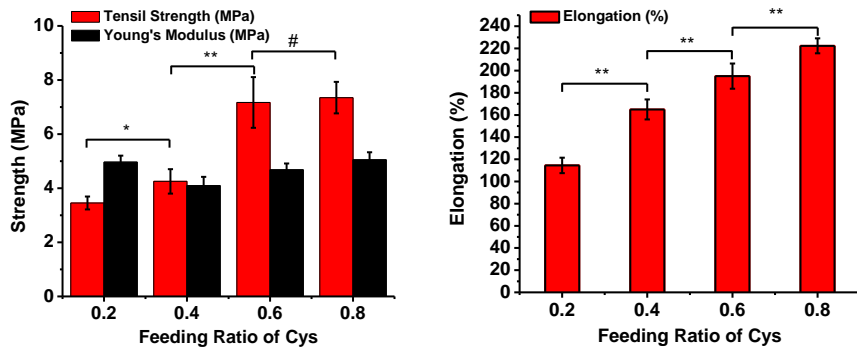
Figure 3.8 Mechanical Properties of BPLP-Cys Films with Different Feeding Ratio of Cys **$p<0.01$, *$p<0.05$, #$p>0.05$; N=8.

3.3.4 In vitro degradation

Degradation studies were conducted in PBS on both pre-BPLPs and oven crosslinked BPLP (Figure 3.9). All of the polymers reached complete degradation after certain time period. Prepolymer degraded within 22 days in PBS. As an important parameter for biodegradable implant, degradation rate is always the concern for choosing right materials [167, 168]. Degradation rate of BPLPs can be tuned by many ways, such as feeding ratio and postpolymerization time. Previous studies show that reaction between the amine and citric acid will first happen to the side carboxyl group from citric acid [169, 170]. This fact will have two consequences. Firstly, the amidation on the side will not affect the degradation of polymer backbone. Therefore, with an increased feeding ratio of cysteine, pre-BPLP-Cys 0.6 reached full degradation 4 days faster than per-BPLP-Cys 0.2 (Figure 3.9A). Secondly, the occupation of side chain of citric acid will results in a lower crosslinking density. Although BPLP-Cys 0.8 had higher mechanical property than BPLP-Cys 0.2 after 4 days postpolymerization, it degraded 8 weeks faster (Figure 3.9B). The manipulation of degradation rates confers BPLP great potential for various biomedical applications that require different degradation rate.
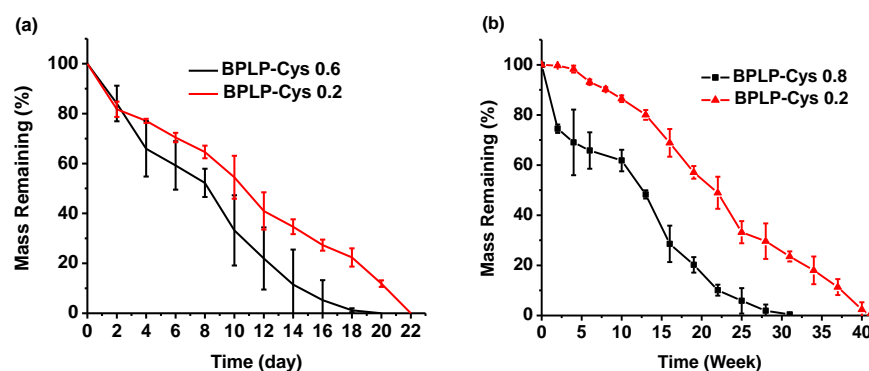
Figure 3.9 In vitro degradation of BPLP-Cys (a) Prepolymer and (b) with 4 day postpolymerization

The fluorescence change over degradation in PBS was also studied. From Figure 3.10, fluorescence of BPLP-Cys dimed completely with full degradation. At the beginning of

degradation, fluorescence showed a slow decrease compared to the degradation rate. This is because that amide bond involved in 6-membered ring is more resistant to hydrolysis than ester bond. After degradation reaches 50%, fluorescence showed a dramatically decrease due to the cleavage of most polymer backbone
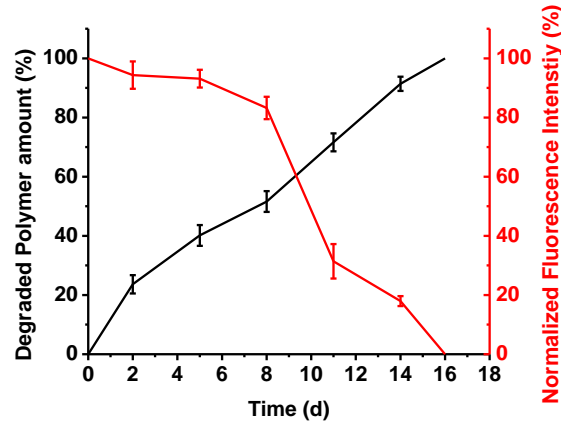
Figure 3.10 Fluorescence change of BPLP-Cys prepolymer over degradation in PBS

3.3.5 In vitro cytotoxicity

In order to analyze the cytocompatibility of BPLP-cys, the 3T3 cells were grown on BPLP-Cys and Ser films. POC and PLGA were used as controls. Cell adhesion and proliferation were quantitatively evaluated by MTT assay (Figure 3.11A). After 1 d cell culture, both BPLP-Cys and BPLP-Ser showed a higher cell adhesion than POC and PLGA. Viable cell numbers on BPLP films were significantly higher than those on controls POC film and PLGA film after 3, 5, and 7 d of cell culture. The morphology of 3T3 on BPLP films were observed by SEM. Images (Figure 3.12) of the cells grown on BPLP-cys films showed the morphology healthy fibroblast after 2 d cell culture. The confluent cell layer can be observed after 6 d. The results demonstrated that BPLP films supported 3T3 mouse fibroblast adhesion and proliferation. Cytotoxicity of degradation products is also important. Cytotoxicity evaluation for degradation products suggested that the degradation of BPLPs and crosslinked BPLPs generated similar cytotoxicity to the controls POC and PLGA (Figure 3.11B).
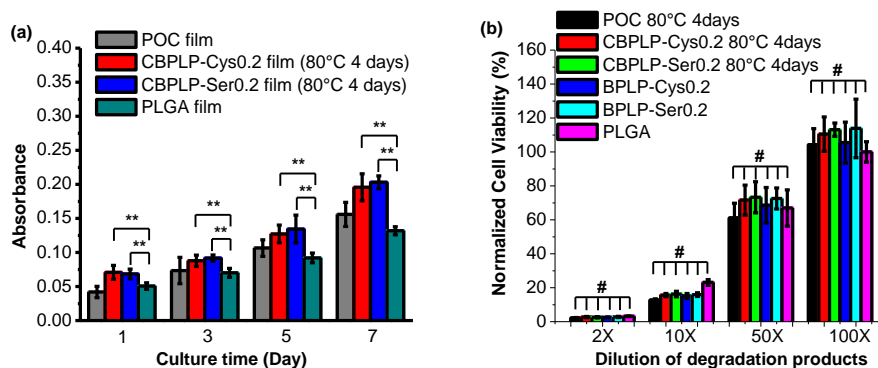
Figure 3.11 In vitro study of cytotoxicity (a) Cell viability and proliferation assay (MTT assay) for 3T3 fibroblasts cultured on BPLP-Cys film. (b) Cytotoxicity evaluation of degradation products of BPLPs (-Cys and -Ser) and crosslinked BPLPs (-Cys and -Ser) at 2x, 10x, 50x and 100x dilutions. All the values of absorbance were normalized to the PLGA at 100x dilution. **p<0.01, *p<0.05, #p>0.05; N=6.

3.3.6 *In vivo Imaging*

In vivo imaging studies has also been conducted for further evaluation. Different concentrations of BPLP-Ser nanoparticles were injected subcutaneously onto the back of Black mice (C57BL/6 J). The fluorescent intensity showed a linear relation with the concentration of BPLP nanoparticles (Figure 3.13a). The *in vivo* cancer targeting of BPLP nanoparticles via an enhanced permeability and retention effect (EPR) [171] was studied by implanting melanoma skin tumors onto the backs of black mice (C57BL/6 J). After intravenous injection of the nanoparticle solution via the tail vein, the mouse was observed for 40h. After 18h a significant increase of fluorescent intensity indicated a remarkable accumulation of BPLP-Ser nanoparticles at the tumor site (Figure 3.13b) (Point of Interest). The results proved that BPLP-Ser nanoparticles could be effectively targeted to tumor site through the EPR effect, and with sufficient functional groups on the surface, BPLP-Ser nanoparticles can be conjugated with variety of tumor specified moieties to further enhance the targeting efficiency.
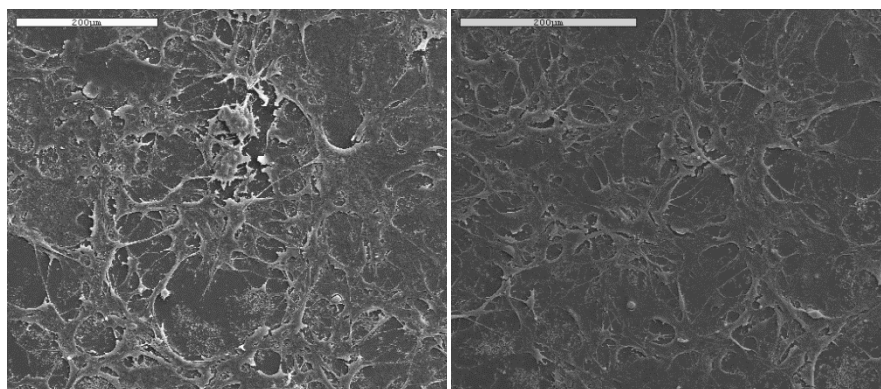
Figure 3.12 SEM images of 3T3 fibroblasts cultured on BPLP-Cys films (a) 2 days and (b) 6 days
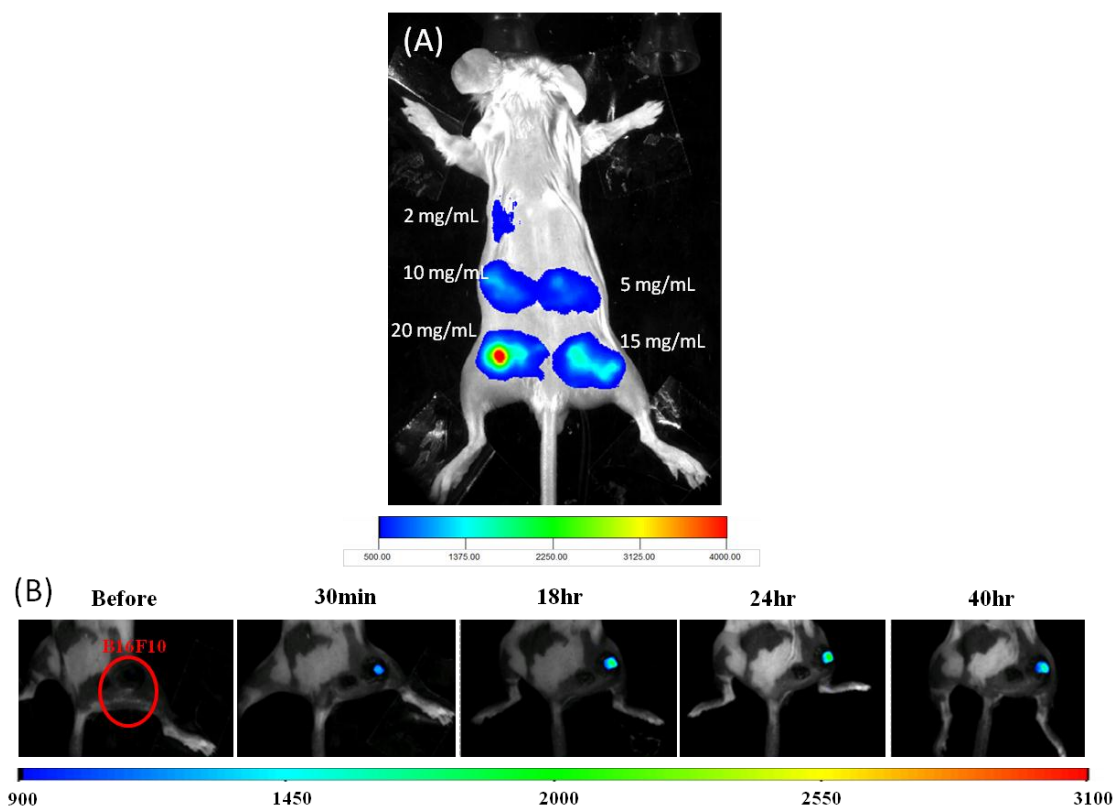
Fig 3.13 In vivo imaging study (a) BPLP-Ser nanoparticles with different concentration injected subcutaneously on the back of white mouse (b) *In vivo* cancer targeting of BPLP-Ser nanoparticles. Photoluminescence of cancer implantation site was recorded at different time point. Exc/emi pair is 550nm/600nm.

3.4 Conclusions

We described the methodology of a family of aliphatic biodegradable photoluminescent polymers that emit tunable, strong, and stable fluorescence. The synthesis and fabrication of BPLPs was straightforward and cost-effective. BPLP families possess excellent processability for micro/nano fabrication and desired mechanical properties, potentially serving as implant materials and bioimaging probes *in vitro* and *in vivo*. The development of BPLPs represent a new direction in developing biodegradable materials and may have wide impact on basic sciences and a broad range of applications such as tissue engineering, drug delivery, and bioimaging.

CHAPTER 4

FLUORESCENT MECHANISM OF BIODEGRADABLE PHOTOLUMINSCENT POLYMERS

4.1 Introduction

Before putting any fluorescent materials into application, the fluorescent mechanism is always the first puzzle to put on. To better exploit this promising fluorescent property of BPLPs, the following sections will be addressed to explore its fluorescent mechanism and the structure fluorescence relationship. Series of BPLPs will be synthesized with expressly selected start monomers to conclude the general fluorophore.   The understanding of structure and fluorescence relationship will be studied in detail, thereby allowing for manipulation of BPLPs to fit for a particular bioimaging application at will.

4.2 Attempts to Explore Fluorophore

4.2.1 Introduction

All fluorescent materials can be concluded into two categories, inorganic and organics. Accordingly, there are two fluorescent mechanisms for each category.

Quantum dot (Qdots) is the major type of inorganic semiconducting fluorescent materials. It not only includes cadmium selenide (CdSe) but also of many other semiconducting materials derived from the II and VI elemental groups (CdTe, CdS, CdHg, ZnS) and III and V elemental groups (InAs, InP, GaAs) of periodic table [172]. The key word for their fluorescent mechanism is energy gap. All semiconductors have an energy gap (E_g) (Figure 4.1a) between conduction band and valence band. When a photon is absorbed, the electron can be excited into conduction band, and leave a hole on valence band. Why only Qdots have fluorescence while bulk semiconductors don't? This question leads us to another key word, quantum confinement. In the case of Qdots, the separation between excited electron and hole is smaller than their Bohr radius so that the exciton was squashed into a smaller space with more energy

[173]. Therefore, the emission of Qdots is size dependent. The smaller size is, the more energetic exciton is, and more blue-shifting emission is. On the contrary, the bigger size is, the more red-shifting emission is. The tunable fluorescence of Qdots has been investigated for multicolor fluorescence imaging of cancer cells under *in vivo* conditions [69]. Since different compositions vary in energy gap, from 0.14 (HgTe) to 3.8 (ZnS) [174, 175], range of emission is different for each Qdots. For example, CdSe can emit from 470nm to 670nm, with a size change from 2nm to 8nm, whereas, PbSe can emit from 1120nm to 1320nm, with a size change from 3nm to 4nm. Generally, small energy gap leads to higher emission wavelength. Recently, quantum dots are capped with a shell of another semiconductor, mostly ZnS [111]. In the case of CdSe core/ZnS shell, quantum yield was raised from 5-15% to 30-50%, and the emission range was also moved to a higher emission.
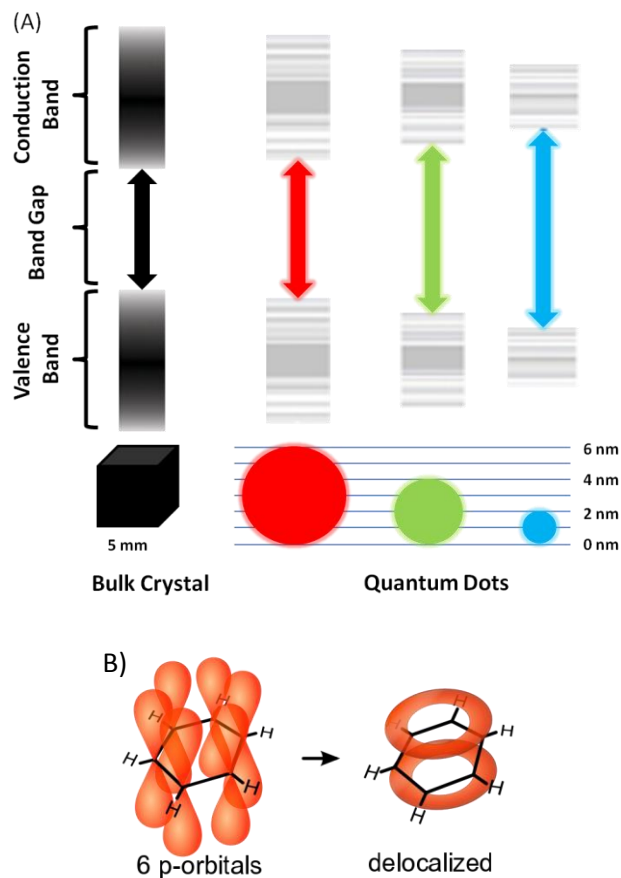
Figure 4.1 Fluorescent mechanism (a) Fluorescent Mechanism of Quantum Dots, (b) Delocalized Electron Structure of Benzene

Organic fluorescent materials include fluorescent polymer, small molecule dye, and green fluorescent protein. The widely accepted fluorescent mechanism is the conjugation system. According to International Union of Pure and Applied Chemistry, conjugation is the overlap of one p-orbital with another across an intervening sigma bond. Therefore, organic compounds with alternating single and multiple bonds, normally an aromatic ring obeying Hückel's rule [162], have a system of connected p-orbitals and allow a delocalization of π electrons across the system (Figure 4.1b). Structure of some traditional small molecule dye is listed in Figure 4.2. The energy gap of these materials is created by the conjugated π system. The more extended conjugation system is, the more red-shifting emission is. Although small

molecular dye has totally different content from Qdots, they have some drawbacks in common, such as cellular toxicity, and poor physical and chemical stability. Therefore, they both have been studied extensively to incorporate with biodegradable polymer for bioimaging application.
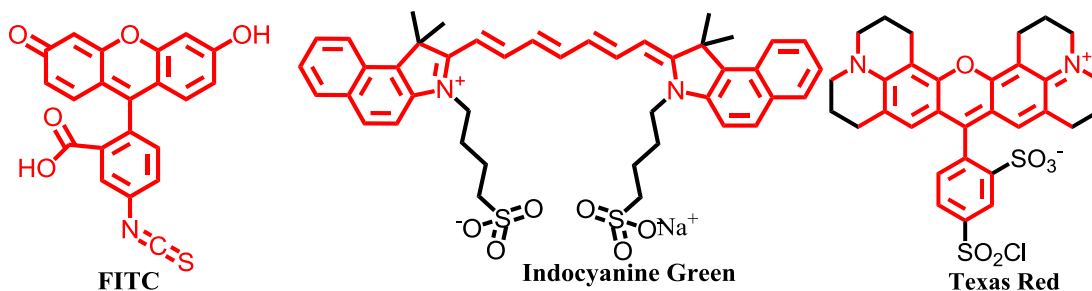
Figure 4.2 Chemical structure of traditional small molecular dye (red represents the conjugated system)

Fluorescent polymers can be divided into two classes. One is having conjugated system pendent to the backbone (Figure 4.3). The other one is with the conjugated system along the backbone, like Poly (p-phenylene vinylene) (Figure 4.3). The fluorescent mechanism is the same as small molecular dye. Recently, there is a new family of fluorescent dendrimers with the tetramine group, including poly (amido amine) (PAMAM), poly (propyleneimine) (PPI), and poly (ethyleneimine) (PEI). The first proposed fluorescent mechanism was the oxidation of hydroxyl end groups of PAMAM [176]. This hypothesis was later disproved by Imae's group that PPI and PEI with various end groups can emit blue fluorescence [97]. With more detail studies, Imae et al. [99] found that a more rigid, crowded structure of tertiary amines exhibits a higher fluorescence yield. Although the fluorescent mechanism still remains unclear, the tertiary amino on the dendritic backbone is speculated to be the key of fluorescence [99], which is still under the rules of conjugation.
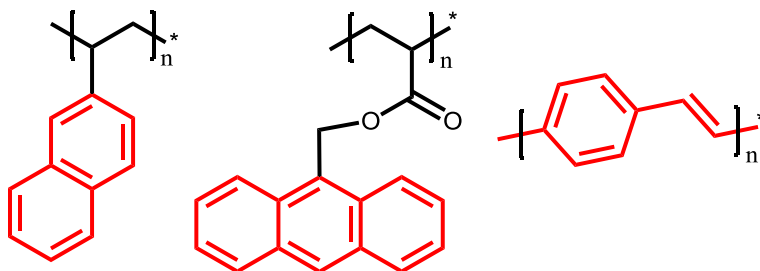
Figure 4.3 Chemical structure of fluorescent polymers, Poly(2-vinylnaphthalene), Poly(9-anthracenylmethyl acrylate), and Poly(p-phenylene vinylene) (from left to right) (red represents the conjugated system)

With the tremendously increased researches on Green Fluorescent Protein (GFP), the fluorescent mechanism has been studied in details. Although there are still some arguments, researchers have agreed on a cyclic ring fluorophore, p-hydroxybenzylideneimidazolinone [134]. With the well-done study on the primary, secondary, tertiary, and quaternary structure of GFP, the cyclic ring is composed of residue Ser or Thr65, Try66, and Gly67. Figure 4.4 illustrates the currently accepted mechanism of the fluorophore formation. After a series of folding, cyclization, dehydration, and aerial oxidation [177], the conjugated system is formed. As a nature organic compound, the fluorescent mechanism of GFP still obeys the conjugated system. Therefore, emission of GFP can also be tuned by extended conjugation system. The task can be achieved by oligomerization and conjugating more aromatic structure onto the fluorophore by series of folding mutation. Gross et al. [178] has reported a red fluorescent protein "DsRed". The red fluorophore results from the autonomous multi-step post-translational modification of residues Gln66, Tyr67, and Gly68 into an imidazolidinone heterocycle with *p*-hydroxybenzylidene and acylimine substituents. Shaner et al. [70, 72] has concluded monomeric fluorescent proteins that emit from yellow to red.
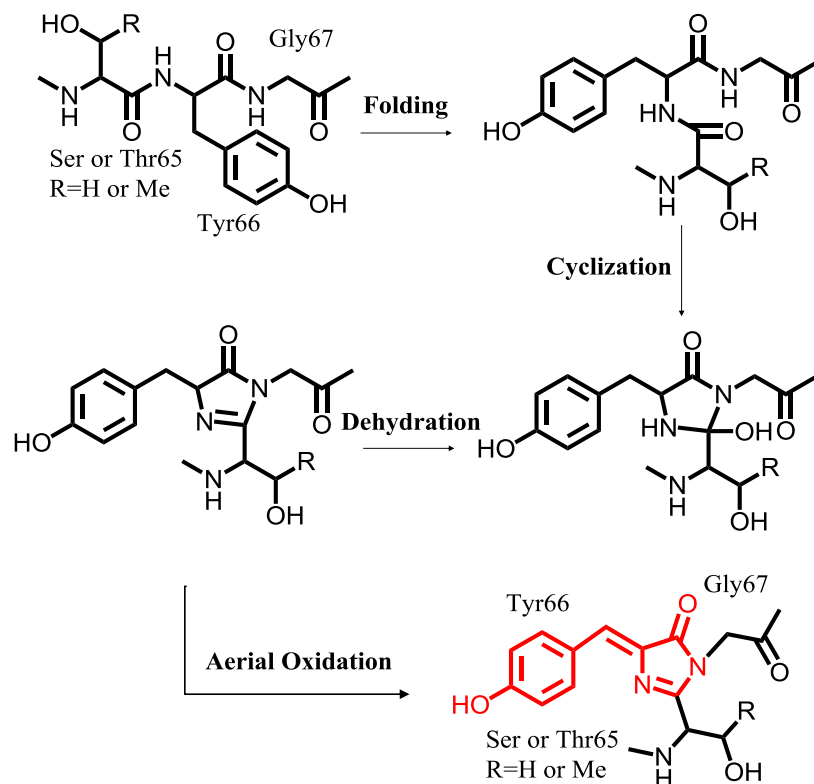
Figure 4.4 Formation and final chemical structure of the fluorophore of GFP

4.2.2 Experimental

4.2.2.1 Synthesis of BPLP with Different Monomers

All chemicals were purchased from Sigma-Aldrich (St. Louis, MO) and used as received, except where mentioned otherwise. To explore the chemical structure of fluorophore, various BPLPs were first synthesized by incorporating different monomers via controlled condensation reaction (Figure 2.5) in the same manner as previously described. Various pre-BPLP polymers were synthesized with different monomers, listed in Table 4.1. The overall ratio between diol, diacid, and amino acid was kept at 1.1:1:0.2.

4.2.2.2 Fluorescent Property of BPLPs Characterization

Photoluminescence spectra of all BPLPs were acquired on a Shimadzu RF-5301 PC fluorospectrophotometer. All polymers were dissolved in 1,4-dioxane and concentration was finalized at 2% (w/v). Both the excitation and the emission slit widths were set at 1.5 nm for all

samples unless otherwise stated. Optimal emission wavelength, quantum yield, and extinction coefficient were measured in the same manner as previously described.

4.2.3 Results and Discussion

The fluorescence of all BPLPs was listed in Table 4.1. We have demonstrated that poly (octamethylene citrate) (POC) synthesized from citric acid and 1,8-octanediol only had negligible fluorescence. Water-soluble BPLP (wsBPLP) was synthesized with 1.8-octanediol replaced with PEG 200. WsBPLP-Cys has strong fluorescence at 434nm, which is same as regular BPLP-Cys. BPLPs-Cys synthesized with poly(propylene glycol) also has the optimal emission wavelength at 434nm. It can be concluded that diol has no contribution of fluorophore. Although citric acid has a melting point at 159 °C, there are reports that it has potential to have thermo-decomposition at lower temperature [179]. To eliminate the effect of decomposition, BPLP-Cys was synthesized under 110 °C, under which no decomposition of citric acid has been reported. The resulted polymer also has same fluorescence as regular synthesized BPLP-Cys. Thus, it has been proved that decomposition has no effect on fluorescence. Fluorescent intensity of BPLPs can be tuned by feeding ratios of amino acid. UV-Abs spectra of BPLP-Cys and BPLP-Ser with different ratio of amino acids were plot in Figure 4.5. It was found that absorbance at optical excitation wavelength was in proportion to the feeding ratio of amino acids. This result further confirmed the hypothesis that the fluorophore is closely related to amino acid.

Table 4.1 Fluorescent properties of BPLPs synthesized with different monomers
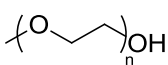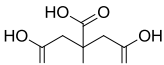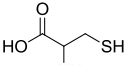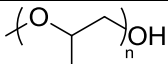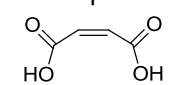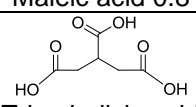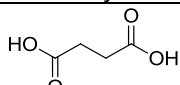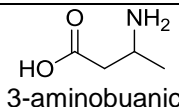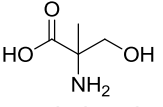
Diol	Diacid	Amino Acid	Optimal Emission (nm)	Quantum Yield	Extinction Coefficient (M^{-1} cm^{-1})
PEG	Citric acid	L-Cysteine	434	32.3%	67.3
PPG	Citric acid	L-Cysteine	434	26.1%	58.1

Table 4.1 – *Continued*

HO⤵OH 8 1,8-octanediol	Citric acid	L-Cysteine	434	62.3%	115.4
1,8-octanediol	Citric acid 0.2 + [structure] HO OH Maleic acid 0.8	L-Cysteine	434	11.1%	90.2
1,8-octanediol	[structure] HO OH Tricarballyic acid	L-Cysteine	No Distinctive Fluorescence		
1,8-octanediol	[structure] HO OH Succinic acid	L-Cysteine	No Distinctive Fluorescence		
1,8-octanediol	Citric acid	[structure] O NH₂ HO 3-aminobuanic acid	No Distinctive Fluorescence		
1,8-octanediol	Citric acid	[structure] HO OH NH₂ α-methyl-serine	434	70.2%	109.37

To understand the structure-property relationship of the pendant functional groups provided by citric acid, tricarballylic acid and succinic acid (Table 4.1) were used to replace citric acid, but neither of the resulting polymers has distinct fluorescence (Figure 4.6A). A fundamental hypothesis can be drawn from those simple reactions in that the side carboxylic and hydroxyl group from citric acid, together with an amino acid, results in fluorescence. All 20 essential α-amino acids have distinct fluorescence, especially glycine (the only achiral nature amino acid). This further excludes the R group of the amino acid from the list of indispensables. Amidation and esterification are two possible reactions among amine, hydroxyl, and carboxyl group. Considering the reacting rate and energy, the fastest reaction is between the amine and the side carboxyl group from citric acid [169, 170] . Based on product of this amidation, we hypothesize a 6-membered ring structure to be the fluorophore (Figure 4.7). This hypothesis was supported by the result that the additional methylene group from β-amino acid switched off

the fluorescence due to a seven-member ring structure, which is unstable in nature. Due to the special chemical environment, α-H of α-amino acid contributes important chemical properties. To eliminate the contribution of α-H to the fluorophore, α-methyl-serine (Table 4.1) was used to synthesize BPLP-MSer. From Figure 4.6B, BPLP-MSer still had even higher fluorescent intensity than BPLP-Cys at 434 nm. This result indicated that α-H has no contribution to the fluorophore. Another unique property of amino acid is that all α-amino acids have two isomers except for glycine. To demonstrate the effect of isomerism on fluorescent property, L-serine, D-serine, and DL-serine have been used for synthesis. From emission spectra (Figure 4.6C), there was no significant difference of optimal emission wavelength and fluorescent intensity. This result indicated that isomerism was irrelevant to the fluorescence of BPLPs.
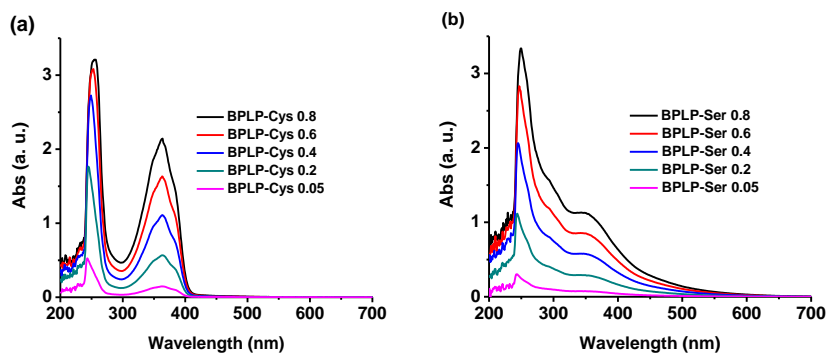
Figure 4.5 UV-Vis absorbance spectra of (a) BPLP-Cys and (b) BPLP-Ser with different feeding ratio of amino acids
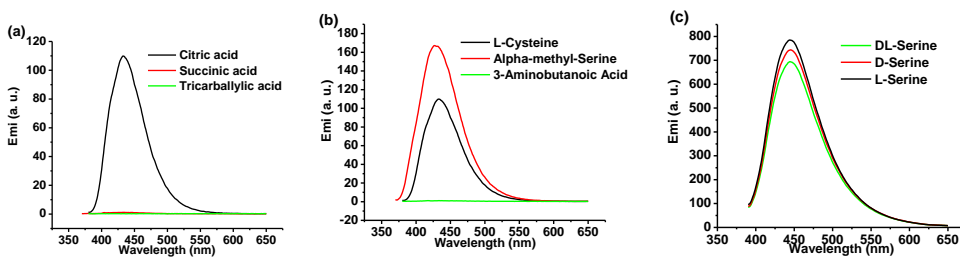
Figure 4.6 Emission spectra of BPLPs solution in 1,4-dioxane synthesized with (a) Different diacids, (b) Different amino acids, and (c) Different optical isomers

^{13}C-NMR also provides evidence for the ring structure. In the ^{13}C-NMR spectrum of BPLP-Cys (Figure 2.6), the peaks ≈170 ppm were assigned to carbonyl (C=O) groups from citric acid and L-cysteine. The peaks ≈63.8 ppm and 28.5 ppm were assigned respectively to -O-$\underline{C}$H$_2$CH$_2$- and -O-CH$_2$$\underline{C}H_2$- from 1,8-octanediol. The -C(=O)-$\underline{C}$H$_2$- carbon from citric acid was assigned to the peak at 61.2 ppm. The –HN-$\underline{C}$H- carbon from L-cysteine was assigned to the peak at 54.5 ppm. There were 4 peaks assigned to the central carbon atoms of citrate units in various chemical environments. Peaks at 72.9 and 73.4 were assigned to C1 when R^1 is -(CH$_2$)$_8$-OH and -H respectively. Peaks at 72.1 and 72.4 ppm were assigned to C2 and C3 respectively. However, the ^{13}C-NMR of pre-POC only showed 2 peaks of central C of citrate units at 72.9 and 73.4 ppm. The ^{13}C-NMR results supported the presence of a 6-membered ring formed on BPLP-Cys.

For organic compounds, conjugation is the only known law of fluorescence. The basic requirement of a structure being conjugated is planarity. The hypothesized 6-membered ring has a similar structure as morpholine-2,5-dione. In present case (Figure 4.7), hydrogen on C2 is substituted with R-group, while hydrogens on C1 are substituted by polymer chains. Studies from other groups have proven the planarity of the ring, when hydrogens on C1 and C2 have been substituted [180]. In order to explain the conjugation of the whole ring structure, the theory of hyperconjugation needed to be introduced. This is a well-studied phenomenon, which was first defined by R. S. Mulliken in the late 1930s. It refers to the interaction of δ with adjacent π orbital. There is evidence to show that hyperconjugation can not only extend the conjugation , but also lead to fluorescence on its own [181]. In the current 6-membered ring, the carbonyl group on C3 and electronic pair from O1 both interact with C-C δ bond on C1 to form hyperconjugation to explain the conjugation of 6-membered ring.

Red part from amino acid
Blue part from citric acid
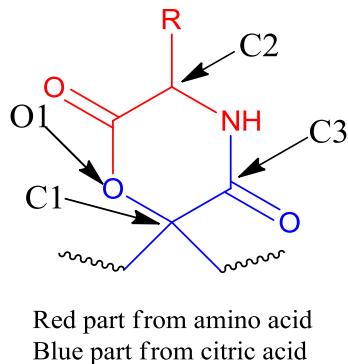
Figure 4.7 Hypothesis of 6-membered Ring as Fluorophore

4.2.4 Conclusion

In this section, a series attempts have been made to obtain the chemical structure of fluorophore. All the possible reactions among monomers have been examined. The contribution of each monomer and functional group to the fluorophore was evaluated by being replaced by other monomers. After synthesizing a series of BPLPs with various diacids, diols, and amino acids, the fluorophore has been concluded as a 6-membered ring structure formed by citric acid and L-cysteine. This ring structure has been confirmed by ^{13}C-NMR, and the conjugation has been explained using both conjugation and hyperconjugation theory. Although no direct characterization has confirmed the structure of this 6-membered ring, it has so far been the most plausible fluorophore structure.

4.3 Factors Affecting Fluorescence

4.3.1 Introduction

As we discussed above, the fluorescent properties of all fluorescent materials can be manipulated in respective ways. Since fluorescence of quantum dots is directly affected by Bohr Radius, size of the quantum dots is the decisive factor to the emission of fluorescence. Due to the different range of Bohr Radius, each quantum dot has unique range of fluorescence. For example, with controlled size, CdS has a range of emission from 400 to 460 nm [172]. By changing the anionic substances, CdSe has a fluorescence at 460~660 nm, while it moves to

530~750 nm for CdTe [172]. With different semiconducting element, PbSe has a range of emission from 1120~1330 nm [172]. Recently, quantum dot with a core-shell structure has been widely studied. The shell is composed of a few atomic layers of a material with a larger band gap on top of the quantum dot core. Materials normally used for coating layer are CdSe and ZnS [79, 120]. Physicochemically, it efficiently averts surface defects, and protects the surface atoms from oxidation. Photophysically, the quantum yield and photostability can be greatly improved, and emission can shift to red [79]. For example, the range of emission of CdTe moves from 530~750 nm to 630~860 nm with a CdSe layer [172].

Different from quantum dots, fluorescence of organic materials is determined by conjugation system. As discussed above, larger conjugation system has more room for the movement of delocalized electrons, thus, leading to a red shift of emission. Based on chemical structure, organic dyes can be divided into several classes, cyanine, porphyrin, squaraine, BODIPY, and xanthenes. All the commonly used dyes are derivates from these classes, such as indocyanine green from cyanine, fluorescein and rhodamineB from xanthenes. To manipulate the emission, different chemical modifications have been made upon traditional dyes to expend conjugation system. Series of commercial organic dyes have been developed, such as Cy® and Alexa Fluor® by Molecular Probes, and DyLight® by Thermo Fisher Scientific. For example of Cy3 and Cy5, with extension of a propylene group, emission moves from 570 nm of Cy3 to 670 nm of Cy5 [182]. Following the same theory, emission of fluorescent polymers can also be manipulated. With different molecular weight and modification of pendant groups, Poly (p-phenylene vinylene) is able to emit from yellow to red [183]. For another special class of fluorescent materials, fluorescent mechanism of Green Fluorescent Protein (GFP) has been discussed above, and its fluorophore also follows the role of conjugation system. Due to the can-core structure of GFP [134], chemical modification is difficult to reach the fluorophore. Therefore, by changing sequence of GFP (mutation) and secondary structure (folding), and

formation of oligomer, emission of fluorescent protein can be tuned from 440 nm (EBFP) to 650 nm (mNeptune) [184].

In the case of BPLPs, the fluorescence can be manipulated in several ways, such as control of initial feeding ratio and using different amino acid. It is noteworthy that BPLP-Ser and BPLP-Cys has different behavior under continuous changing excitation. BPLP-Cys has a fixed emission at 434 nm, independent from concentration, feeding ratio, and excitation. On the other hand, emission of BPLP-Ser is dependent on various factors. Most remarkably, the emission is able to shift as red as 725 nm [52]. This phenomenon demonstrates that BPLP has its own way to make itself fluorescent at near infrared without any modification of fluorophore. As the tremendously growing of near infrared fluorescent materials development, BPLP-Ser has a great potential as a biodegradable NIR dye for biomedical application. The following sections will synthesize a series of BPLPs with different amino acids. The fluorescent property of those polymers will be studied to explore the fluorescence-structure relation of BPLP.

4.3.2 Experimental

All chemicals were purchased from Sigma-Aldrich (St. Louis, MO), except where mentioned otherwise. To study the fluorescence of BPLP-Cys, three s-containing amino acids were involved in synthesize. They are Homocysteine, S-methyl-cysteine, and Penicillamine, yielding BPLP-HMCys, BPLP-SMCys, and BPLP-Pen, respectively (Table 4.2).

Photoluminescence spectra of all BPLPs were acquired on a Shimadzu RF-5301 PC fluorospectrophotometer. All polymers were dissolved in 1,4-dioxane and concentration was finalized at 2% (w/v), except where mentioned otherwise.

Table 4.2 Excitation dependent emission of BPLPs with different α-amino acids
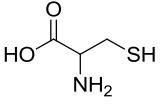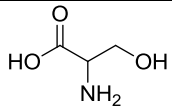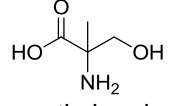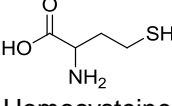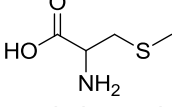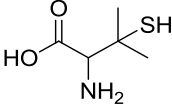
Polymer	Amino acid	Excitation Dependent Emission
BPLP-Cys	L-Cysteine	No

Table 4.2 – *Continued*

BPLP-Ser	L-Serine	Yes
BPLP-MSer	α-methyl-serine	No
BPLP-HMCys	Homocysteine	No
BPLP-SMCys	S-methyl-cysteine	Yes
BPLP-Pen	Penicillamine	Yes

4.3.3 Results and Discussion

The emission spectra of BPLP-Cys, BPLP-Ser, BPLP-MSer, BPLP-HMCys, BPLP-SMCys, and BPLP-Pen with changing excitation wavelength have been shown in Figure 4.8 and 4.9. All involved BPLPs have distinctive fluorescence. The spectra of those polymers showed that only BPLP-SMCys has excitation dependent emission similar to BPLP-Ser, while all the rest showed no excitation dependence. More important is that all the excitation independent BPLPs show similar emission around 435 nm. It can be assumed that all the excitation independent BPLPs have some similarity in structure. It was found that hydrogen sulfide was released during the synthesis of BPLP-Cys. This phenomenon gives us a clue that release of hydrogen sulfide leaves a double bond attached to the fluorophore. This is further confirmed on ^{1}H-NMR (Figure 2.6) with two peaks at 5.85 and 6.57 ppm [[165]]. In the case of BPLP-Ser, due to the higher bond energy of C-O than C-S, the elimination of one molecule of H_2O is more difficult than hydrogen sulfide, which has a boiling point of only 60°C. Considering the steric hindrance of polymer chain and lack of strong base, the elimination of hydrogen

sulfide is believed to go through E1 mechanism, during which a carbocation was formed as intermediate. In order to form the most stable carbocation, Wagner-Meerwein rearrangement has taken place, and is illustrated in (Figure 4.10). For BPLP-Cys, the thiol group first leaves the structure, and forms a carbocation. This primary carbocation is the least stable form. Therefore, it will migrate to form a more stable tertiary carbocation. Since tertiary carbocation is the most stable, second step of E1 elimination will happen on this tertiary carbocation. Thus, a double bond will be formed pendent to 6-membered ring. Same carbocation rearrangement also happens to BPLP-HMCys (Figure 4.10). Only difference is that there are two step of rearrangement. As illustrated in Figure 4.10, the primary carbocation will first be formed and rearrange to form a more stable secondary carbocation. Then, a second rearrangement will take place to form the tertiary carbocation. The elimination will happen on this carbocation. For BPLP-Pen, when the thiol group leaves, a tertiary carbocation will be directly formed. Thus, there is no rearrangement happen in the synthesis of BPLP-Pen. In the case of BPLP-SMCys, the alkanethiol group is not able to leave as easily as thiol group. Therefore, no elimination will take place. Interestingly, BPLP with a non s-containing amino acid, α-methyl-serine (MSer), has the exactly same emission wavelength as BPLP-Cys. Its emission is also independent from excitation. Therefore, it can be hypothesized that BPLP-MSer should have the similar structure to BPLP-Cys. As illustrated in Figure 4.10, the hydroxyl group leaves the structure and forms primary carbocation. After one-step rearrangement, the tertiary carbocation is formed and elimination takes place. After elimination, all the fluorophores have a double bond that extends the conjugation system. This may also explain the enhanced fluorescence of BPLP-Cys and BPLP-MSer.
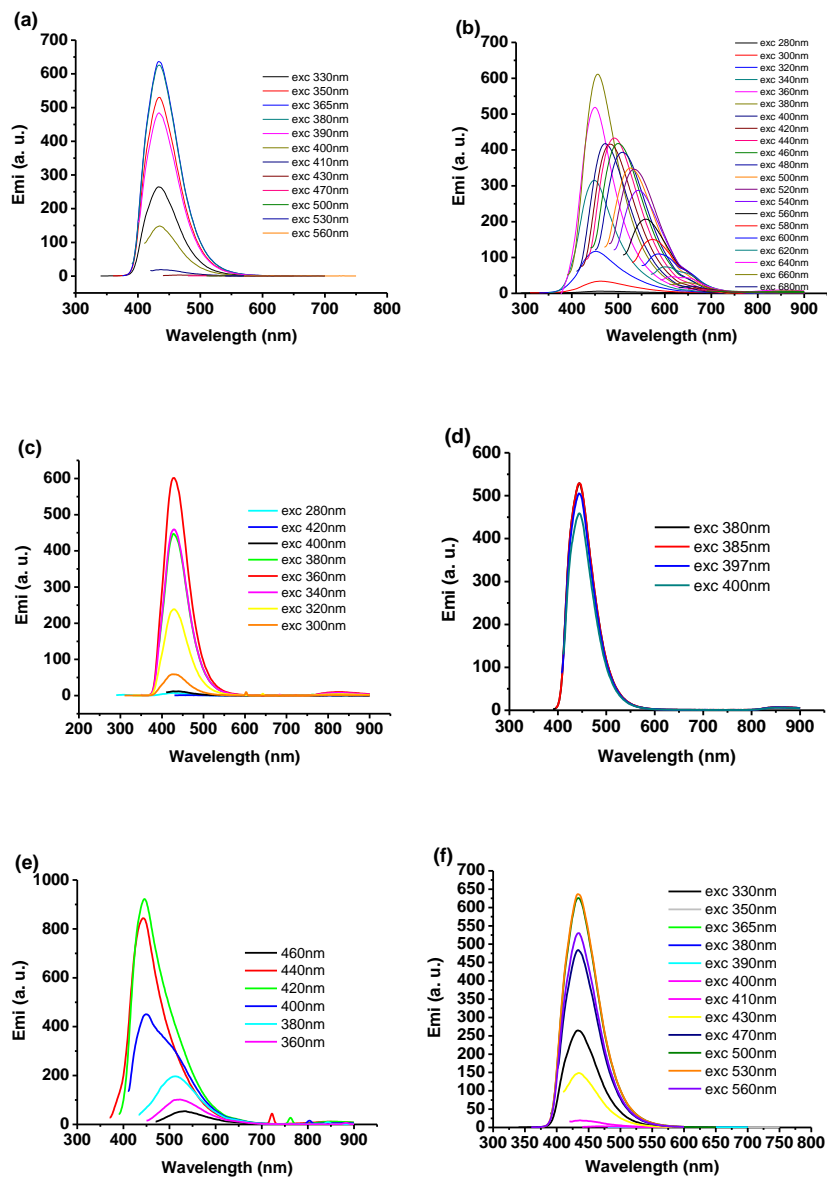
Figure 4.8 Emission spectra under different excitation of (a) BPLP-Cys, (b) BPLP-Ser, (c) BPLP-MSer, (d) BPLP-HMCys, (e) BPLP-SMCys, and (f) BPLP-Pen. (2% w/v)
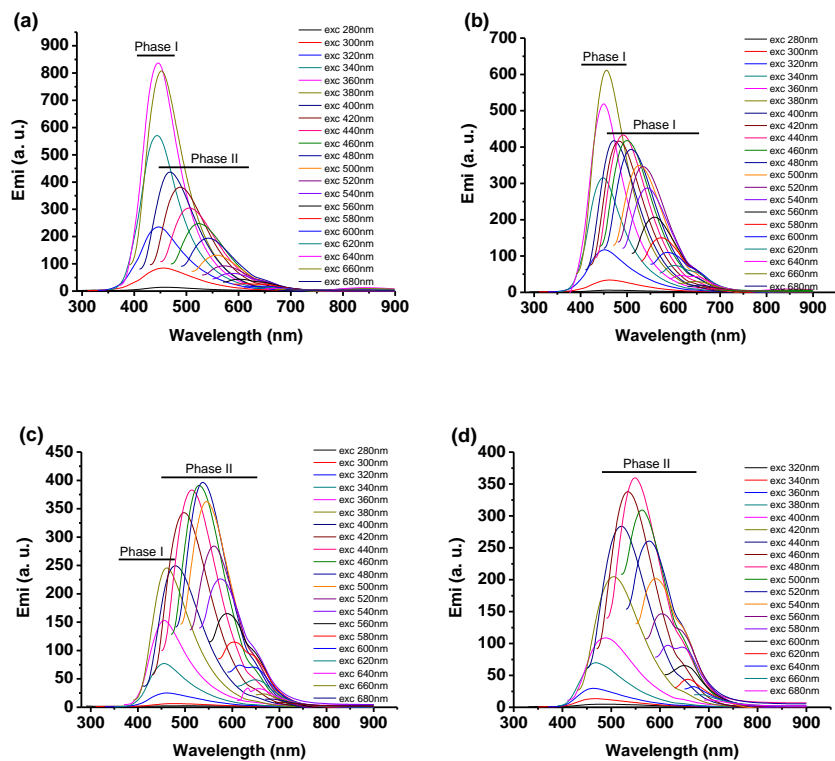
Figure 4.9 Emission Spectra under Different Excitation of BPLP-Ser with Different Concentration: (a) 1% w/v, (b) 2% w/v, (c) 4% w/v, and (d) 6% w/v.
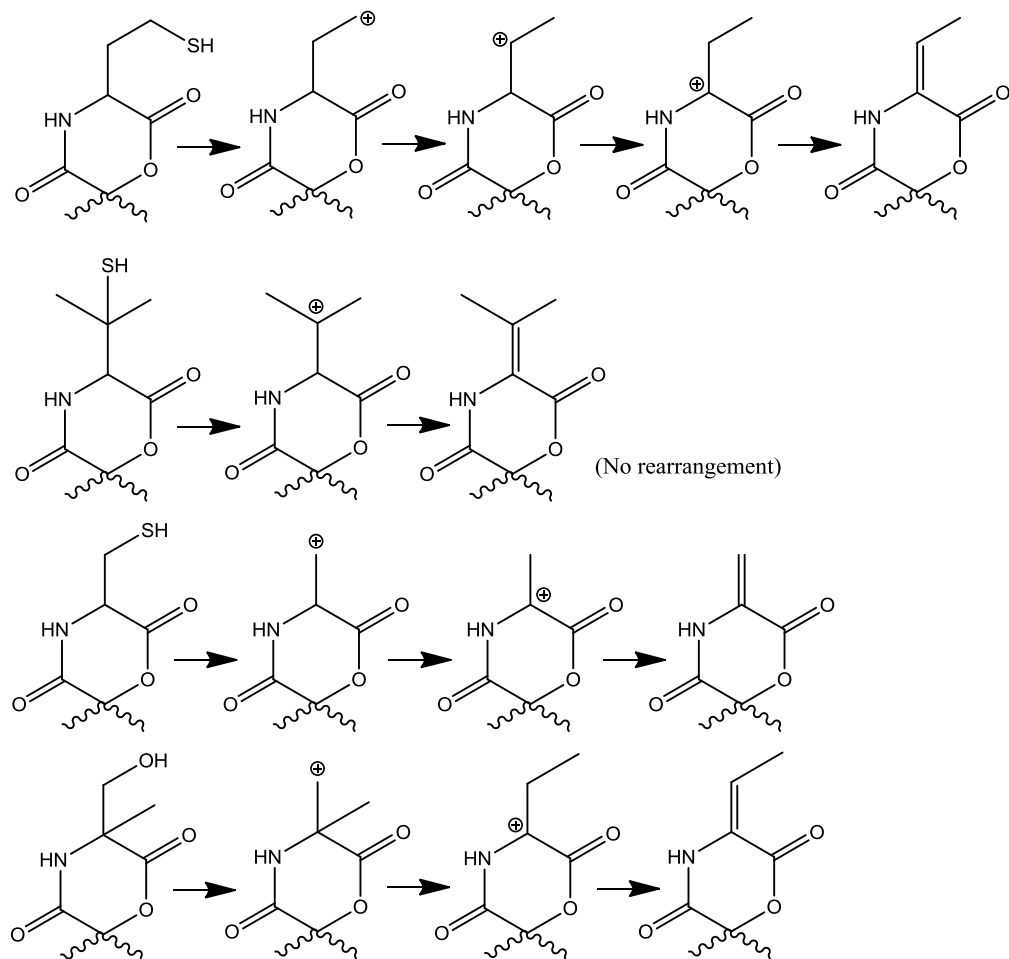
Fig 4.10 Wagner-Meerwein rearrangement of BPLP-HMCys, BPLP-Pen, BPLP-Cys, and BPLP-MSer (from top to bottom)

The excitation dependent emission of BPLP-Ser is a remarkable property, not only because it makes the fluorescence more controllable, but also pushes it into the window of near infrared. After careful characterization, all BPLPs based on 19 essential amino acids except for cysteine have this property. However, only BPLP-Ser still sustains strong fluorescence at near infrared. From the emission spectra of BPLP-Ser (Figure 4.9), the emission spectra are shifting to red with the increasing excitation wavelength. Moreover, under lower concentration (Figure 4.9A and B), the emission spectra can be analyzed in two phases. In phase I, BPLP-Ser emits at 434 nm, with varying excitation wavelength under 434nm. This phase is similar to BPLP-Cys.

91

In phase II, with the excitation higher than 434nm, it begins to show the shifting spectra with increasing excitation wavelength. From the emission spectra of BPLP-Ser at higher concentration (Figure 4.9C and D), the phase I begin to fade. Only phase II can be observed from the emission spectra of BPLP-Ser with concentration higher than 6% w/v.

These excitation dependent emission spectra has been studied in detail and termed as Red-Edge Effect (REE) [185-187]. It can be concluded that fluorescence spectra can depend on excitation wavelength, when polar fluorophores embedded into different rigid and highly viscous media [186]. It is applicable for almost all kinds of organic dyes, including small molecule dyes [188], fluorescent polymer [186], and GFP [187]. The fluorophore of BPLPs is a pendent structure on the polymer chain. Thus, although the concentration of BPLP-Ser is only under 8% (w/v), the polymer backbone still provides a rigid media to the pendent fluorophore. This is confirmed by the fact that the REE of BPLP-Ser is more distinct in higher concentration. Fletcher [[188]] pointed out that a rotatable auxochrome (or chromophore) is necessary for a fluorophore to have REE. This well explains that BPLP-Cys does not having REE because of the not rotatable double bond. Consequently, all the BPLPs that go through elimination and result in double bond do not have Red Edge Effect.

4.3.4 Conclusion

The strong fluorescence and excitation dependent emission of BPLP-Ser was explored. After evaluating the fluorescent property of a set of BPLPs synthesized with sulfur-containing amino acids, the occurrence of elimination was demonstrated and possible rearrangement of carbocation was hypothesized. The happening of elimination was found to be crucial to the excitation dependence.

<u>4.4 Conclusion</u>

The fluorescent mechanism of BPLPs family has been explored. The plausible general fluorophore of this newly developed biodegradable polymer family was a 6-membered ring structure. This ring structure is a conjugation system with both usual conjugation and

hyperconjugation. As an organic compound, fluorescent mechanism of BPLPs follows the theory of conjugation. The unique excitation dependent emission of BPLPs has been studied with synthesizing a set of careful designed BPLPs. The results of fluorescent property show that the occurrence of elimination on the fluorophore leads to the high fluorescence and excitation independent emission of BPLP-Cys and BPLP-MSer. With no elimination of BPLP-Ser, it has a red edge effect to yield an excitation dependent emission. This unique property confers near infrared fluorescence on BPLP-Ser, and make it competitive candidate in various bioimaging applications, which will be the focus of the following sections. The understanding of structure fluorescence relationship will provide solid foundation for designing versatile biodegradable fluorescent polymers.

CHAPTER 5

URETHANE DOPED BIODEGRADABLE PHOTOLUMINESCENT POLYMERS

5.1 Introduction

During the last two decades, biodegradable materials have become the ideal choice for the non-permanent biomedical device, such as tissue engineering scaffolds, drug delivery vehicles, and bioimaging probes [32, 157, 189, 190]. Using biodegradable polymers as implant materials is beneficial as the implants may be degraded and cleared by the body once their missions are complete, leaving no foreign materials in the body. Large number of biodegradable polymers has been studied for various biomedical applications. Two FDA approved biodegradable polymers, poly (L-lactic acid) (PLLA) and poly (glycolic acid) (PGA), including their copolymers, are successful in engineering hard tissues [191, 192]. The controlled degradation and ready-to-use surface functional groups agitated their extensive applications as drug delivery carrier [157, 193]. Although those biodegradable polymers showed success, they are not suitable for all kinds of applications. For tissue engineering, aliphatic polyesters failed to be used for vascular tissue engineering due to the mismatch of the mechanical property from native tissue. Recently, some elastomers, such as poly (octylene citrates) (POC) and poly (glycerol sebacate) have attracted much attention due to their soft and elastic property [31, 50]. Nevertheless, the tremendously loss of mechanical property under wet condition and fabrication of porous scaffold created a mismatch from the mechanical property of native blood vessel. Studies have showed that chemically doping urethane bond into polymers can significantly increase mechanical strength, for instance, from 6.7MPs tensile strength (POC) to 33.35MPa after urethane doping [194]. This high strength is not only providing sufficient room for loss from scaffold fabrication or physiological environment, but also strong enough to support surgical handling. For drug delivery, PLGA has several drawbacks including low stability (negative surface charge) and low

94

drug loading capacity [195, 196]. Many newly developed biodegradable polymers, especially amphiphilic copolymers, have been proved to be beneficial in many aspects [197, 198]. However, stability of nanoparticles, low loading efficiency, and burst initial release facilitate the pace on searching new biodegradable materials as drug carrier.

Meanwhile, the fluorescent labeling and imaging endowed biodegradable materials with more promising potentials. Fluorescence incorporated tissue engineering scaffold helps some fundamental understandings on the key elements, such as predicting *in vivo* degradation rate [199, 200]. The non-invasive imaging also provided real-time monitoring *in situ* scaffold degradation and tissue regeneration/infiltration. For drug delivery, biodegradable polymeric nanoparticles combined with fluorescence enable the theranostic probes. Most commonly, traditional dyes, such as small molecule organic dye and inorganic quantum dots, were incorporated to enable fluorescence [201, 202]. However, those fluorescent dyes have drawbacks that limit their further use. Small molecule organic dyes, such as Indocyanine Green (ICG) and fluorescein, have been proved to be cytotoxic at cellular level, and have low dye-to-reporter molecule labeling ratios [203]. Quantum dots have been extensively studied in fluorescent-based bio-applications such as *in vitro* cellular labeling and *in vivo* cancer labeling. However, toxicity from heavy metal content evoked great concern for their biomedical application [204]. Green fluorescent protein (GFP) has attracted tremendous attention for their unique intrinsic fluorescence. However, it suffers from photobleaching and instability, and may cause cellular toxicity from aggregation inside the cells [205]. All those fluorescent dyes require incorporation with biodegradable polymers to achieve implantable fluorescent materials, which brings complexity to the system. Recently, a family of biodegradable photoluminescent polymers (BPLPs) has been developed in author's lab. BPLPs have strong (quantum yield as high as 62.33) and tunable intrinsic fluorescence (up to 725nm) that requires no need of fluorescent dyes. Due to its good processability, BPLPs can be fabricated into dense films, porous scaffolds, and micro/nanoparticles without losing fluorescent properties. However, the tensile strength (6.5 ± 0.8 MPa tensile strength) is not high enough for vascular tissue engineering. In aspect of theranostic

probe, although BPLP nanoparticle showed suitable size (80 nm) and stable zeta potential (-20.2 mV), the sticky nature and low molecular weight increased aggregation potential.

In this study, we reported the synthesis and characterization of a urethane doped biodegradable photoluminescent polymer (UBPLP), and showed the proof of concept for a triphasic graft used for *in situ* tissue engineered vascular grafts and stable biodegradable theranostic probes. The synthesis and fabrication are described. Crosslinked UBPLPs (CUBPLPs) process desire mechanical property and elasticity. The porous triphasic scaffold not only meets the requirements for tissue engineering vascular graft and surgical handling, but also retains strong and tunable fluorescence. The *in vivo* detectable fluorescence confers the real-time monitoring of scaffold degradation and tissue infiltration/regeneration. Fabrication and characterization of UBPLPs nanoparticles as theranostic probe for cancer treatment are also described. Stable and evenly distributed nanoparticles can be formed in PBS. Therapeutic function is demonstrated with loading 5-fluorouracil by chosen formula. This cyto-compatible nanoparticle exhibits high drug loading efficiency and sustained release. The *in vivo* imaging demonstrates its potential as diagnostic probe. Taken together, UBPLPs have several advantages: (1) hydrolyzable ester bond and urethane bond leading to biodegradability (2) cyto-compatible (3) strong mechanical property retaining strength of porous scaffold (4) increased stability of nanoparticles (5) sustained release of anti-cancer drug (6) *in vivo* detectable fluorescence provided real-time monitoring of tissue engineering scaffold and cancer diagnosis.

<div align="center">5.2 Experimental</div>

5.2.1 UBPLP synthesis

UBPLP pre-polymers were synthesized in two distinct steps (Figure 5.1A). The step one involves the synthesis of BPLP pre-polymer same to previously published methods [52]. Briefly, BPLP was first synthesized by reacting 1:1.1:0.2 monomer ratio of citric acid, 1,8-octanediol, and L-Cysteine/L-Serine, respectively, in a three-necked round bottom flask fitted with an inlet and outlet adapter at 160°C under a constant flow of nitrogen. Once all the monomers had

melted, the temperature of the system was lowered to 140°C, and the reaction mixture was allowed to continue for 2h to create the BPLP pre-polymer. The obtained pre-polymer was then purified by drop-wise precipitation in deionized water. The precipitated pre-polymer was collected and lyophilized for 24h to obtain the purified BPLP.
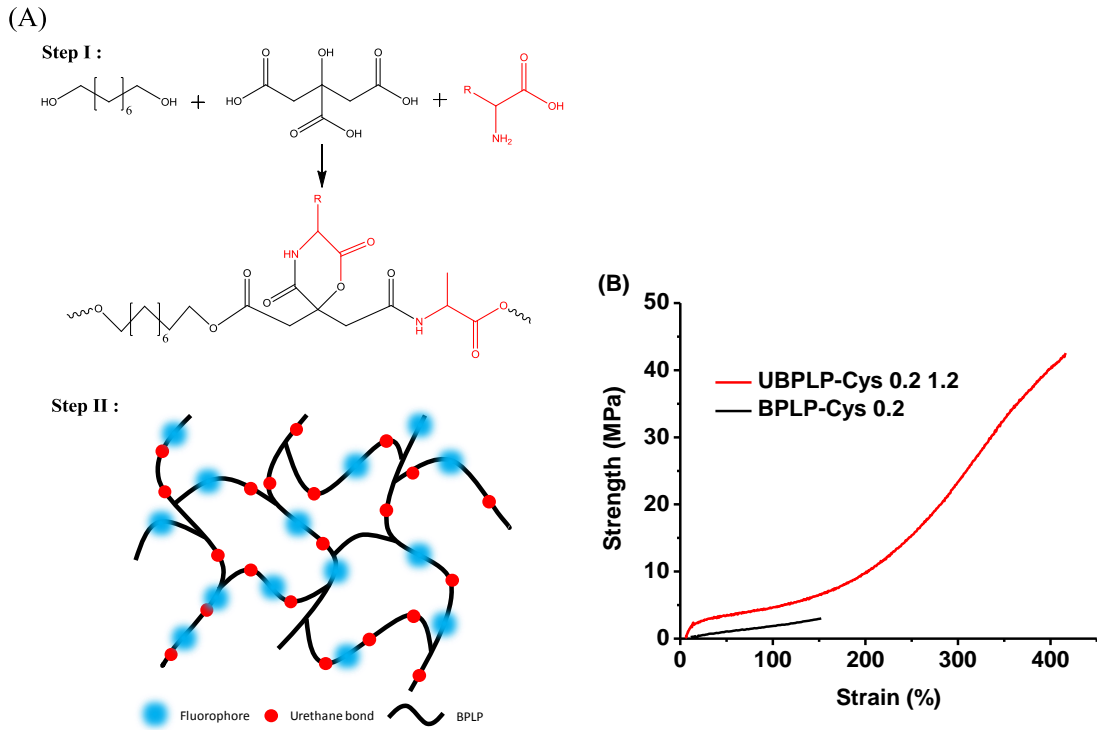
Figure 5.1 Synthesis of UBPLPs (a) Synthesis schematic of UBPLP polymers. (b) Stress-Strain curve of UBPLP-Cys 0.2 1.2 and BPLP-Cys

In the second step, BPLP was used as precursor to react with 1,6-hexamethyl diisocyanate (HDI) to obtain UBPLP. BPLP was dissolved in 1,4-dioxane (3% w/v), and the resulting solution was allowed to react with HDI in a clean reaction flask under constant stirring at 55°C using stannous octoate as a catalyst (0.1% w/v). Various UBPLP pre-polymers were synthesized using different molar feeding ratios of BPLP:HDI (1:0.9, and 1:1.2), and different precursor (BPLP-Cys, and BPLP-Ser), which are referred to as UBPLP-Cys 0.9, UBPLP-Cys 1.2, UBPLP-Ser 0.9, and UBPLP-Cys 1.2). The reaction was terminated upon the

97

disappearance of the isocyanate peak located at 2267 cm^{-1}, which was determined by FT-IR analysis. UBPLP polymers can further be thermally cured to form a crosslinked UBPLP (CUBPLP).

5.2.2 Fluorescent property

Photoluminescence spectra of UBPLP solutions were acquired on a Shimadzu RF-5301 PC fluorospectrophotometer. All samples were set to concentration of 3% (w/v). Both the excitation and the emission slit widths were set at 1.5 nm for all samples unless otherwise stated. The emission spectra of UBPLP-Cys, and UBPLP-Ser under different excitation wavelength were recorded under same circumstance. The Williams method was used to measure the fluorescent quantum yield of the BPLP polymers.

5.2.3 In vitro degradation

Degradation studies were conducted in both phosphate buffered saline (PBS, pH=7.4) and NaOH solutions (0.01M). NaOH degradation was used to screen the polymer degradation in a short period of time. The polymer films were cut into 7mm disc using a cork borer. The initial weight of the samples was noted as W1, and they were placed in test tubes containing 10ml degradation fluids and incubated at 37°C for the period of study. At pre-determined time points, the samples were removed and washed thoroughly with deionized water (3 times) to remove any residual salt or base. The samples were then lyophilized for 3d to remove traces of water and weighted as W2. Degradation was determined as (W1-W2) / W1 x 100%.

5.2.4 Triphasic graft fabrication

Multi-phasic small diameter vascular grafts were fabricated to replicate the stratified architecture of native vessels. Briefly, 3 mm outer diameter steel rods were dip coated with a pre-polymer solution (3% w/v) in 1,4-dioxane, and coated with NaCl (99% purity) with an average size of 1-20μm. Next, NaCl with an average size of 1-20 um was mixed with a pre-polymer solution in a 1:5 polymer to salt ratio, and mixed until a viscous paste was formed. The paste was then transferred onto the steel rods to create a 200 um-thick layer. Next, NaCl with

an average size of 150-250µm was mixed with a pre-polymer solution in a 1:10 polymer to salt ratio, and mixed until a viscous paste was formed. The paste was then transferred onto the steel rods to create an 800 µm thick layer. The steel rods were placed in a laminar flow hood overnight, and then transferred to an oven maintained at 80C for 4 days. After polymer crosslinking, the steel rods were immersed in deionized water with complete water changes every 6 hours. The complete removal of NaCl was determined with silver nitrate, and the vascular grafts were dried using lyophilization. Graft morphology was examined by scanning electron microscopy (SEM) (Hitachi S-3000N, Hitachi Science System, Ibaaki, Japan).

5.2.5 Mechanical Test

Tensile testing, suture retention, and burst pressure were carried out on the biphasic scaffolds. All mechanical testing was carried out on a MTS Insight2 mechanical tester (MTS System, Minneapolis, MN) fitted with a 10N load cell (Model 569326-02, MTS System, Minneapolis, MN). A sample size of n=5 was used for all the following tests.

For tensile tests, the triphasic scaffolds were cut into rectangular strips and their dimensions were recorded using a digital caliper. The samples were pulled at a rate of 500mm/min and elongated to failure. Values were converted to strss-strain and the initial modulus was calculated from the initial gradient of the resulting curve (0-10% elongation). The results are presented as the means ± standard deviation. Suture retention was tested as previously described methods. Briefly, the scaffolds were cut into rectangular specimens with 15 x 6mm (length x width) dimensions. At 2mm from the short edge of the rectangular segment, a Prolene 5-0 suture (Ethicon) was inserted and tied to form a loop. One set of clamps of the tensile tester was used to secure the sample and the second set was used to clamp and pull the looped suture at a deflection rate of 2mm/s, till suture pull out occurred. The peak load recorded was reported as the suture retention strength. Burst pressure of triphasic graft was evaluated using previously described technique. Briefly, one end of the graft was connected to a digital pressure gauge (VWR International) and the other end was connected to a 60mL syringe. The

syringe was filled with PBS and mounted on an Infusion/Withdrawal pump (Harvard Apparatus, Millis, MA) which have been pre-programmed with an output rate of 0.67 mL/min. The burst pressure was recorded as the maximum pressure measured by the gauge before the graft burst.

5.2.6 Nanoparticle Fabrication and drug release

The UBPLPs nanoparticles were prepared using a nanoprecipitation technique. To prepare polymer solutions for nanoprecipitation, UBPLPs were synthesized in tetrahydrofuran (THF) instead of 1,4-dioxane. Concentration of final solution was finalized to 3% (w/v). 10 mL of a polymer solution was added dropwisely to 20 ml of deionized water/PBS under magnetic stirring at a speed of about 400 rpm. The setup was left overnight in a chemical hood to let the acetone evaporate. Particle size was measured by Dynamic Laser Scattering (DLS). Morphology of nanoparticles was observed by transmission electron microscope (TEM).

For drug release, 5-fluouracil (5F) was loaded into nanoparticles by two formulae. Formula A: 0.01g 5F was dissolved in 10mL UBPLPs polymer solution (in THF) with gentle heating in a sealed glass tube. The mixture was added dropwisely into 20mL PBS. Formula B: 10mL regular polymer solution was added dropwisely into 20mL PBS with 0.01g 5F pre-dissolved in. Setup of both formulae was left overnight in a chemical hood to let the acetone evaporate. To determine the drug loading efficiency, 1mL 5F-loaded nanoparticle solution was diluted in PBS to make a final volume of 20mL. The diluted nanoparticle solution was ultra-speed centrifuged, and absorbance of the liquid was examined by Infinite200 microplate reader (Tecan Group Ltd., Switzerland) at 270nm. Loading efficiency was calculated using following equation:

Loading efficiency% = $\frac{Initial\ amount\ of\ drug - amount\ of\ drug\ in\ solution}{Initial\ amount\ of\ drug}$

The in vitro drug release study was performed in an sealed glass beaker with 100mL phosphate buffer saline (PBS, pH 7.4) at 37 °C. Next, 5-FU-loaded UBPLP nanoparticles from each formula were placed in a dialysis bag (Mw cut-off of 1000 Da). The dialysis bag was then

immersed in the release medium and kept in a horizontal laboratory shaker at a constant temperature (37 °C) and stirring (100 rpm). To measure the drug release content, samples (1 mL) were removed periodically and an equivalent volume was replaced by the fresh PBS. The amount of released 5-FU was analyzed with a microplate reader at 270 nm. 5 samples were tested to obtain average.

5.2.7 In Vitro Cytotoxicity

Cytotoxicity of UBPLP was evaluated *in vitro* by seeding the polymer films with the NIH 3T3 fibroblasts (ATCC). The cell proliferation was performed using Methylthiazoletetrazolium (MTT) cell proliferation and viability assay kit. PLGA (25/75) film was used as control. All testing films were cut into cylindrical discs (7mm in diameter) and sterilized in 70% ethanol for 3h, followed by another 30min of UV light exposure. The cells were cultured in Dulbecco's modified eagle's medium (DMEM), which had been supplemented with 10% fetal bovine serum (FBS) and 1% penicillin streptomycin. The culture flasks were maintained in an incubator at 37°C, 5% CO_2m and 95% relative humidity. The cells were allowed to grow to the fourth passage, trypsinized, centrifuged, and suspended into media to obtain a seeding density of 1 x 10^5 cells/mL. MTT assay analysis was performed at 1, 3, and 7d of culture. At the end of each time point, the assay was performed as per the manufacturer's protocol. Briefly, the old media was aspirated, and each specimen was thoroughly washed 3 times with PBS to remove any loosely attached cells and dead cells. 100 ml of incomplete media (DMEM without serum) was added to these specimens. 10 ml of 3-(4,5-dimethylthiazol-2yl)-diphenyltetrazolium bromide solution was then added to the wells containing the cells and the blanks, and they were incubated at 37 °C for 3 h. At the end of incubation period, the mixture of the MTT solution and incomplete media was aspirated and replaced with 100 ml of MTT solvent. Dissolution of formazan crystals was facilitated by constantly agitating the well plate on an orbital shaker for 15 min. Absorbance was analyzed with an Infinite200 microplate reader (Tecan Group Ltd., Switzerland) at 570 nm, with a reference wavelength of 690 nm, within 30 min of MTT solvent addition.

5.2.8 In vivo fluorescence Imaging

For nanoparticle/scaffold bioimaging in vivo, UBPLP-Ser 1.2 nanoparticles (2% wt in PBS, 80 nm in diameter, sterilized by filtering through a syringe filter (0.22 μm) and UBPLPs triphasic scaffolds (5mm in length, sterilized by 70% ethanol and UV light) were injected/implanted s.c. in Black mice (C57BL/6 J). The mice were then imaged using a Kodak Imaging System, as described previously immediately after the implantation. Animals were cared for in compliance with the regulations of the animal care and use committee of The University of Texas at Arlington.

5.2.9 Statistical Method

Data were expressed as the mean ± standard deviation. The statistical significance between two sets of data was calculated using a One-way ANOVA. Data were considered to have significant difference, when a p-value of 0.05 or less was obtained.

<u>5.3 Results and Discussions</u>

In previous study, BPLPs showed strong elasticity and good processability. However, the great loss of mechanical property upon scaffold fabrication jeopardizes its use for cardiovascular tissue engineering. In the other hand, the instability of BPLP nanoparticles makes it difficult to be exploited as theranostic probes. A higher molecular weight and stronger mechanical property need to be achieved to address those issues. Urethane bond doping is a commonly used method for chemically crosslinking and increasing mechanical properties [194]. The mild reaction condition and specificity of isocyanate chemistry will only consume hydroxyl and carboxylic groups and keep fluorophore intact. The consumption of functional groups will also reduce the sticky nature, thus increase the stability of nanoparticles.

The stress-strain curves were characteristic of elastomers (Figure 5.1B). After 1d postpolymerization, tensile strength of CUBPLP-Cys 1.2 has been increased by 8 folds, compared to BPLP-Cys. Elongation was also raised from 160% of BPLP-Cys to 420%. The results not only confirm the successful incorporation of urethane bond, but also prove the

concept that urethane bond doping will dramatically increase the mechanical strength and elasticity. The effect of postpolymerization conditions on the mechanical properties of UBPLP-Cys 1.2 was also investigated. From Figure 5.2A and B, postpolymerization increased polymer tensile strength and Young's modulus with a corresponding decrease in elongation. However, mechanical property of UBPLP-Cys 1.2 showed no significant change after 1d postpolymerization. This is because the side hydroxyl and carboxyl groups of octylene citrates have been partially occupied by cysteine and also partially reacted by isocyanate, which lowered the postpolymerization potential. It was found that mechanical property could be controlled by feeding formulae (Figure 5.2C and D). After 1d postpolymerization, tensile strength has been raised from 13.708±2.192 MPa of CUBPLP-Cys 0.9 to 39.314±6.966 MPa of CUBPLP-Cys 1.2. Stronger mechanical property and elasticity with increased feeding ratio of diisocyanate is due to the increased amount of urethane bond. CUBPLP-Ser 1.2 had a tensile strength of 49.926±7.002MPa which is higher than that of CUBPLP-Cys 1.2. Due to the –OH containing R-group of serine, BPLP-Ser provided more active sites for isocyanate reaction. The increased crosslinking site resulted in loss of elasticity. Compared with CUBPLP-Cys 1.2, Young's modulus of CUBPLP-Ser 1.2 was 18.867±2.234MPa, which is higher than 13.293±1.962MPa. The elongation was also decreased from 381.838±25.340% to 313.22±26.139%. Conclusions can be drawn that mechanical property of UBPLPs can be manipulated by (1) postpolymerization condition (2) feeding ratio of diisocyanate and (3) choice of amino acids. Tensile strength up to 49.410±6.165MPa and elongation up to 456.603±62.499% were obtained under the investigated synthesis conditions. This is a dramatic improvement over the previously reported mechanical property of BPLP, which had tensile strength up to 6.5±0.8MPa and elongation up to 240±36% [52]. The elasticity of UBPLP can be tailored to match that of the cardiovascular tissue, such as smooth muscle tissue that exhibit elongation of 300% [8].
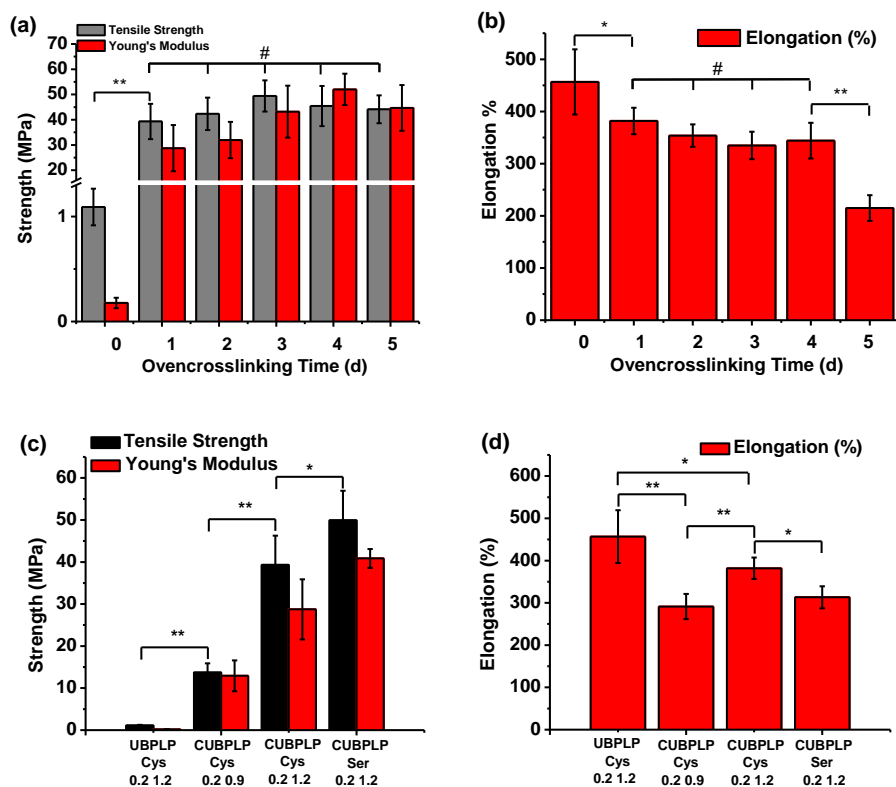
Figure 5.2 Mechanical properties of UBPLPs. Effects of postpolymerization conditions on the UBPLP-Cys 1.2 (a) tensile strength and Young's modulus, and (b) elongation. Effects of feeding formulation on the (c) tensile strength and Young's modulus, and (d) elongation. **p<0.01, *p<0.05, #p>0.05; N=8.

Fluorescent property of UBPLPs was also evaluated. The fluorophore of BPLPs has been studied in detail previously, and 6-membered ring structure was claimed to contribute to the fluorescence. Among all BPLPs based on 20 essential amino acids, BPLP-Cys and BPLP-Ser had strongest fluorescence with quantum yield of 62.3% and 26.0% respectively. Due to the Red-edge Effect (REE) [186] BPLP-Ser exhibited excitation-dependent emission spectra which are different from BPLP-Cys which had a fixed emission wavelength. The emission spectra of UBPLP-Cys 1.2 and UBPLP-Ser 1.2 solution were first recorded under different excitation wavelength. Figure 5.3A showed that UBPLP-Cys 1.2 inherited excitation-independent emission spectra from its precursor. Same inheritance from BPLP-Ser to UBPLP-Ser has been proved.

UBPLP-Ser emitted different emission with changing excitation wavelength (Figure 5.3B). This result provided evidence that 6-membered ring structure was remained intact during the synthesis of UBPLPs. Quantum yield of UBPLP-Cys 1.2 was 38.65%, and UBPLP-Ser 1.2 had a quantum yield of 19.38%. Due to the chain extension of BPLPs, average number of fluorophores per polymer chain was increased, which leads to self-quenching of the fluorescence [206]. This explained the loss of fluorescence intensity after urethane bond doping.
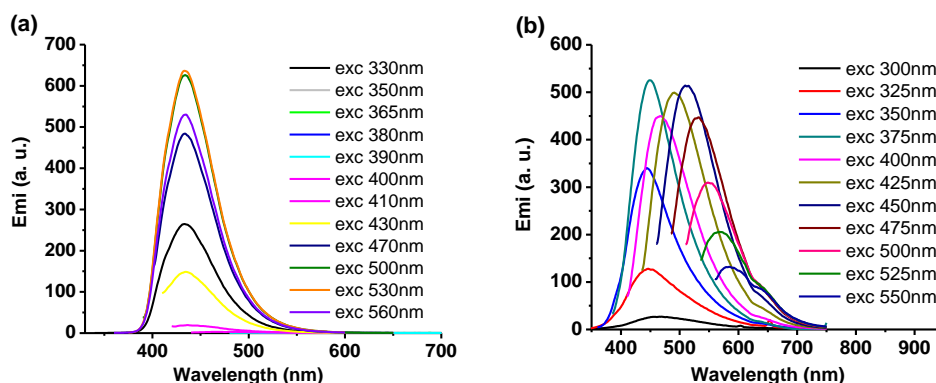
Figure 5.3 Emission spectra under different excitation wavelength (a) UBPLP-Cys and (b) UBPLP-Ser.

Degradation profiles of CUBPLPs under different conditions are presented in Figure 5.4. All tested polymers were post-polymerized for 1d. From the accelerated degradation (in NaOH), with less urethane bond doping, CUBPLP-Cys 0.9 reached complete degradation faster than CUBPLP-Cys 1.2. This is because of the higher resistance to hydrolysis of urethane bond than ester bond. A longer degradation time of CUBPLP-Ser 1.2 was observed. This result further confirmed that the –OH group from serine joined reaction with isocyanate group, which lead to formation of more urethane bonds. The compelet degradation in physiological condition was proved with PBS as degradation fluids. CUBPLP-Cys 1.2 degraded completely within 80 days. It can be concluded that degradation rate of UBPLPs can be adjusted by feeding ratio of diisocyanate and choice of amino acids, which is same as mechanical property. Therefore,

UBPLPs with a tunable mechanical property and degradation rate can be tailored to meet the requirements of various soft tissue engineering applications.
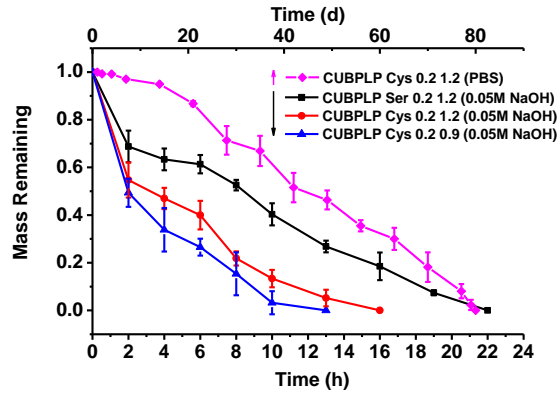
Figure 5.4 In vitro degradation study of CUBPLP-Cys and CUBPLP-Ser in different degradation fluids

In addition to matching the mechanical property of native tissue, a successful design of graft should also be made to replicate the stratified architecture of native blood vessel. Due to the complexity of the microarchitectural of native vascular tissue, facilitating cell growth and extracellular matrix (ECM) compartmentalization is critical to mimic a native-like tissue and also enable *in situ* vascular tissue engineering. To address this issue, a triphasic scaffold composed of a rough surface as inner lumen, middle layer of porous scaffold with pore size of 1-20μm, and outer layer of porous scaffold with pore size of 150-250μm was fabricated. It has been demonstrated that a rough surface is more favorable for endothelial cells [207], and pore size of 1-20μm is preferable for cell migration [208]. Pore size of 150-250μm has been proven to be ideal for growth of fibroblast and formation of ECM [209]. SEM images were taken to observe scaffold morphology (Figure 5.5). From Figure 5.5A, it can be seen that CUBPLPs can be easily fabricated into tubular architecture. Since layers were welded by postpolymerization, the integration was seamless. It can be clearly observed in Figure 5.5B. The pore size of middle layer and outer layer can also be confirmed. The roughness of the inner surface and porous

106

surface of outer layer were shown in Figure 5.5C and 5.5D respectively. This design can allowed separated seeding for different cell types. Endothelial cells can be seeded specifically on the inner surface, and dynamic bioreactor may also be applied to improve cell growth and phenotype [210]. Smooth muscle cells and fibroblasts can be seeded directly on outer layer, and the large pore size can improve cell growth and ECM secretion. This design of triphasic tubular scaffold was also addressed to be exploited for *in situ* vascular tissue engineering. Previous studies showed that surface roughness improved stem cell attach and differentiation [211].
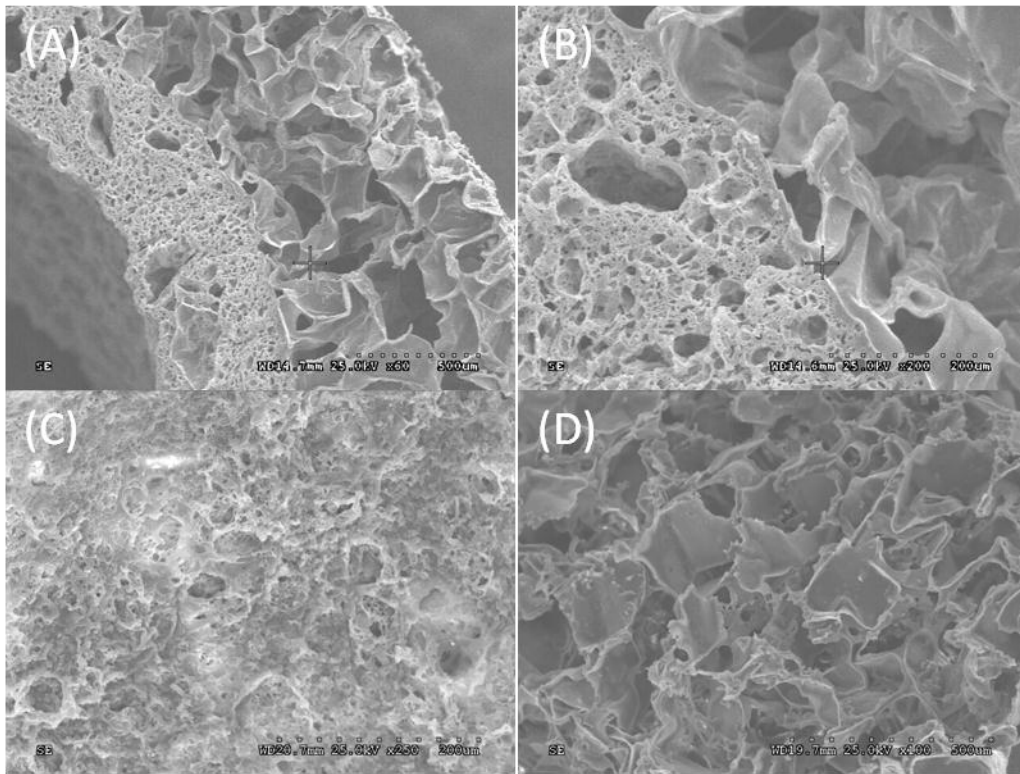
Figure 5.5 SEM images of UBPLPs triphasic scaffold (a) cross-section (b) seamless integration of outer layer and middle layer (c) Inner lumen of surface roughness (d) outer lumen of porous structure.

To evaluate the mechanical property of this triphasic scaffold, burst pressure and suture retention were investigated. Burst pressure is the key parameter of the vessel strength of a

tissue engineering vascular graft, and suture retention is critical for surgery handling. From Figure 5.6, mechanical property of scaffold was affected by feeding ratio of diisocyanate. As all resistance to arterial blood pressure is mainly provided by the middle layer of less porosity, there was no significant difference between CUBPLP-Cys 1.2 and CUBPLP-Ser 1.2. Both of them exhibited burst pressure around 800 mmHg. In previous studies, biphasic scaffold with a non-porous inner layer has been designed for POC [143]. The solid inner layer contributed most of mechanical strength. With layer thickness of 400μm, POC biphasic scaffold had a burst pressure below 1000mmHg. However, the solid inner layer completely blocks the cell migration. With a porous middle layer, current design of triphasic scaffold not only allowed cellular infiltration, but also maintained a burst pressure of 800mmHg, which was sufficient to withstand arterial blood pressure [212]. As shown in Figure 5.6, triphasic scaffold of CUBPLP-Cys 1.2 had the highest suture retention of 1.79±0.1N, which was significantly higher than the surgical requirement [212]. In addition to achieving the desired mechanical property of tissue engineering vascular graft, the design of triphasic scaffold showed great improvements in replicating native structure of blood vessel than previous biphasic scaffold.
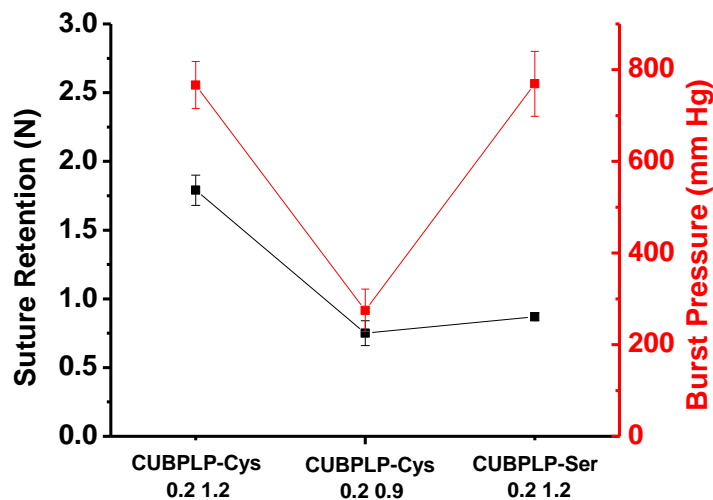
Figure 5.6 Suture retention strength and burst pressure of triphasic scaffold of different CUBPLPs

The biocompatibility of UBPLPs was evaluated in forms of both films and degradation products. From Figure 5.7A, comparable cell viability was obtained on all CUBPLPs and PLGA films. All films showed increasing cell number during the 7d cell culture. The growth and proliferation of 3T3 fibroblasts in the *in vitro* study demonstrated good material-cell interaction of CUBPLPs. From SEM image, 3T3 fibroblasts had stretched morphology and formed a cell layer that covered film surface. The healthy cell morphology confirmed the cell friendly surface of CUBPLPs. As a family of fully biodegradable polymers, the cytotoxicity of degradation products is also important. Since degradation of urethane, amide, and ester bonds are mostly hydrolysis, maximum amount of degradation products were yielded by accelerated degradation in strong base solution [213].The MTT results presented in Figure 5.7B indicated that after 24h incubation, all investigated UBPLPs and CUBPLPs exhibited comparable cytotoxicity as PLGA at all dilutions, which has been proved by FDA. Therefore, in view of high dilution by plasma of *in vivo* degradation, degradation products of CUBPLPs and UBPLPs can potentially meet safety requirements of biomedical applications.
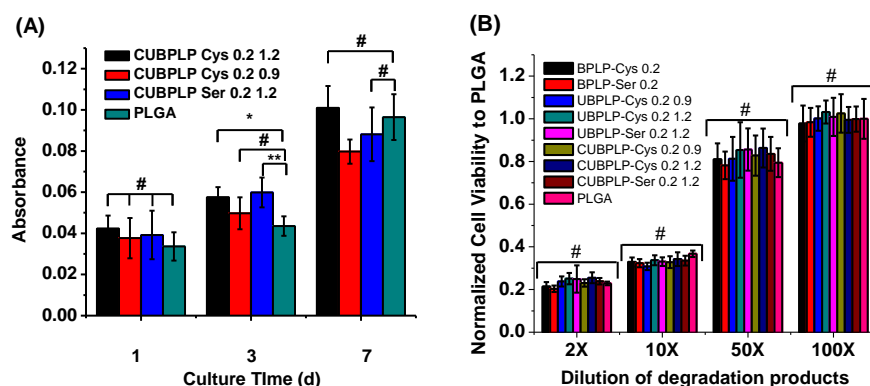
Figure 5.7 In vitro cytotoxicity of UBPLPs (A) Evaluation of UBPLPs films at different time period, PLGA films as control (B) Evaluation of UBPLPs degradation products after 24h. All values of absorbance were normalized to the PLGA at 100x dilution. **$p<0.01$, *$p<0.05$, #$p>0.05$; N=6.

UBPLPs have also been fabricated into nanoparticles to evaluate the potential for successful theranostic probe. Previously, BPLPs have been fabricated into nanoparticles with a

size of 80nm via nanoprecipation technique [52]. Due to the sticky nature and acidity, BPLP nanoparticles were only stable in DI water, and dispersed in PBS. This critical defect limited its use in physiological environment. The main cause was considered as the superfluous hydrophilic groups of polymer backbone. During the reaction between BPLPs and diisocyanate, large amount of carboxyl and hydroxyl groups have been consumed, which can be confirmed by a neutralized pH of UBPLPs nanoparticles solution compared to BPLPs nanoparticles (from 4.3 to 6.3). Using nanoprecipitation technique, UBPLP-Ser 1.2 was able to form stable nanoparticles in PBS. The average size of nanoparticle was 103nm, measured by DLS. This result was confirmed by TEM images of nanoparticles in PBS. From Figure 5.8A, nanoparticles showed a sphere shape with an average diameter of 103nm. An evenly dispersion of nanoparticles was also observed (Figure 5.8A inset). The cytotoxicity of UBPLPs nanoparticles was also evaluated by MTT assay (Figure 5.8B). All the values of absorbance were normalized to the PLGA at 100x dilution. Due to the reduced acidity, UBPLPs nanoparticles were found to be more cyto-compatible than BPLPs at high concentration (10mg/mL, 2x dilution). Cell viability of UBPLPs nanoparticles was found to be significantly higher than quantum dots under all dilution, and UBPLPs nanoparticles showed a comparable cytotoxicity of PLGA nanoparticles at 2x, 10x, and 50x dilution. Since all nanoparticles as a delivery system or imaging probe will have dilution in the body fluids [214], cytotoxicity of low concentration is critical to nanoparticle solutions. At 100x dilution, cell viability of UBPLP-Cys 1.2 nanoparticles is significantly higher than that of PLGA nanoparticles. All the results supported the good cytocompatibility of UBPLPs nanoparticles.
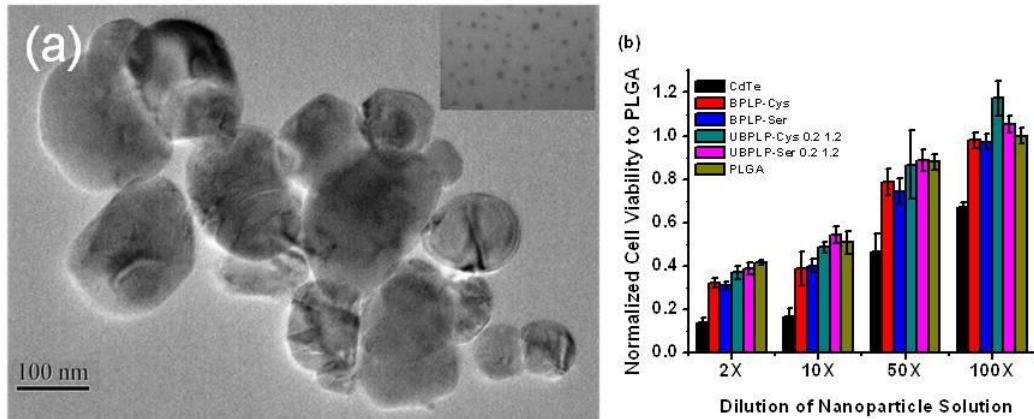
Figure 5.8 Characterization of UBPLPs nanoparticles (a) Morphology of UBPLP-Ser 1.2 nanoparticles, and inset was captured under higher magnification showing evenly dispersion of nanoparticles. (b) Evaluation of cytotoxicity of BPLPs and UBPLPs nanoparticle solutions at different dilution.

The capability of UBPLPs nanoparticles as a drug delivery device was evaluated by *in vitro* encapsulation and release of 5-fluorouracil (5F). Since 5F can be dissolved in both PBS and THF, two formulae of drug encapsulation were conducted. When 5F was dissolved in polymer solution (formula A), a loading efficiency of 57.6% was obtained. Interestingly, loading efficiency was dramatically increased to 91.84% when 5F was dissolved in PBS (formula B). This is because of the loose physical bonding between drug and nanoparticle surface in formula B. This difference also influenced *in vitro* drug release profile (Figure 5.9). From Figure 5.9A, formula B reached 90% release of 5F within 24h. However, formula A reached complete release after 120h. For the first 24h release (Figure 5.9B), formula B showed a 53% burst release within 2h, while formula A exhibited a more sustained drug release. It can be concluded that potential of UBPLPs nanoparticles as controlled drug delivery device was demonstrated by both formulae. Although high loading efficiency can be obtained by formula B, the loose bonding between drug and nanoparticle surface lead to burst release. Since majority of anti-cancer drug is hydrophobic, formula A can be served as protocol for future studies.
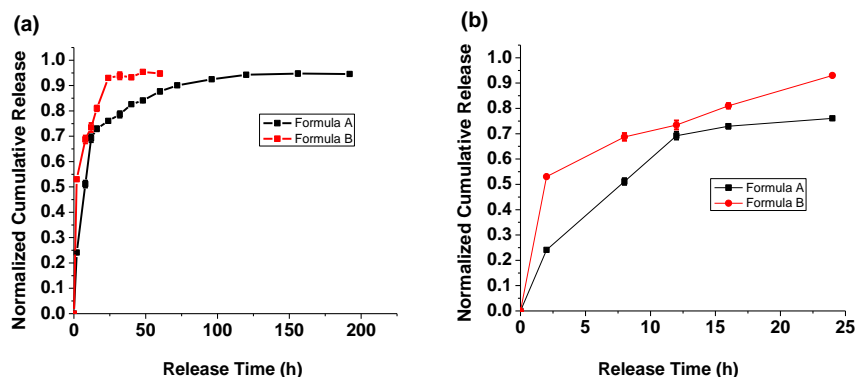
Figure 5.9 In vitro drug release profiles of two loading formulae (a) complete release and (b) 24h

In vivo imaging studies has also been conducted for evaluation of conspicuity. Both CUBPLP-Cys 1.2 and CUBPLP-Ser 1.2 tubular triphasic scaffolds were implanted subcutaneously onto the back of Black mice (C57BL/6 J). From Figure 5.10A, both scaffolds were readily detected by a non-invasive imaging system. Due to the different fluorescent properties of UBPLP-Cys and UBPLP-Ser, two exc/emi pairs were used for detection. Taking into account the following, light scattering, absorption by hemoglobin, strong infrared filtration of water, and tissue autofluorescence, fluorescent materials with NIR emission is ideal for *in vivo* non-invasive bioimaging [5]. Therefore, with an optimal exc/emi pair at 550nm/600nm, UBPLP-Ser was more suitable than UBPLP-Cys. However, many attentions have been focused on development of minimally invasive imaging techniques [215]. Eliminating the interference from physiological environment, minimally invasive imaging will be ideal to provide real-time monitoring of the ultra-strong blue fluorescence from UBPLP-Cys. The real-time monitoring of UBPLPs scaffold *in situ* is able to provide accurate information on scaffold degradation and tissue infiltration/regeneration without traumatically explanting samples or sacrificing animals. Same procedure was conducted to evaluate *in vivo* conspicuity of UBPLP-Ser nanoparticles (Fgure 5.10B). It was found that clear fluorescence signal was detected with a concentration of 5mg/ml. Since the capability of UBPLP-Ser 1.2 nanoparticles as drug delivery device has been

demonstrated, the successful *in vivo* detection proved that UBPLP-Ser 1.2 nanoparticles had great potential for theranostic probes. Although polymer-fluorescent dye composites have showed promising results, UBPLP nanoparticles, as a "biodegradable polymeric dots", not only are able to avoid long-term toxicity associated with traditional fluorescent dye, but also greatly reduce the complexity of the system. Moreover, with the flexible and simple synthesis of UBPLPs, much functionality can be introduced by using specific monomers, such as vinyl group containing diacid, water soluble diol, and stimulus-responsible monomers. Thus, UBPLPs can be manipulated for various biomedical applications on demand. Due to the uniqueness of excitation-dependent emission of UBPLP-Ser, smart design of UBPLP-Ser and Cys pair can be obtained based on fluorescence resonance energy transfer (FRET). We are confident to predict that UBPLPs will bring a paradigm shift in the use of biodegradable implant polymers in a broad range of biological and biomedical fields including biosensors, cellular bioimaging, fluorescence-guided surgery, theranostic nanomedicine, drug delivery, and regenerative medicine.
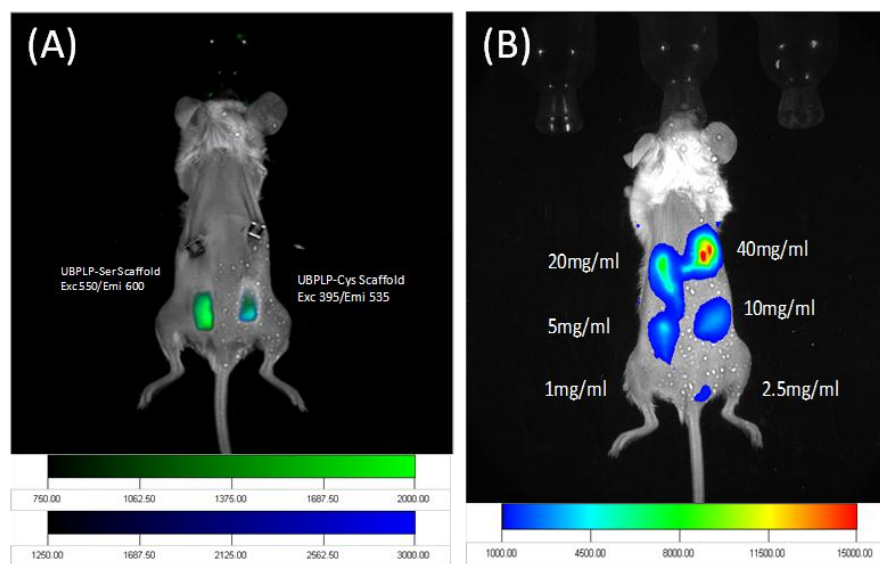
Figure 5.10 In vivo imaging study (a) Combined fluorescent imaging of *In vivo* implantation of UBPLP-Cys and Ser triphasic scaffold under different emi/exc pairs. UBPLP-cys under exc 395nm/emi 535nm and UBPLP-Ser under exc 550nm/ emi 600nm (b) UBPLP-Ser nanoparticles with different concentrations injected subcutaneously on the back of white mouse. 100 μl was injected at each point. Exc/emi pair is 550nm/600nm

113

5.4 Conclusion

We have developed a new class of urethane-doped biodegradable photoluminescent polymers (UBPLPs). UBPLPs demonstrated a soft but strong mechanical property. The triphasic scaffold met the mechanical requirements for tissue engineering vascular graft and was strong enough for surgical handling. UBPLPs were also fabricated into stable nanoparticles in PBS, and showed a controlled release of anti-cancer drug. Degradation products and nanoparticles of UBPLPs showed comparable cytotoxicity as PLGA. Fluorescence of both UBPLPs scaffolds and nanoparticles were clearly detected *in vivo*. The development of UBPLPs should contribute to fundamental science of biomaterials for tissue engineering and shed new light on "biodegradable polymeric dots" for theranostic application.

REFERENCE

1. Anderson JM, Shive MS. Biodegradation and biocompatibility of PLA and PLGA microspheres. Advanced Drug Delivery Reviews 1997 Oct 13;28(1):5-24.

2. Kim K, Yu M, Zong XH, Chiu J, Fang DF, Seo YS, et al. Control of degradation rate and hydrophilicity in electrospun non-woven poly(D,L-lactide) nanofiber scaffolds for biomedical applications. Biomaterials 2003 Dec;24(27):4977-4985.

3. Nerem RM, Seliktar D. Vascular tissue engineering. Annual Review of Biomedical Engineering 2001;3:225-243.

4. Shin H, Jo S, Mikos AG. Biomimetic materials for tissue engineering. Biomaterials 2003 Nov;24(24):4353-4364.

5. Terai T, Nagano T. Fluorescent probes for bioimaging applications. Current Opinion in Chemical Biology 2008 Oct;12(5):515-521.

6. Artzi N, Oliva N, Puron C, Shitreet S, Artzi S, bon Ramos A, et al. In vivo and in vitro tracking of erosion in biodegradable materials using non-invasive fluorescence imaging. Nat Mater Sep;10(9):704-709.

7. Janib SM, Moses AS, MacKay JA. Imaging and drug delivery using theranostic nanoparticles. Advanced Drug Delivery Reviews 2010 Aug 30;62(11):1052-1063.

8. Webb AR, Yang J, Ameer GA. Biodegradable polyester elastomers in tissue engineering. Expert Opin Biol Ther 2004 Jun;4(6):801-812.

9. Wang Y, Ameer GA, Sheppard BJ, Langer R. A tough biodegradable elastomer. Nat Biotechnol 2002 Jun;20(6):602-606.

10. Andrzejewska E. Photopolymerization kinetics of multifunctional monomers. Progress in Polymer Science 2001 May;26(4):605-665.

11. Wang F, Tan WB, Zhang Y, Fan XP, Wang MQ. Luminescent nanomaterials for biological labelling. Nanotechnology 2006 Jan 14;17(1):R1-R13.

12. Dey J, Xu H, Shen J, Thevenot P, Gondi SR, Nguyen KT, et al. Development of biodegradable crosslinked urethane-doped polyester elastomers. Biomaterials 2008 Dec;29(35):4637-4649.

13. Wang SG, Cui WJ, Bei JZ. Bulk and surface modifications of polylactide. Analytical and Bioanalytical Chemistry 2005 Feb;381(3):547-556.

14. Middleton JC, Tipton AJ. Synthetic biodegradable polymers as orthopedic devices. Biomaterials 2000 Dec;21(23):2335-2346.

15. Meredith JC, Tona A, Elgendy H, Karim A, Amis E. Combinatorial characterization of biodegradable polymers. Abstracts of Papers of the American Chemical Society 2001 Apr 1;221:U299-U300.

16. Vroman I, Tighzert L. Biodegradable Polymers. Materials 2009 Jun;2(2):307-344.

17. Amsden B. Curable, biodegradable elastomers: emerging biomaterials for drug delivery and tissue engineering. Soft Matter 2007;3(11):1335-1348.

18. Nijst CLE, Bruggeman JP, Karp JM, Ferreira L, Zumbuehl A, Bettinger CJ, et al. Synthesis and characterization of photocurable elastomers from poly(glycerol-co-sebacate). Biomacromolecules 2007 Oct;8(10):3067-3073.

19. Finn MG, Fokin VV. Click chemistry: function follows form. Chemical Society Reviews 2010;39(4):1231-1232.

20. Hong J, Luo Q, Wan XM, Petrovic ZS, Shah BK. Biopolymers from Vegetable Oils via Catalyst- and Solvent-Free "Click" Chemistry: Effects of Cross-Linking Density. Biomacromolecules 2012 Jan;13(1):261-266.

21. Langer R, Vacanti JP. Tissue Engineering. Science 1993 May 14;260(5110):920-926.

22. Sun BJ, Lai HJ, Wu PY. Integrated Microdynamics Mechanism of the Thermal-Induced Phase Separation Behavior of Poly(vinyl methyl ether) Aqueous Solution. Journal of Physical Chemistry B 2011 Feb 17;115(6):1335-1346.

23. Salerno A, Di Maio E, Iannace S, Netti PA. Tailoring the pore structure of PCL scaffolds for tissue engineering prepared via gas foaming of multi-phase blends. Journal of Porous Materials 2012 Apr;19(2):181-188.

24. Dahms SE, Piechota HJ, Dahiya R, Lue TF, Tanagho EA. Composition and biomechanical properties of the bladder acellular matrix graft: comparative analysis in rat, pig and human. British Journal of Urology 1998 Sep;82(3):411-419.

25. Chandran KB. Cardiovascular Biomechanics. New York: New York University Press, 1992.

26. Balguid A, Rubbens MP, Mol A, Bank RA, Bogers AJJC, Van Kats JP, et al. The role of collagen cross-links in biomechanical behavior of human aortic heart valve leaflets - Relevance for tissue engineering. Tissue Engineering 2007 Jul;13(7):1501-1511.

27. Millesi H, Zoch G, Reihsner R. Mechanical-Properties of Peripheral-Nerves. Clinical Orthopaedics and Related Research 1995 May(314):76-83.

28. Monson KL, Goldsmith W, Barbaro NM, Manley GT. Axial mechanical properties of fresh human cerebral blood vessels. Journal of Biomechanical Engineering-Transactions of the Asme 2003 Apr;125(2):288-294.

29. Wren TAL, Yerby SA, Beaupre GS, Carter DR. Mechanical properties of the human Achilles tendon. Clinical Biomechanics 2001 Mar;16(3):245-251.

30. Moon DK, Woo SL, Takakura Y, Gabriel MT, Abramowitch SD. The effects of refreezing on the viscoelastic and tensile properties of ligaments. J Biomech 2006;39(6):1153-1157.

31. Wang YD, Ameer GA, Sheppard BJ, Langer R. A tough biodegradable elastomer. Nature Biotechnology 2002 Jun;20(6):602-606.

32. Liu QY, Jiang L, Shi R, Zhang LQ. Synthesis, preparation, in vitro degradation, and application of novel degradable bioelastomers-A review. Progress in Polymer Science 2012 May;37(5):715-765.

33. Santerre JP, Woodhouse K, Laroche G, Labow RS. Understanding the biodegradation of polyurethanes: From classical implants to tissue engineering materials. Biomaterials 2005 Dec;26(35):7457-7470.

34. Guelcher SA. Biodegradable polyurethanes: synthesis and applications in regenerative medicine. Tissue Eng Part B Rev 2008 Mar;14(1):3-17.

35. Gisselfalt K, Edberg B, Flodin P. Synthesis and properties of degradable poly(urethane urea)s to be used for ligament reconstructions. Biomacromolecules 2002 Sep-Oct;3(5):951-958.

36. Spaans CJ, Belgraver VW, Rienstra O, de Groot JH, Veth RPH, Pennings AJ. Solvent-free fabrication of micro-porous polyurethane amide and polyurethane-urea scaffolds for repair and replacement of the knee-joint meniscus. Biomaterials 2000 Dec;21(23):2453-2460.

37. Stachelek SJ, Song C, Alferiev I, Defelice S, Cui X, Connolly JM, et al. Localized gene delivery using antibody tethered adenovirus from polyurethane heart valve cusps and intra-aortic implants. Gene Therapy 2004 Jan;11(1):15-24.

38. Martina M, Hutmacher DW. Biodegradable polymers applied in tissue engineering research: a review. Polymer International 2007 Feb;56(2):145-157.

39. Sun HL, Meng FH, Dias AA, Hendriks M, Feijen J, Zhong ZY. alpha-Amino Acid Containing Degradable Polymers as Functional Biomaterials: Rational Design, Synthetic Pathway, and Biomedical Applications. Biomacromolecules 2011 Jun;12(6):1937-1955.

40. Cohn D, Salomon AF. Designing biodegradable multiblock PCL/PLA thermoplastic elastomers. Biomaterials 2005 May;26(15):2297-2305.

41. Cohn D, Hotovely-Salomon A. Biodegradable multiblock PEO/PLA thermoplastic elastomers: molecular design and properties. Polymer 2005 Mar 10;46(7):2068-2075.

42. Heijkants RGJC, van Calck RV, van Tienen TG, de Groot JH, Buma P, Pennings AJ, et al. Uncatalyzed synthesis, thermal and mechanical properties of polyurethanes based on poly(epsilon-caprolactone) and 1,4-butane diisocyanate with uniform hard segment. Biomaterials 2005 Jul;26(20):4219-4228.

43. Kavlock KD, Pechar TW, Hollinger JO, Guelcher SA, Goldstein AS. Synthesis and characterization of segmented poly(esterurethane urea) elastomers for bone tissue engineering. Acta Biomaterialia 2007 Jul;3(4):475-484.

44. Wang WS, Ping P, Yu HJ, Chen XS, Jing XB. Synthesis and characterization of a novel biodegradable, thermoplastic polyurethane elastomer. Journal of Polymer Science Part a-Polymer Chemistry 2006 Oct 1;44(19):5505-5512.

45. Hong Y, Guan JJ, Fujimoto KL, Hashizume R, Pelinescu AL, Wagner WR. Tailoring the degradation kinetics of poly(ester carbonate urethane)urea thermoplastic elastomers for tissue engineering scaffolds. Biomaterials 2010 May;31(15):4249-4258.

46. Tang DL, Noordover BAJ, Sablong RJ, Koning CE. Metal-Free Synthesis of Novel Biobased Dihydroxyl-Terminated Aliphatic Polyesters as Building Blocks for Thermoplastic Polyurethanes. Journal of Polymer Science Part a-Polymer Chemistry 2011 Jul 1;49(13):2959-2968.

47. Nagata M, Kiyotsukuri T, Ibuki H, Tsutsumi N, Sakai W. Synthesis and enzymatic degradation of regular network aliphatic polyesters. Reactive & Functional Polymers 1996 Jun;30(1-3):165-171.

48. Sundback CA, Shyu JY, Wang YD, Faquin WC, Langer RS, Vacanti JP, et al. Biocompatibility analysis of poly(glycerol sebacate) as a nerve guide material. Biomaterials 2005 Sep;26(27):5454-5464.

49. Fidkowski C, Kaazempur-Mofrad MR, Borenstein J, Vacanti JP, Langer R, Wang YD. Endothelialized microvasculature based on a biodegradable elastomer. Tissue Engineering 2005 Jan;11(1-2):302-309.

50. Yang J, Webb AR, Ameer GA. Novel citric acid-based biodegradable elastomers for tissue engineering. Advanced Materials 2004 Mar 18;16(6):511-+.

51. Yang J, Webb AR, Pickerill SJ, Hageman G, Ameer GA. Synthesis and evaluation of poly(diol citrate) biodegradable elastomers. Biomaterials 2006 Mar;27(9):1889-1898.

52. Yang J, Zhang Y, Gautam S, Liu L, Dey J, Chen W, et al. Development of aliphatic biodegradable photoluminescent polymers. Proceedings of the National Academy of Sciences of the United States of America 2009 Jun 23;106(25):10086-10091.

53. Konig G, McAllister TN, Dusserre N, Garrido SA, Iyican C, Marini A, et al. Mechanical properties of completely autologous human tissue engineered blood vessels compared to human saphenous vein and mammary artery. Biomaterials 2009 Mar;30(8):1542-1550.

54. L'Heureux N, McAllister TN, de la Fuente LM. Tissue-engineered blood vessel for adult arterial revascularization. N Engl J Med 2007 Oct 4;357(14):1451-1453.

55. Bruggeman JP, de Bruin BJ, Bettinger CJ, Langer R. Biodegradable poly(polyol sebacate) polymers. Biomaterials 2008 Dec;29(36):4726-4735.

56. Bruggeman JP, Bettinger CJ, Langer R. Biodegradable xylitol-based elastomers: In vivo behavior and biocompatibility. Journal of Biomedical Materials Research Part A 2010 Oct;95A(1):92-104.

57. Sun ZJ, Wu L, Lu XL, Meng ZX, Zheng YF, Dong DL. The characterization of mechanical and surface properties of poly (glycerol-sebacate-lactic acid) during degradation in phosphate buffered saline. Applied Surface Science 2008 Nov 15;255(2):350-352.

58. Sun ZJ, Wu L, Huang W, Zhang XL, Lu XL, Zheng YF, et al. The influence of lactic on the properties of Poly (glycerol-sebacate-lactic acid). Materials Science & Engineering C-Biomimetic and Supramolecular Systems 2009 Jan 1;29(1):178-182.

59. Migneco F, Huang YC, Birla RK, Hollister SJ. Poly(glycerol-dodecanoate), a biodegradable polyester for medical devices and tissue engineering scaffolds. Biomaterials 2009 Nov;30(33):6479-6484.

60. Gyawali D, Nair P, Zhang Y, Tran RT, Zhang C, Samchukov M, et al. Citric acid-derived in situ crosslinkable biodegradable polymers for cell delivery. Biomaterials Dec;31(34):9092-9105.

61. Hu XL, Chen XS, Cheng HB, Jing XB. Cinnamate-Functionalized Poly(ester-carbonate): Synthesis and Its UV Irradiation-Induced Photo-Crosslinking. Journal of Polymer Science Part a-Polymer Chemistry 2009 Jan 1;47(1):161-169.

62. Wang SF, Yaszemski MJ, Knight AM, Gruetzmacher JA, Windebank AJ, Lu LC. Photo-crosslinked poly(epsilon-caprolactone fumarate) networks for guided peripheral nerve regeneration: Material properties and preliminary biological evaluations. Acta Biomaterialia 2009 Jun;5(5):1531-1542.

63. Ifkovits JL, Devlin JJ, Eng G, Martens TP, Vunjak-Novakovic G, Burdick JA. Biodegradable fibrous scaffolds with tunable properties formed from photo-cross-linkable poly(glycerol sebacate). ACS Appl Mater Interfaces 2009 Sep;1(9):1878-1886.

64. Gyawali D, Tran RT, Guleserian KJ, Tang L, Yang J. Citric-acid-derived photo-cross-linked biodegradable elastomers. J Biomater Sci Polym Ed;21(13):1761-1782.

65. Slaughter BV, Khurshid SS, Fisher OZ, Khademhosseini A, Peppas NA. Hydrogels in Regenerative Medicine. Advanced Materials 2009 Sep 4;21(32-33):3307-3329.

66. Hou QP, Grijpma DW, Feijen J. Creep-resistant elastomeric networks prepared by photocrosslinking fumaric acid monoethyl ester-functionalized poly(trimethylene carbonate) oligomers. Acta Biomaterialia 2009 Jun;5(5):1543-1551.

67. Bat E, Kothman BHM, Higuera GA, van Blitterswijk CA, Feijen J, Grijpma DW. Ultraviolet light crosslinking of poly(trimethylene carbonate) for elastomeric tissue engineering scaffolds. Biomaterials 2010 Nov;31(33):8696-8705.

68. Nagata M, Sato Y. Biodegradable elastic photocured polyesters based on adipic acid, 4-hydroxycinnamic acid and poly(epsilon-caprolactone) diols. Polymer 2004 Jan 1;45(1):87-93.

69. Chung LWK, Gao XH, Cui YY, Levenson RM, Nie SM. In vivo cancer targeting and imaging with semiconductor quantum dots. Nature Biotechnology 2004 Aug;22(8):969-976.

70. Shaner NC, Steinbach PA, Tsien RY. A guide to choosing fluorescent proteins. Nature Methods 2005 Dec;2(12):905-909.

71. Luo S, Zhang E, Su Y, Cheng T, Shi C. A review of NIR dyes in cancer targeting and imaging. Biomaterials Oct;32(29):7127-7138.

72. Shaner NC, Campbell RE, Steinbach PA, Giepmans BNG, Palmer AE, Tsien RY. Improved monomeric red, orange and yellow fluorescent proteins derived from Discosoma sp red fluorescent protein. Nature Biotechnology 2004 Dec;22(12):1567-1572.

73. Chang K, Jaffer F. Advances in fluorescence imaging of the cardiovascular system. Journal of Nuclear Cardiology 2008 May-Jun;15(3):417-428.

74. Paganin-Gioanni A, Bellard E, Paquereau L, Ecochard V, Golzio M, Teissie J. Fluorescence imaging agents in cancerology. Radiology and Oncology 2010 Sep;44(3):142-148.

75. Derfus AM, Chan WCW, Bhatia SN. Probing the cytotoxicity of semiconductor quantum dots. Nano Letters 2004 Jan;4(1):11-18.

76. Kirchner C, Liedl T, Kudera S, Pellegrino T, Javier AM, Gaub HE, et al. Cytotoxicity of colloidal CdSe and CdSe/ZnS nanoparticles. Nano Letters 2005 Feb;5(2):331-338.

77. Han DW, Matsumura K, Kim B, Hyon SH. Time-dependent intracellular trafficking of FITC-conjugated epigallocatechin-3-O-gallate in L-929 cells. Bioorganic & Medicinal Chemistry 2008 Nov 15;16(22):9652-9659.

78. Liu HS, Jan MS, Chou CK, Chen PH, Ke NJ. Is green fluorescent protein toxic to the living cells? Biochemical and Biophysical Research Communications 1999 Jul 14;260(3):712-717.

79. Hezinger AFE, Tessmar J, Gopferich A. Polymer coating of quantum dots - A powerful tool toward diagnostics and sensorics. European Journal of Pharmaceutics and Biopharmaceutics 2008 Jan;68(1):138-152.

80. Donaldson L. 'Cornell Dots' receive approval for clinical trials. Materials Today 2011 Apr;14(4):131-131.

81. Schipper ML, Iyer G, Koh AL, Cheng Z, Ebenstein Y, Aharoni A, et al. Particle Size, Surface Coating, and PEGylation Influence the Biodistribution of Quantum Dots in Living Mice. Small 2009 Jan;5(1):126-134.

82. Hild WA, Breunig M, Goepferich A. Quantum dots - Nano-sized probes for the exploration of cellular and intracellular targeting. European Journal of Pharmaceutics and Biopharmaceutics 2008 Feb;68(2):153-168.

83. Escobedo JO, Rusin O, Lim S, Strongin RM. NIR dyes for bioimaging applications. Current Opinion in Chemical Biology 2010 Feb;14(1):64-70.

84. Resch-Genger U, Grabolle M, Cavaliere-Jaricot S, Nitschke R, Nann T. Quantum dots versus organic dyes as fluorescent labels. Nature Methods 2008 Sep;5(9):763-775.

85. Rautio J, Kumpulainen H, Heimbach T, Oliyai R, Oh D, Jarvinen T, et al. Prodrugs: design and clinical applications. Nature Reviews Drug Discovery 2008 Mar;7(3):255-270.

86. Zhao H, Rubio B, Sapra P, Wu DC, Reddy P, Sai P, et al. Novel prodrugs of SN38 using multiarm poly(ethylene glycol) linkers. Bioconjugate Chemistry 2008 Apr;19(4):849-859.

87. Larson N, Ghandehari H. Polymeric Conjugates for Drug Delivery. Chemistry of Materials 2012 Mar 13;24(5):840-853.

88. Melancon MP, Wang W, Wang Y, Shao R, Ji X, Gelovani JG, et al. A novel method for imaging in vivo degradation of poly(L-glutamic acid), a biodegradable drug carrier. Pharm Res 2007 Jun;24(6):1217-1224.

89. Lu ZR. Molecular imaging of HPMA copolymers: visualizing drug delivery in cell, mouse and man. Adv Drug Deliv Rev Feb 17;62(2):246-257.

90. Jensen KD, Kopeckova P, Bridge JH, Kopecek J. The cytoplasmic escape and nuclear accumulation of endocytosed and microinjected HPMA copolymers and a basic kinetic study in Hep G2 cells. AAPS PharmSci 2001;3(4):E32.

91. Helmchen F, Denk W. Deep tissue two-photon microscopy. Nat Methods 2005 Dec;2(12):932-940.

92. Hong X, Guo W, Yuang H, Li J, Liu YM, Ma L, et al. Periodate oxidation of nanoscaled magnetic dextran composites. Journal of Magnetism and Magnetic Materials 2004 Feb;269(1):95-100.

93. Bhadra D, Bhadra S, Jain S, Jain NK. A PEGylated dendritic nanoparticulate carrier of fluorouracil. Int J Pharm 2003 May 12;257(1-2):111-124.

94. Sokolova V, Neumann S, Kovtun A, Chernousova S, Heumann R, Epple M. An outer shell of positively charged poly(ethyleneimine) strongly increases the transfection efficiency of calcium phosphate/DNA nanoparticles. Journal of Materials Science 2010 Sep;45(18):4952-4957.

95. Nam HY, Nam K, Hahn HJ, Kim BH, Lim HJ, Kim HJ, et al. Biodegradable PAMAM ester for enhanced transfection efficiency with low cytotoxicity. Biomaterials 2009 Feb;30(4):665-673.

96. Majoros IJ, Myc A, Thomas T, Mehta CB, Baker JR, Jr. PAMAM dendrimer-based multifunctional conjugate for cancer therapy: synthesis, characterization, and functionality. Biomacromolecules 2006 Feb;7(2):572-579.

97. Wang D, Imae T, Miki M. Fluorescence emission from PAMAM and PPI dendrimers. Journal of Colloid and Interface Science 2007 Feb 15;306(2):222-227.

98. Imae T, Wang DJ. Fluorescence emission from dendrimers and its pH dependence. Journal of the American Chemical Society 2004 Oct 20;126(41):13204-13205.

99. Chu CC, Imae T. Fluorescence Investigations of Oxygen-Doped Simple Amine Compared with Fluorescent PAMAM Dendrimer. Macromolecular Rapid Communications 2009 Jan 16;30(2):89-93.

100. Santra S, Malhotra A. Fluorescent nanoparticle probes for imaging of cancer. Wiley Interdiscip Rev Nanomed Nanobiotechnol Apr 8.

101. Brigger I, Dubernet C, Couvreur P. Nanoparticles in cancer therapy and diagnosis. Adv Drug Deliv Rev 2002 Sep 13;54(5):631-651.

102. Lee YR, Lee YH, Im SA, Kim K, Lee CK. Formulation and Characterization of Antigen-loaded PLGA Nanoparticles for Efficient Cross-priming of the Antigen. Immune Netw Jun;11(3):163-168.

103. Le Droumaguet B, Souguir H, Brambilla D, Verpillot R, Nicolas J, Taverna M, et al. Selegiline-functionalized, PEGylated poly(alkyl cyanoacrylate) nanoparticles: Investigation of interaction with amyloid-beta peptide and surface reorganization. Int J Pharm Sep 20;416(2):453-460.

104. Kim SH, Jeong JH, Chun KW, Park TG. Target-specific cellular uptake of PLGA nanoparticles coated with poly(L-lysine)-poly(ethylene glycol)-folate conjugate. Langmuir 2005 Sep 13;21(19):8852-8857.

105. Chung YI, Kim JC, Kim YH, Tae G, Lee SY, Kim K, et al. The effect of surface functionalization of PLGA nanoparticles by heparin- or chitosan-conjugated Pluronic on tumor targeting. J Control Release May 10;143(3):374-382.

106. Kocbek P, Obermajer N, Cegnar M, Kos J, Kristl J. Targeting cancer cells using PLGA nanoparticles surface modified with monoclonal antibody. Journal of Controlled Release 2007 Jul 13;120(1-2):18-26.

107. Liu Q, Li R, Zhu Z, Qian X, Guan W, Yu L, et al. Enhanced antitumor efficacy, biodistribution and penetration of docetaxel-loaded biodegradable nanoparticles. Int J Pharm Apr 12.

108. Nam T, Park S, Lee SY, Park K, Choi K, Song IC, et al. Tumor targeting chitosan nanoparticles for dual-modality optical/MR cancer imaging. Bioconjug Chem Apr 21;21(4):578-582.

109. Qi LF, Gao XH. Emerging application of quantum dots for drug delivery and therapy. Expert Opinion on Drug Delivery 2008 Mar;5(3):263-267.

110. Walling MA, Novak JA, Shepard JR. Quantum dots for live cell and in vivo imaging. Int J Mol Sci 2009 Feb;10(2):441-491.

111. Tomczak N, Janczewski D, Han MY, Vancso GJ. Designer polymer-quantum dot architectures. Progress in Polymer Science 2009 May;34(5):393-430.

112. Cheng YY, Zhao LB, Li YW, Xu TW. Design of biocompatible dendrimers for cancer diagnosis and therapy: current status and future perspectives. Chemical Society Reviews 2011;40(5):2673-2703.

113. Bharali DJ, Khalil M, Gurbuz M, Simone TM, Mousa SA. Nanoparticles and cancer therapy: A concise review with emphasis on dendrimers. International Journal of Nanomedicine 2009;4(1):1-7.

114. Crouch D, Norager S, O'Brien P, Park JH, Pickett N. New synthetic routes for quantum dots. Philosophical Transactions of the Royal Society of London Series a-Mathematical Physical and Engineering Sciences 2003 Feb 15;361(1803):297-310.

115. Choi HS, Liu W, Misra P, Tanaka E, Zimmer JP, Ipe BI, et al. Renal clearance of quantum dots. Nature Biotechnology 2007 Oct;25(10):1165-1170.

116. Zhang YJ, Clapp A. Overview of Stabilizing Ligands for Biocompatible Quantum Dot Nanocrystals. Sensors 2011 Dec;11(12):11036-11055.

117. Hou XD, Li QB, Jia L, Li Y, Zhu YD, Cao AM. New Preparation of Structurally Symmetric, Biodegradable Poly(L-lactide) Disulfides and PLLA-Stabilized, Photoluminescent CdSe Quantum Dots. Macromolecular Bioscience 2009 Jun 11;9(6):551-562.

118. Tian HY, Tang ZH, Zhuang XL, Chen XS, Jing XB. Biodegradable synthetic polymers: Preparation, functionalization and biomedical application. Progress in Polymer Science 2012 Feb;37(2):237-280.

119. Choi HS, Liu WH, Liu FB, Nasr K, Misra P, Bawendi MG, et al. Design considerations for tumour-targeted nanoparticles. Nature Nanotechnology 2010 Jan;5(1):42-47.

120. Murcia MJ, Shaw DL, Long EC, Naumann CA. Fluorescence correlation spectroscopy of CdSe/ZnS quantum dot optical bioimaging probes with ultra-thin biocompatible coatings. Optics Communications 2008 Apr 1;281(7):1771-1780.

121. Dubertret B, Skourides P, Norris DJ, Noireaux V, Brivanlou AH, Libchaber A. In vivo imaging of quantum dots encapsulated in phospholipid micelles. Science 2002 Nov 29;298(5599):1759-1762.

122. Kumar N, Ravikumar MNV, Domb AJ. Biodegradable block copolymers. Advanced Drug Delivery Reviews 2001 Dec 3;53(1):23-44.

123. Di Corato R, Quarta A, Piacenza P, Ragusa A, Figuerola A, Buonsanti R, et al. Water solubilization of hydrophobic nanocrystals by means of poly(maleic anhydride-alt-1-octadecene). Journal of Materials Chemistry 2008;18(17):1991-1996.

124. Mattoussi H, Palui G, Na HB. Luminescent quantum dots as platforms for probing in vitro and in vivo biological processes. Adv Drug Deliv Rev Feb;64(2):138-166.

125. Zanetti-Ramos BG, Lemos-Senna E, Soldi V, Borsali R, Cloutet E, Cramail H. Polyurethane nanoparticles from a natural polyol via miniemulsion technique. Polymer 2006 Nov 8;47(24):8080-8087.

126. Cheng FY, Wang SPH, Su CH, Tsai TL, Wu PC, Shieh DB, et al. Stabilizer-free poly(lactide-co-glycolide) nanoparticles for multimodal biomedical probes. Biomaterials 2008 May;29(13):2104-2112.

127. Nehilla BJ, Allen PG, Desai TA. Surfactant-free, drug-quantum-dot coloaded poly(lactide-co-glycolide) nanoparticles: Towards multifunctional nanoparticles. Acs Nano 2008 Mar;2(3):538-544.

128. Kim JS, Cho KJ, Tran TH, Nurunnabi M, Moon TH, Hong SM, et al. In vivo NIR imaging with CdTe/CdSe quantum dots entrapped in PLGA nanospheres. Journal of Colloid and Interface Science 2011 Jan 15;353(2):363-371.

129. Kim BYS, Jiang W, Oreopoulos J, Yip CM, Rutka JT, Chan WCW. Biodegradable Quantum Dot Nanocomposites Enable Live Cell Labeling and Imaging of Cytoplasmic Targets. Nano Letters 2008 Nov;8(11):3887-3892.

130. Cao J, Zhu HY, Deng DW, Xue B, Tang LP, Mahounga D, et al. In vivo NIR imaging with PbS quantum dots entrapped in biodegradable micelles. Journal of Biomedical Materials Research Part A 2012 Apr;100A(4):958-968.

131. Xu YL, Shi LQ, Ma RJ, Zhang WQ, An YL, Zhu XX. Synthesis and micellization of thermo- and pH-responsive block copolymer of poly (N-isopropylacrylamide)-block-poly(4-vinylpyridine). Polymer 2007 Mar 8;48(6):1711-1717.

132. Gong YJ, Gao MY, Wang DY, Mohwald H. Incorporating fluorescent CdTe nanocrystals into a hydrogel via hydrogen bonding: Toward fluorescent microspheres with temperature-responsive properties. Chemistry of Materials 2005 May 17;17(10):2648-2653.

133. Wu CL, Ma RJ, He H, Zhao LZ, Gao HJ, An YL, et al. Fabrication of Complex Micelles with Tunable Shell for Application in Controlled Drug Release. Macromolecular Bioscience 2009 Dec 8;9(12):1185-1193.

134. Tsien RY. The green fluorescent protein. Annual Review of Biochemistry 1998;67:509-544.

135. Tavare JM, Fletcher LM, Welsh GI. Review - Using green fluorescent protein to study intracellular signalling. Journal of Endocrinology 2001 Aug;170(2):297-306.

136. Chudakov DM, Matz MV, Lukyanov S, Lukyanov KA. Fluorescent Proteins and Their Applications in Imaging Living Cells and Tissues. Physiological Reviews 2010 Jul;90(3):1103-1163.

137. Piston DW, Kremers GJ. Fluorescent protein FRET: the good, the bad and the ugly. Trends in Biochemical Sciences 2007 Sep;32(9):407-414.

138. Miyawaki A, Llopis J, Heim R, McCaffery JM, Adams JA, Ikura M, et al. Fluorescent indicators for Ca2+ based on green fluorescent proteins and calmodulin. Nature 1997 Aug 28;388(6645):882-887.

139. Neidert MR, Tranquillo RT. Tissue-engineered valves with commissural alignment. Tissue Eng 2006 Apr;12(4):891-903.

140. Robinson PS, Johnson SL, Evans MC, Barocas VH, Tranquillo RT. Functional tissue-engineered valves from cell-remodeled fibrin with commissural alignment of cell-produced collagen. Tissue Eng Part A 2008 Jan;14(1):83-95.

141. Engelmayr GC, Jr., Sales VL, Mayer JE, Jr., Sacks MS. Cyclic flexure and laminar flow synergistically accelerate mesenchymal stem cell-mediated engineered tissue formation: Implications for engineered heart valve tissues. Biomaterials 2006 Dec;27(36):6083-6095.

142. Zhao Y, Lin H, Zhang J, Chen B, Sun W, Wang X, et al. Crosslinked three-dimensional demineralized bone matrix for the adipose-derived stromal cell proliferation and differentiation. Tissue Eng Part A 2009 Jan;15(1):13-21.

143. Yang J, Motlagh D, Webb AR, Ameer GA. Novel biphasic elastomeric scaffold for small-diameter blood vessel tissue engineering. Tissue Engineering 2005 Nov;11(11-12):1876-1886.

144. Guan J, Sacks MS, Beckman EJ, Wagner WR. Synthesis, characterization, and cytocompatibility of elastomeric, biodegradable poly(ester-urethane)ureas based on poly(caprolactone) and putrescine. J Biomed Mater Res 2002 Sep 5;61(3):493-503.

145. Guan J, Sacks MS, Beckman EJ, Wagner WR. Biodegradable poly(ether ester urethane)urea elastomers based on poly(ether ester) triblock copolymers and putrescine: synthesis, characterization and cytocompatibility. Biomaterials 2004 Jan;25(1):85-96.

146. Guan J, Wagner WR. Synthesis, characterization and cytocompatibility of polyurethaneurea elastomers with designed elastase sensitivity. Biomacromolecules 2005 Sep-Oct;6(5):2833-2842.

147. Zhang C, Wen X, Vyavahare NR, Boland T. Synthesis and characterization of biodegradable elastomeric polyurethane scaffolds fabricated by the inkjet technique. Biomaterials 2008 Oct;29(28):3781-3791.

148. Chen QZ, Bismarck A, Hansen U, Junaid S, Tran MQ, Harding SE, et al. Characterisation of a soft elastomer poly(glycerol sebacate) designed to match the mechanical properties of myocardial tissue. Biomaterials 2008 Jan;29(1):47-57.

149. Du Y, Lo E, Ali S, Khademhosseini A. Directed assembly of cell-laden microgels for fabrication of 3D tissue constructs. Proc Natl Acad Sci U S A 2008;105(28):9522-9527.

150. Khademhosseini A, Eng G, Yeh J, Fukuda J, Blumling J, Langer R, et al. Micromolding of photocroslinkable hyaluronic acid for cell encapsulation and entrapment. J Biomed Mater Res 2006;79A:522-532.

151. Yu L, Ding JD. Injectable hydrogels as unique biomedical materials. Chemical Society Reviews 2008;37(8):1473-1481.

152. Timmer MD, Shin H, Horch RA, Ambrose CG, Mikos AG. In vitro cytotoxicity of injectable and biodegradable poly(propylene fumarate)-based networks: unreacted macromers, cross-linked networks, and degradation products. Biomacromolecules 2003 Jul-Aug;4(4):1026-1033.

153. Guan J, Stankus JJ, Wagner WR. Biodegradable elastomeric scaffolds with basic fibroblast growth factor release. J Control Release 2007 Jul 16;120(1-2):70-78.

154. Yang J, Gywali D, Tran RT, inventors. Composition and method of biodegradable elastic polymers. US Patent Pending, 2008.

155. Yang SF, Leong KF, Du ZH, Chua CK. The design of scaffolds for use in tissue engineering. Part 1. Traditional factors. Tissue Engineering 2001 Dec;7(6):679-689.

156. Yeganeh H, Lakouraj MM, Jamshidi S. Synthesis and characterization of novel biodegradable epoxy-modified polyurethane elastomers. Journal of Polymer Science Part a-Polymer Chemistry 2005 Jul 15;43(14):2985-2996.

157. Panyam J, Labhasetwar V. Biodegradable nanoparticles for drug and gene delivery to cells and tissue. Advanced Drug Delivery Reviews 2003 Feb 24;55(3):329-347.

158. Kim JH, Park K, Nam HY, Lee S, Kim K, Kwon IC. Polymers for bioimaging. Progress in Polymer Science 2007 Aug-Sep;32(8-9):1031-1053.

159. Yang J, Lee CH, Park J, Seo S, Lim EK, Song YJ, et al. Antibody conjugated magnetic PLGA nanoparticles for diagnosis and treatment of breast cancer. Journal of Materials Chemistry 2007;17(26):2695-2699.

160. Cho H, Kwon GS. Polymeric Micelles for Neoadjuvant Cancer Therapy and Tumor-Primed Optical Imaging. Acs Nano 2011 Nov;5(11):8721-8729.

161. Gurskaya NG, Verkhusha VV, Shcheglov AS, Staroverov DB, Chepurnykh TV, Fradkov AF, et al. Engineering of a monomeric green-to-red photoactivatable fluorescent protein induced by blue light. Nature Biotechnology 2006 Apr;24(4):461-465.

162. Hirsch A, Chen ZF, Jiao HJ. Spherical aromaticity in 1(h) symmetrical fullerenes: The 2(N+1)(2) rule. Angewandte Chemie-International Edition 2000;39(21):3915-+.

163. Campbell RE, Tour O, Palmer AE, Steinbach PA, Baird GS, Zacharias DA, et al. A monomeric red fluorescent protein. Proceedings of the National Academy of Sciences of the United States of America 2002 Jun 11;99(12):7877-7882.

164. Martini M, Montagna M, Ou M, Tillement O, Roux S, Perriat P. How to measure quantum yields in scattering media: Application to the quantum yield measurement of fluorescein molecules encapsulated in sub-100 nm silica particles. Journal of Applied Physics 2009 Nov 1;106(9).

165. Cossec B, Cosnier F, Burgart M. Methyl Mercapturate Synthesis: An Efficient, Convenient and Simple Method. Molecules 2008 Oct;13(10):2394-2407.

166. Pinto MR, Kristal BM, Schanze KS. A water-soluble poly(phenylene ethynylene) with pendant phosphonate groups. Synthesis, photophysics, and layer-by-layer self-assembled films. Langmuir 2003 Aug 5;19(16):6523-6533.

167. Hutmacher DW. Scaffolds in tissue engineering bone and cartilage. Biomaterials 2000 Dec;21(24):2529-2543.

168. Amass W, Amass A, Tighe B. A review of biodegradable polymers: Uses, current developments in the synthesis and characterization of biodegradable polyesters, blends of biodegradable polymers and recent advances in biodegradation studies. Polymer International 1998 Oct;47(2):89-144.

169. Larsen J, Cornett C, Jaroszewski JW, Hansen SH. Reaction between drug substances and pharmaceutical excipients: Formation of citric acid esters and amides of carvedilol in the solid state. Journal of Pharmaceutical and Biomedical Analysis 2009 Jan 15;49(1):11-17.

170. Larsen J, Staerk D, Cornett C, Hansen SH, Jaroszewski JW. Identification of reaction products between drug substances and excipients by HPLC-SPE-NMR: Ester and amide formation between citric acid and 5-aminosalicylic acid. Journal of Pharmaceutical and Biomedical Analysis 2009 Apr 5;49(3):839-842.

171. Torchilin V. Tumor delivery of macromolecular drugs based on the EPR effect. Advanced Drug Delivery Reviews 2011 Mar 18;63(3):131-135.

172. Michalet X, Pinaud FF, Bentolila LA, Tsay JM, Doose S, Li JJ, et al. Quantum dots for live cells, in vivo imaging, and diagnostics. Science 2005 Jan 28;307(5709):538-544.

173. Smyder J, Krauss T. Coming attractions for semiconductor quantum dots. Materials Today 2011;14(9):16.

174. Rajeshwar K, de Tacconi NR, Chenthamarakshan CR. Semiconductor-based composite materials: Preparation, properties, and performance. Chemistry of Materials 2001 Sep;13(9):2765-2782.

175. Trindade T, O'Brien P, Pickett NL. Nanocrystalline semiconductors: Synthesis, properties, and perspectives. Chemistry of Materials 2001 Nov;13(11):3843-3858.

176. Lee WI, Bae YJ, Bard AJ. Strong blue photoluminescence and ECL from OH-terminated PAMAM dendrimers in the absence of gold nanoparticles. Journal of the American Chemical Society 2004 Jul 14;126(27):8358-8359.

177. Cubitt AB, Heim R, Adams SR, Boyd AE, Gross LA, Tsien RY. Understanding, improving and using green fluorescent proteins. Trends Biochem Sci 1995 Nov;20(11):448-455.

178. Gross LA, Baird GS, Hoffman RC, Baldridge KK, Tsien RY. The structure of the chromophore within DsRed, a red fluorescent protein from coral. Proceedings of the National Academy of Sciences of the United States of America 2000 Oct 24;97(22):11990-11995.

179. Rochelle GT, Gibson MM. Thermal-Degradation of Sodium-Citrate Solutions Containing So2 and Thiosulfate. Industrial & Engineering Chemistry Process Design and Development 1982;21(4):569-574.

180. Martinez-Palau M, Urpi L, Solans X, Puiggali J. Morpholine-2,5-dione. Acta Crystallographica Section C-Crystal Structure Communications 2006 May;62:O262-O264.

181. Knyazhanskii k, Karmazin P, Olekhnovich P, Dorofeenko N. Spectral luminescence properties caused by hyperconjugation in the 2-methylchromylium cation. Journal of Applied Spectroscopy 1975;23(2):3.

182. Levitus M. Sequence-dependent photophysical properties of Cy3-labeled DNA. Reporters, Markers, Dyes, Nanoparticles, and Molecular Probes for Biomedical Applications Ii 2010;7576.

183. Zhang XJ, Jenekhe SA. Electroluminescence of multicomponent conjugated polymers. 1. Roles of polymer/polymer interfaces in emission enhancement and voltage-tunable multicolor emission in semiconducting polymer/polymer heterojunctions. Macromolecules 2000 Mar 21;33(6):2069-2082.

184. Piatkevich KD, Malashkevich VN, Almo SC, Verkhusha VV. Engineering ESPT Pathways Based on Structural Analysis of LSSmKate Red Fluorescent Proteins with Large Stokes Shift. Journal of the American Chemical Society 2010 Aug 11;132(31):10762-10770.

185. Chattopadhyay A, Mukherjee S. Fluorophore Environments in Membrane-Bound Probes - a Red Edge Excitation Shift Study. Biochemistry 1993 Apr 13;32(14):3804-3811.

186. Demchenko AP. The red-edge effects: 30 years of exploration. Luminescence 2002 Jan-Feb;17(1):19-42.

187. Haldar S, Chattopadhyay A. Dipolar relaxation within the protein matrix of the green fluorescent protein: A red edge excitation shift study. Journal of Physical Chemistry B 2007 Dec 27;111(51):14436-14439.

188. Fletcher AN. Fluorescence Emission Band Shift with Wavelength of Excitation. Journal of Physical Chemistry 1968;72(8):2742-&.

189. Li YL, Rodrigues J, Tomas H. Injectable and biodegradable hydrogels: gelation, biodegradation and biomedical applications. Chemical Society Reviews 2012;41(6):2193-2221.

190. Nair LS, Laurencin CT. Biodegradable polymers as biomaterials. Progress in Polymer Science 2007 Aug-Sep;32(8-9):762-798.

191. Zhang RY, Ma PX. Poly(alpha-hydroxyl acids) hydroxyapatite porous composites for bone-tissue engineering. I. Preparation and morphology. Journal of Biomedical Materials Research 1999 Mar 15;44(4):446-455.

192. Tateishi T, Chen G. Biodegradable polymer scaffold for tissue engineering. Asbm6: Advanced Biomaterials Vi 2005;288-289:59-62.

193. Govender T, Stolnik S, Garnett MC, Illum L, Davis SS. PLGA nanoparticles prepared by nanoprecipitation: drug loading and release studies of a water soluble drug. Journal of Controlled Release 1999 Feb 1;57(2):171-185.

194. Dey J, Xu H, Shen JH, Thevenot P, Gondi SR, Nguyen KT, et al. Development of biodegradable crosslinked urethane-doped polyester elastomers. Biomaterials 2008 Dec;29(35):4637-4649.

195. Vij N, Min T, Marasigan R, Belcher CN, Mazur S, Ding H, et al. Development of PEGylated PLGA nanoparticle for controlled and sustained drug delivery in cystic fibrosis. J Nanobiotechnology;8:22.

196. Kashi TS, Eskandarion S, Esfandyari-Manesh M, Marashi SM, Samadi N, Fatemi SM, et al. Improved drug loading and antibacterial activity of minocycline-loaded PLGA nanoparticles prepared by solid/oil/water ion pairing method. Int J Nanomedicine;7:221-234.

197. Bagwe RP, Kanicky JR, Palla BJ, Patanjali PK, Shah DO. Improved drug delivery using microemulsions: Rationale, recent progress, and new horizons. Critical Reviews in Therapeutic Drug Carrier Systems 2001;18(1):77-140.

198. Yokoyama M. Polymeric micelles as a new drug carrier system and their required considerations for clinical trials. Expert Opinion on Drug Delivery 2010 Feb;7(2):145-158.

199. Gong Y, Zhou Q, Gao C, Shen J. In vitro and in vivo degradability and cytocompatibility of poly(l-lactic acid) scaffold fabricated by a gelatin particle leaching method. Acta Biomater 2007 Jul;3(4):531-540.

200. Artzi N, Oliva N, Puron C, Shitreet S, Artzi S, Ramos AB, et al. In vivo and in vitro tracking of erosion in biodegradable materials using non-invasive fluorescence imaging (vol 10, pg 704, 2011). Nature Materials 2011 Nov;10(11):896-896.

201. Petros RA, DeSimone JM. Strategies in the design of nanoparticles for therapeutic applications. Nat Rev Drug Discov Aug;9(8):615-627.

202. Yakimansky AV, Menshikova AY, Shevchenko NN, Shabsels BM, Bazhenova AG, Sel'kin AV, et al. From polymeric nanoparticles to dye-containing photonic crystals: synthesis, self-assembling, optical features, and possible applications. Polymers for Advanced Technologies 2009 Jun;20(6):581-588.

203. Jaiswal JK, Mattoussi H, Mauro JM, Simon SM. Long-term multiple color imaging of live cells using quantum dot bioconjugates. Nature Biotechnology 2003 Jan;21(1):47-51.

204. Jamieson T, Bakhshi R, Petrova D, Pocock R, Imani M, Seifalian AM. Biological applications of quantum dots. Biomaterials 2007 Nov;28(31):4717-4732.

205. Yanushevich YG, Staroverov DB, Savitsky AP, Fradkov AF, Gurskaya NG, Bulina ME, et al. A strategy for the generation of non-aggregating mutants of Anthozoa fluorescent proteins. Febs Letters 2002 Jan 30;511(1-3):11-14.

206. Phillips RL, Kim IB, Tolbert LM, Bunz UH. Fluorescence self-quenching of a mannosylated poly(p-phenyleneethynylene) induced by concanavalin A. J Am Chem Soc 2008 Jun 4;130(22):6952-6954.

207. Chung TW, Liu DZ, Wang SY, Wang SS. Enhancement of the growth of human endothelial cells by surface roughness at nanometer scale. Biomaterials 2003 Nov;24(25):4655-4661.

208. Karageorgiou V, Kaplan D. Porosity of 3D biornaterial scaffolds and osteogenesis. Biomaterials 2005 Sep;26(27):5474-5491.

209. Li WJ, Laurencin CT, Caterson EJ, Tuan RS, Ko FK. Electrospun nanofibrous structure: A novel scaffold for tissue engineering. Journal of Biomedical Materials Research 2002 Jun 15;60(4):613-621.

210. Sodian R, Lemke T, Fritsche C, Hoerstrup SP, Fu P, Potapov EV, et al. Tissue-engineering bioreactors: A new combined cell-seeding and perfusion system for vascular tissue engineering. Tissue Engineering 2002 Oct;8(5):863-870.

211. Deligianni DD, Katsala ND, Koutsoukos PG, Missirlis YF. Effect of surface roughness of hydroxyapatite on human bone marrow cell adhesion, proliferation, differentiation and detachment strength. Biomaterials 2001 Jan;22(1):87-96.

212. Huynh T, Abraham G, Murray J, Brockbank K, Hagen PO, Sullivan S. Remodeling of an acellular collagen graft into a physiologically responsive neovessel. Nature Biotechnology 1999 Nov;17(11):1083-1086.

213. Marques AP, Reis RL, Hunt JA. The biocompatibility of novel starch-based polymers and composites: in vitro studies. Biomaterials 2002 Mar;23(6):1471-1478.

214. Kataoka K, Harada A, Nagasaki Y. Block copolymer micelles for drug delivery: design, characterization and biological significance. Advanced Drug Delivery Reviews 2001 Mar 23;47(1):113-131.

215. Abraham T, Wadsworth S, Carthy JM, Pechkovsky DV, McManus B. Minimally invasive imaging method based on second harmonic generation and multiphoton excitation fluorescence in translational respiratory research. Respirology 2011 Jan;16(1):22-33.

BIOGRAPHICAL INFORMATION

Born in Shanghai, People's Republic of China, Yi Zhang finished his Junior and High school at Jingye School, Shanghai, China. He started his undergraduate study at Department of Macromolecular science, Fudan University, Shanghai, China, and earned his Bachelor of Science degree in 2007. During his undergraduate studies, Yi was received several rewards for his excellent academic records, and research work, including People's Scholarship, and Tangs' Research Foundation.

Yi joined Dr. Zhou's research group on spring, 2006. He finished his thesis on "Growth of Human Smooth Muscle Cells on the Silk Fibroin Modified-Polyhydroxyalkanoate Scaffold", and published this work on Acta Chimica Sinica. In 2007, Yi was accepted into the joint Graduate Program in Biomedical Engineering at the University of Texas at Arlington and the University of Texas Southwestern Medical Center at Dallas. Under the guidance of Dr. Jian Yang, he began his doctoral work, which focused on biodegradable photoluminescnet polymer development and biomedical applications and earned a Ph. D in Bioengineering in the summer of 2012. During his doctoral work, Yi had 11 publications on significant journal from Science Citation Index. He published his major work, "Development of aliphatic biodegradable photoluminescent polymers", on Proceedings of the National Academy of Sciences of the United States of America.